

Moritz Pallua, BSc

**Hydrogenation of CO<sub>2</sub> to methanol:  
Development of a novel semi batch reactor concept  
and validation of a fixed bed reactor setup**

Master's Thesis

to achieve the university degree of

Diplom-Ingenieur

in

Verfahrenstechnik

submitted to

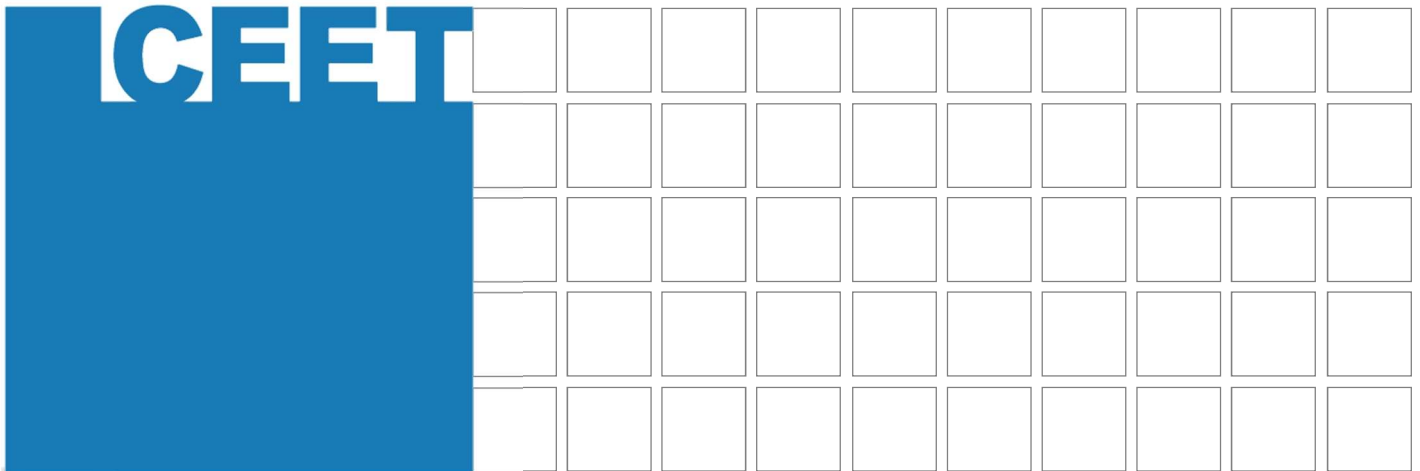
Graz University of Technology

Supervisor:

Ass.Prof. Dipl.-Ing. Dr.techn. Lux Susanne

Institute of Chemical Engineering and Environmental Technology

Graz, May 2020



## Hydrogenation of CO<sub>2</sub> to methanol: Development of a novel semi batch reactor concept and validation of a fixed bed reactor setup

Moritz Pallua, BSc

Graz, May 2020

**Master's Thesis**  
**by**  
**Moritz Pallua, BSc**

**Task description**

The aim of this work is to prepare a solid fundament for future research in two different fields. One approach aims at the investigation of a new  $Cu/MgO$  catalyst for the hydrogenation of  $CO_2$  to methanol. Therefore, a suitable lab scale plug flow reactor (PFR) plant has to be built, commissioned and validated with the catalyst of interest in the first part of this work. The second part of this work includes a novel reactor set-up. It consists of a discontinuous stirred tank reactor (DSTR) in combination with a condenser and a product vessel. The novelty of this concept is the idea of a fluid flow introduction, caused by volume contraction during the condensation of vaporous products in the condenser. Additionally, the withdrawal of liquid products should hinder the formation of an equilibrium state in the reactor. Therefore, the setup has to be built and validated. As design criteria for both reactor setups,  $p_R = 50 \text{ bar}$  and  $T_R = 300 \text{ }^\circ\text{C}$  are defined. The results of this thesis shall be used as a basis for future research regarding the introduced  $Cu/MgO$  catalyst and the novel reactor concept.

---

## STATUTORY DECLARATION

I declare that I have authored this thesis independently, that I have not used other than the declared sources / resources, and that I have explicitly marked all material which has been quoted either literally or by content from the used sources.

Graz, .....

date

.....

(signature)

## EIDESSTÄTTLICHE ERKLÄRUNG

Ich erkläre an Eides statt, dass ich die vorliegende Arbeit selbstständig verfasst, andere als die angegebenen Quellen/Hilfsmittel nicht benutzt, und die den benutzten Quellen wörtlich und inhaltlich entnommenen Stellen als solche kenntlich gemacht habe.

Graz, am .....

.....  
(Unterschrift)



---

## Abstract

In times of global warming, mankind is continuously seeking for alternatives to fossil fuels, as well as new technologies for the minimization of anthropogenic  $CO_2$  emissions. Hydrogenation of  $CO_2$  to methanol could contribute in providing a possible solution. Therefore, new reactor concepts and catalysts are needed. To make such a process profitable on a large scale, these catalysts need to show a higher performance, selectivity and lifetime than the conventional  $Cu/ZnO/Al_2O_3$  catalysts. This work aims to contribute to these topics, by building, commissioning and validating two lab-scale reactor setups, as well as a new  $Cu/MgO$  catalyst. The validated reactor setups and the tested catalyst will form the basis for future research.

The proposed catalyst is based on recognizable results of  $Ni/MgO$  catalysts in the methanation of  $CO_2$ . The catalyst is adapted by exchanging the active  $Ni$  species to  $Cu$ , which is the standard active site in methanol synthesis from  $CO$  and  $CO_2$  and  $H_2$ . By impregnation of  $MgO$  with  $Cu(NO_3)_2$ , a catalyst is prepared with a  $Cu/Mg$  ratio of 3/1. Its activation, as well as validation, are performed in the first lab-scale plug flow reactor (PFR) setup. The second lab-scale reactor setup is based on a discontinuous stirred tank reactor (DSTR). Both reactor setups consist of a reactor, followed by a condenser and a product vessel. The new concept of the second setup is based on the idea of a product flow, which establishes as vaporous products are condensed in the condenser. By the withdrawal of vapour, the reaction equilibrium will not be established in the reactor, which leads to higher total conversions of reactants. For its validation, a proofed  $Cu/ZnO/Al_2O_3$  catalyst is used with  $H_2$ ,  $N_2$  and  $CO_2$  in the feed stream. Before the actual activation and validation different pressure tests are performed to avoid unwanted leakage and to ensure safe operation. The activation of the catalysts is performed in a mixed atmosphere of  $H_2$  and  $N_2$  at reaction conditions. The following validations are performed at  $p_R \cong 50 \text{ bar}$  and  $T_R \cong 300 \text{ }^\circ\text{C}$  in a  $H_2/CO_2$  ratio of 3/1. At the end of the validation experiments, methanol is detected in the formed liquids, which proves the functionality of the lab-scale plants and the  $Cu/MgO$  catalyst.

---

## Kurzfassung

In Zeiten globaler Klimaerwärmung ist die Menschheit ununterbrochen auf der Suche nach Alternativen zu fossilen Brennstoffen sowie innovativen Technologien zur Minimierung anthropogener  $CO_2$  Emissionen. Die Hydrierung von  $CO_2$  zu Methanol könnte zur Lösung dieser Probleme einen wertvollen Beitrag leisten. Diesbezüglich besteht ein Bedarf an verbesserten Reaktorkonzepten und Katalysatoren. Letztere müssen höhere Aktivitäten, Selektivitäten und Lebenserwartungen als konventionelle  $Cu/ZnO/Al_2O_3$  Katalysatoren vorweisen können, um die Rentabilität großtechnischer Prozesse zu garantieren. Die in dieser Arbeit behandelten Labormaßstabsreaktorkonzepte, deren Aufbau und Inbetriebnahme, sowie die Validierung derselben und eines neuartigen  $Cu/MgO$  Katalysators stellen einen Beitrag zu diesem Forschungsgebiet dar. Die validierten Reaktorkonzepte und der getestete Katalysator bilden die Basis für zukünftige Forschungsarbeit.

Der hier vorgestellte Katalysator beruht auf beachtlichen Ergebnissen von  $Ni/MgO$  Katalysatoren in der Methanisierung von  $CO_2$ . Angepasst wird dieser durch Austauschen der aktiven  $Ni$  Spezies durch  $Cu$ , welche die standardmäßig aktive Spezies in der Hydrierung von  $CO$  und  $CO_2$  zu Methanol ist. Seine Herstellung erfolgt durch Imprägnierung von  $MgO$  mit  $Cu(NO_3)_2$ , wobei ein  $Cu/Mg$ -Verhältnis von 3/1 angestrebt wird. Die Aktivierung und Validierung desselben erfolgt im ersten Labormaßstabsrohrreaktoraufbau. Der zweite Labormaßstabsreaktoraufbau basiert auf einem diskontinuierlichen Rührkessel. Beide Aufbauten bestehen aus einem Reaktor, welchem ein Kondensator und ein Produktbehälter nachgeschaltet sind. Das neuartige Konzept des zweiten Aufbaus beruht auf der Idee eines sich, aufgrund von kondensierendem Produktdampf im Kondensator, einstellenden Produktstroms. Durch den Abzug des Produktdampfes aus dem Reaktorraum kann sich kein Reaktionsgleichgewicht im Reaktor einstellen, wodurch mehr Edukt zu Produkt umgesetzt werden kann. Die Validierung dieses Aufbaus erfolgt mit einem erprobten  $Cu/ZnO/Al_2O_3$  Katalysator. Vor der eigentlichen Aktivierung und Validierung werden verschiedene Drucktests durchgeführt, um einen sicheren Ablauf zu gewährleisten. Die Aktivierung der Katalysatoren erfolgt unter Reaktionsbedingungen in einer Atmosphäre aus  $H_2$  und  $N_2$ . Die Validierung derselben erfolgt bei  $p_R \cong 50 \text{ bar}$  und  $T_R \cong 300 \text{ °C}$  in einer  $H_2/CO_2$  Atmosphäre im Verhältnis 3/1. Am Ende der Validierungsexperimente kann Methanol in den gebildeten Flüssigphasen nachgewiesen werden, wodurch die Funktionalität der verschiedenen Reaktoraufbauten und des neuen  $Cu/MgO$  Katalysators bewiesen werden.

---

## Content

Abstract.....	III
1 Introduction .....	1
2 Theoretical basics .....	3
2.1 Thermodynamics .....	3
2.2 Reaction kinetics.....	5
2.3 Ideal isothermal reactors.....	6
2.4 Catalysis .....	7
2.4.1 Heterogeneous catalysis.....	8
3 Methanol synthesis .....	13
3.1 Methanol from syngas.....	14
3.1.1 Syngas preparation.....	14
3.1.2 Reactor systems .....	16
3.2 Methanol from $CO_2$ .....	18
3.2.1 Hydrogenation of $CO_2$ .....	19
3.2.2 Current research.....	21
3.3 Catalyst of interest .....	26
4 Process design .....	30
4.1 Standard equipment .....	30
4.1.1 Fittings and piping.....	30
4.1.2 Valves.....	31
4.1.3 Mass flow controllers .....	32
4.1.4 Condenser .....	33
4.1.5 Product vessel .....	35
4.1.6 Safety equipment.....	36

---

4.2	PFR plant.....	37
4.2.1	Working principle and build up.....	37
4.2.2	Process control.....	39
4.2.3	Pressure test .....	42
4.2.4	Experiments.....	43
4.2.5	Optimization and future improvements .....	52
4.3	DSTR plant.....	54
4.3.1	Working principle and build up.....	54
4.3.2	Process control.....	56
4.3.3	Pressure test .....	59
4.3.4	Risk assessment.....	65
4.3.5	Experiments.....	68
4.3.6	Optimization and future improvements .....	76
5	Conclusion.....	83
6	References .....	86
7	List of figures .....	90
8	List of tables.....	94
9	List of abbreviations and symbols .....	95
10	Appendix.....	99

# 1 Introduction

In times of global warming, environmental pollution and constant fear of the ending of fossil fuels, mankind is on the search for alternatives to the current, fossil fuel dominated system. Politics is, therefore, trying to accelerate this switch with a mix of financial supports and penalties. The industry can profit from subsidies for climate-friendly investments, while financial penalties must be paid for over proportional carbon emissions to the atmosphere. Thus, the *European Union* has introduced the “*European Union Emissions Trading System*” [1]. This system defines a cap for greenhouse gas emissions for defined industries. A company is, therefore, allowed to emit a certain amount, depending on its share on the total cap, of greenhouse gases at a specific time. If more greenhouse gases are emitted, more certificates are needed, which can be bought from other market participants. In addition to the European system, the People’s Republic of China is currently working on an emissions trading system. Furthermore, an emissions trading system is available in Korea, including companies that are responsible for 68% of Korea’s greenhouse gas emissions. The goal of all of these systems is the minimization of greenhouse gas emissions by the market itself. Since fewer allowances will be handed out than needed, the idea is that the market will optimize itself. Investments will be done in sectors where greenhouse gas emissions can be achieved with little money. While until now emission gases were treated as waste products, their usage and therefore the minimization of their emission, in combination with the produced valuables, becomes a financial opportunity.

Prior to the synthesis of new valuables, adequate capture technology is necessary. For  $CO_2$  capture pre-, post-, and oxy-fuel combustion capture are known. These strategies rely on different technologies, such as ad- and absorption, membranes, and many more, to separate and concentrate the  $CO_2$ . Post-combustion capture technology can be added to existing  $CO_2$  emitters, which allows the minimization of their ecological footprint [2].

A promising process for  $CO_2$  usage as a feedstock is its catalytic hydrogenation to methanol. Methanol, as the simplest alcohol, can be used for a large variety of products. It finds its use as a feedstock for fuel production, as a basic chemical or for energy-related purposes. In addition to the wide variety of application possibilities, methanol and most of its derivatives have similar properties to fossil fuel products. Therefore, they have the huge advantage that in case of an uprising, fossil fuel replacing methanol industry, the existing infrastructure could

still be used [3–5]. For the synthesis of most of the nowadays produced methanol, syngas, which is produced by the reforming of fossil fuels [6], is used. Catalysts for conventional methanol synthesis from syngas use copper as their active species and a mixture of zinc- and aluminum-oxide as their support. As an alternative to methanol from syngas processes, many research projects investigate the direct catalytic conversion of  $CO_2$  to methanol. This work aims to contribute to this research field. Since catalysts shall be tested, suitable lab-scale plants are needed. Accordingly, two different reactor setups, a lab-scale plug flow reactor (PFR) plant and a lab-scale discontinuous stirred tank reactor (DSTR) plant, are built and validated. The catalyst of interest, which will be validated, consists of copper and magnesium oxide. This composition is chosen because of the acknowledgeable results of a  $Ni/MgO$  catalyst in the methanation. The mentioned catalyst allows constant  $CO_2$  conversion of 87% with a selectivity > 99% for methane at 330 °C and ambient pressure [7, 8]. The combination of the validated plants and catalyst shall be the cornerstone for future research efforts.

## 2 Theoretical basics

This chapter can be considered as a short introduction in the relevant theory and is meant to explain the basic considerations taken into account in this work. It includes a brief insight into reaction thermodynamics, kinetics as well as the basic principles of reactor design.

### 2.1 Thermodynamics

Before any investigation about the rate law or a reaction mechanism can be performed, knowledge about the thermodynamics of a reactions is crucial. Thermodynamics can provide answers to crucial questions about the feasibility and the character of a reaction.

Therefore, the enthalpy of reaction  $\Delta H_R$  is introduced, which at standard conditions ( $T = 298.15\text{ K}$ ,  $p = 1.013\text{ bar}$ ) can be calculated using the standard enthalpies of formation  $\Delta H_F^0$  of the products  $P$  and the Educts  $E$  as:

$$\Delta H_R^0 = \sum \nu_P \Delta H_{F,P}^0 - \sum \nu_E \Delta H_{F,E}^0 \quad (1)$$

Where  $\Delta H_R^0$  indicates if a reaction is exothermic ( $< 0$ ) or endothermic ( $> 0$ ). Endothermic reactions depend on external heat supply at isothermal conditions, while exothermic reactions release heat to their surrounding. In addition to the knowledge about the thermal characteristics of a reaction, a quantity is needed to judge if a reaction is likely to occur. The standard Gibbs free energy of reaction is, consequently, the quantity of interest. Congruent to the enthalpy of reaction, negative values ( $< 0$ ) correspond to exergonic (spontaneous) reactions and positive values ( $> 0$ ) to endergonic (non-spontaneous) reactions. Its standard form can be calculated analogously to the standard enthalpy of reaction as:

$$\Delta G_R^0 = \sum \nu_P \Delta G_{F,P}^0 - \sum \nu_E \Delta G_{F,E}^0 \quad (2)$$

The connection between the standard Gibbs free energy, the standard enthalpy of reaction and the standard entropy of reaction can be described using the Gibbs-Helmholtz equation.

$$\Delta G_R^0 = \Delta H_R^0 - T * \Delta S_R^0 \quad (3)$$

In this equation, a new extensive variable of state, the standard entropy of reaction, is used. It can be calculated as the difference between the entropy of product and educts:

$$\Delta S_R^0 = \sum \nu_P \Delta S_{F,P}^0 - \sum \nu_E \Delta S_{F,E}^0 \quad (4)$$

For the prediction of the change in entropy during a reaction, rules of thumb can be applied. Reactions, where the number of particles increase, result in an increase in entropy and vice versa. Phase transitions from solid to liquid to gaseous as well as hydration reactions are also increasing the system's entropy. As both, the standard entropy of reaction as well as the standard enthalpy of reaction, are known, also the standard Gibbs free energy of reaction can be calculated. Finally, a connection between the equilibrium constant and the standard Gibbs free energy of reaction can be derived as:

$$\Delta G_R^0 = -R * T * \ln (K_{298}) \quad (5)$$

The equilibrium constant, here noted at standard conditions, describes the, at reaction equilibrium, constant ratio of product to reactant concentration. Looking at the  $K_{298}$  and the  $\Delta G_R^0$  of a reaction, predictions about the reaction process can be done. A very low  $\Delta G_R^0$  ( $-60 \text{ kJ/mol}$ ) and, consequently, a very high  $K_{298}$  ( $> 10^{10}$ ), indicate processes, in which reactants will react completely. With increasing  $\Delta G_R^0$  and decreasing  $K_{298}$ , the share of products is decreasing. This trend continues until a reaction will not occur at all.

In addition to the behavior of the reaction at standard conditions, the influence of temperature and pressure are of interest. Herefore, Equation (5) can be combined with Equation (3) to obtain the *Van't Hoff* equation:

$$-\ln(K_{298}) = \frac{\Delta H_R^0}{R * T_{298}} - \frac{\Delta S_R^0}{R} \quad (6)$$

If the equilibrium constant at a reference point (e.g. standard conditions) is known, the equilibrium constant at any other temperature can be calculated. Therefore, a combination of the *Van't Hoff* equation, formulated at both temperatures, is used. In these temperature ranges, the assumption of temperature-independent  $\Delta H_R$  and  $\Delta S_R$  must be valid:

$$K_i = K_{298} * \text{Exp} \left[ \frac{\Delta H_R^0}{R} * \left( \frac{1}{T_{298}} - \frac{1}{T_i} \right) \right] \quad (7)$$

In addition to the temperature dependency, knowledge about the influence of pressure on a reaction is beneficial for process development. Therefore, an exemplary chemical reaction shall be defined as:





Noting the law of mass action as a function of the partial pressures as

$$K_p = \frac{p_C}{p_A^2 * p_B} \quad (9)$$

and by applying *Dalton's law*

$$p_i = x_i * p_{tot} \quad (10)$$

one can derive

$$K_p = \frac{x_C}{x_A^2 * x_B} * (p_{tot})^{-2}. \quad (11)$$

The molar ratio of products to educts according to Equation (11) for a reaction at a certain temperature at equilibrium is constant and has a characteristic value (depending on the exact reaction). Accordingly, the influence of the total pressure, as well as the changes in concentration, can be evaluated. Increasing the total pressure in Equation (11) results in a shift of the reaction to form more product C, since  $K_p$  must be constant. Equation (11) can furthermore be used to demonstrate the effect of adding or withdrawing components. The addition of reactants results in the formation of more products and vice-versa.

## 2.2 Reaction kinetics

In addition to the thermodynamics of a process, rate laws are needed for the design of reactors. Rate equations describe the rate of disappearance of a component over time (and therefore also the formation of products over time), which for a simple irreversible reaction  $aA + bB \rightarrow cC$  can be noted as:

$$-r_A = -\frac{1}{V} * \frac{dN_A}{dt} \text{ which can be rewritten as } -r_A = -\frac{dc_A}{dt} \text{ for } V = \text{const.} \quad (12)$$

The function which describes the change in concentration can usually not be predicted from the concentration and must be determined experimentally. For an irreversible reaction where two components, (A and B), react to a third component, (C), a power law can be noted as:

$$-r_A = k * c_A^i * c_B^j \quad (13)$$

The sum of the exponents can be noted as the reaction order  $n$ , while  $k$  is the so-called reaction rate constant. By evaluating experimental data with different methods [9], the reaction order  $n$  as well as the reaction rate constants  $k$ , and the corresponding rate law can be found. The temperature dependency of  $k$  can be described by the Arrhenius equation as

$$k = A * \text{Exp} \left[ -\frac{E_A}{R * T} \right], \quad (14)$$

where  $A$  is the pre-exponential factor,  $R$  the universal gas constant ( $8314 \text{ J}/(\text{kmol} * \text{K})$ ),  $T$  the absolute Temperature and  $E_A$  the activation energy.

### 2.3 Ideal isothermal reactors

The design of ideal reactors can be derived from general material balances. Therefore, entering streams, exiting streams as well as the conversion of the considered species and the accumulation in the system are considered.

$$F_{A,0} = F_{A,out} + \int_0^V -r_A * dV + \frac{dN_A}{dt} \quad (15)$$

Since the design of reactors must take the equilibrium of a reaction into account, the relative conversion  $X_A$  is introduced for better comparability.  $X_A$  describes the relative amount of reactant  $A$  which has been reacted to products at a specific time:

$$X_A = \frac{N_{A,0} - N_A}{N_{A,0}} \quad (16)$$

By solving the balances, the design equations for the basic reactor types can be derived as described in *Table 1*. The discontinuous stirred tank reactor (DSTR) is the simplest type of reactor. It is operated batch-wise, resulting in a decrease of initial concentration over time, while the concentration in the reactor at a certain time is constant over space (Ideal mixing). The continuous stirred tank reactor (CSTR) is equipped with an entering feed stream as well as an exiting product stream. Hence, the concentration profile over time, as well as the spatial concentration, are constant. Another basic reactor concept is the (tubular) plug flow reactor (PFR). Analogous to the CSTR, a feed stream enters and a product stream leaves the reactor, without any type of product accumulation. Just when the reactants enter the reactor, the

reaction begins, leading to a decrease of reactant concentration in the axial direction. Ideal mixing is assumed in the radial direction, leading to constant concentration over the reactor's cross-section.

**Table 1:** Design equations of ideal isothermal reactors

Reactor type	Design equation
DSTR	$t = N_{A,0} \int_0^{X_A} \frac{dX_A}{-r_A * V} \quad (17)$
CSTR	$V = \frac{X_A * F_{A,0}}{-r_A} \quad (18)$
PFR	$V = F_{A,0} * \int_0^{X_A} \frac{dX_A}{-r_A} \quad (19)$

In practice, only quasi isothermal reactors can be achieved in constructively complicated and therefore expensive reactors [6, 10, 11]. Additional terms can be added to the design equations to account for volume-, pressure- or temperature-changes during a reaction [9]. Furthermore, the design equations, as well as the rate laws, have to be modified for catalytic reactions. For solid catalyzed reactions, formulations which consider the catalyst mass or surface area are more suited than the volume-dependent formulations.

## 2.4 Catalysis

Catalysts are used in a large variety of industrial processes, allowing economic production of many different products. To shortly describe the working principle of catalysts, a simple exothermic reversible reaction is introduced:



Thermodynamics allows the determination of the reaction equilibrium of such a reaction and its feasibility of occurrence. However, statements about the velocity of a reaction cannot be derived therefrom. The difference in enthalpy of formation between the product and reactants does not take into account, that certain energy can be required to break and rebuild bounds. This energy can be described by the energy of activation  $E_A$ . The Arrhenius Equation (14) links the reaction rate constant  $k$  with the activation energy. Therefore, large  $E_A$  result in lower  $k$

and accordingly lower reaction rates. Additionally, high temperatures lead to higher  $k$  and as a consequence faster reaction rates.

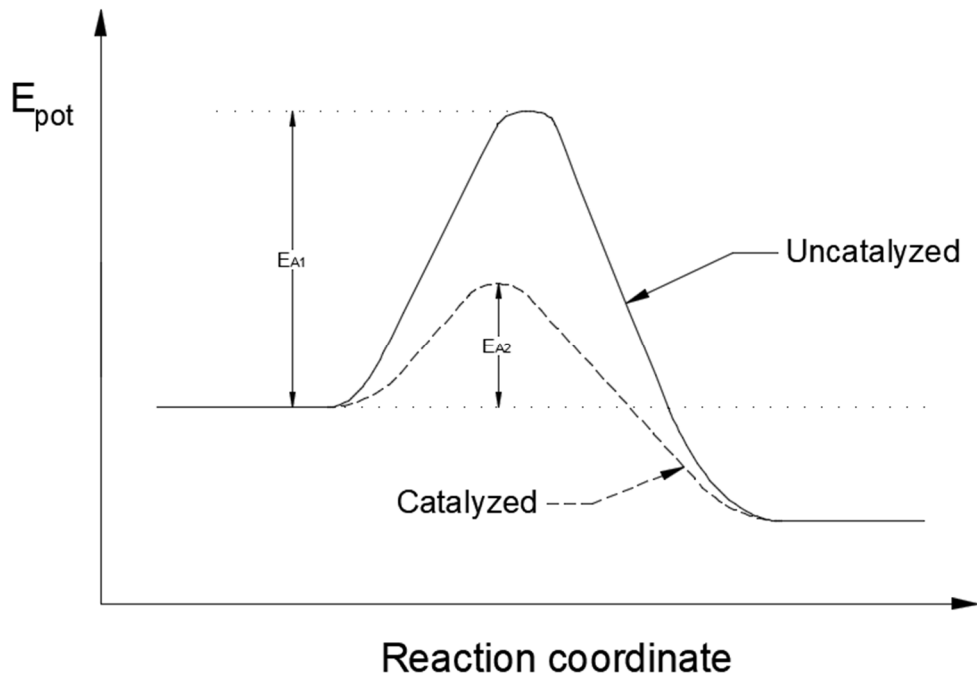


**Figure 1:** Energy levels of a catalyzed and an uncatalyzed exothermic reaction (schematically)

Figure 1 shows the impact of a catalyst on the activation energy of a reaction schematically. Catalysts can have an impact on the reaction rates and therefore on the velocity by which the equilibrium of a reaction can be achieved, while (theoretically) not being affected by the reaction itself. Depending on the parameters and conditions of a reaction homogeneous-, bio- or heterogenous-catalysis is possible. As the main focus of this work lies in the production of methanol, the concepts of heterogenous catalysis shall be discussed in more detail, since it is the common type of catalysis in methanol production [6].

#### 2.4.1 Heterogeneous catalysis

As mentioned before, the most common combination of phases in heterogeneous catalysis is the combination of a fluid phase, containing reactants, with a solid catalyst [6, 12–14]. These catalysts provide a new path for the reaction mechanisms since reactions do not have to occur in the gas-phase only anymore. As visible in Figure 2 different energy levels, corresponding to intermediate products or reaction steps, occur as a consequence of the interaction of fluid phase and the catalyst surface.

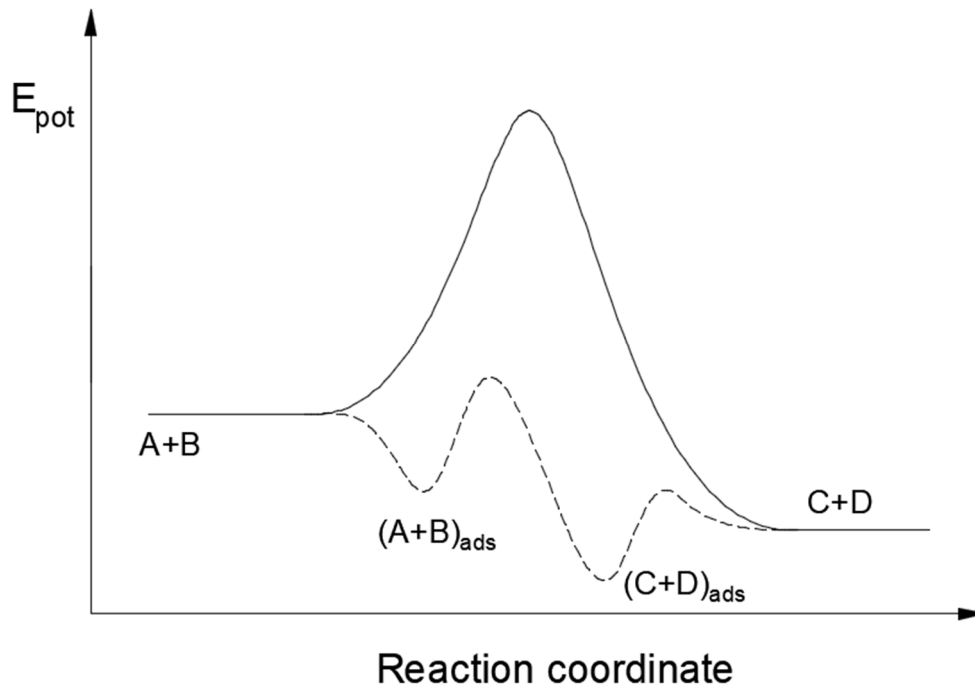


**Figure 2:** Energy levels of the uncatalyzed reaction as well as a catalyzed path, where the reactants react on the catalyst surface

For the evaluation of the overall reaction, the principle of the rate-determining step is introduced. Since for most heterogeneous catalytic reactions, mass transfer and reaction do occur in series, the overall reaction rate is determined by the slowest step. *Figure 3* shows all steps, occurring on/in a porous catalyst:

1. Transport of reactants from the bulk phase to the geometric surface through convection
2. Diffusion of reactants to the active sites
3. Adsorption to active sites
4. The chemical reaction
5. Desorption of products
6. Diffusion from the active sites
7. Transport of reactants from the geometric surface through convection to the bulk phase

In practice, the rate of each step must be evaluated and compared to determine which one is the slowest. Mass transfer limitations can be minimized either by increasing the volumetric flow rate or, if a maximum is reached, by downsizing the catalyst particles. For the investigation of ad- or desorption, ad- and desorption rates are formulated as functions of the partial pressures. Regarding the surface reaction, different surface reactions may occur:

- An adsorbed reactant reacts directly at the active site
- An adsorbed reactant needs a second active spot for conversion
- Two adsorbed reactants react at an active site (Langmuir-Hinshelwood mechanism [10])
- An adsorbed reactant reacts with a gaseous reactant (Eley-Rideal mechanism [10])

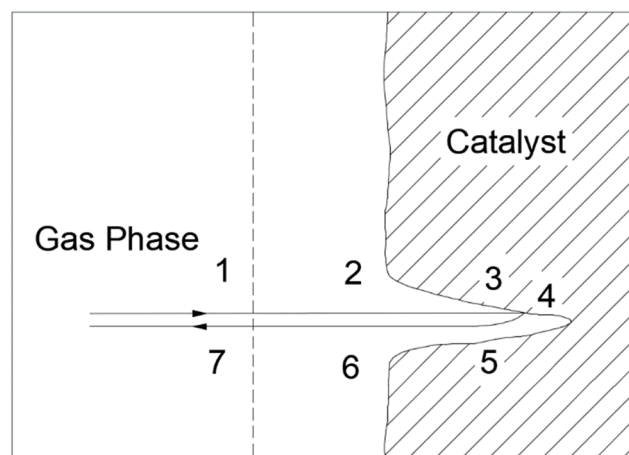


**Figure 3:** Schematic representation of the reaction steps during a heterogeneously catalyzed reaction

In addition to the determination of the rate-determining step, investigations about the heat and mass transfer are necessary. For exothermic reactions, heat must be conducted to the particle surface and expelled to the fluid stream. If this is not possible, adiabatic acceleration, and as a consequence, catalyst aging, may occur. The removal of heat from the inside of particles becomes a very important factor during upscaling from lab tested catalysts to the ones used in industrial applications. Compared to catalysts used in lab-scale applications larger pellets are used instead of small particles [10].

As proposed by the idea of active sites as the place of a reaction to occur, a large surface of the catalyst is very important. The active sites, respectively active species, are most commonly metals, oxides, and sulfides. A high surface area of the active species can be achieved by dispersing the finest particles on a support species. They hinder the dispersed phase from coalescing, which is particularly important at temperatures, at which a species is immobilized and tends to sinter [15]. In addition to the immobilization of active species, support species should have a relatively high surface area and large pores. This assures that active sites are

accessible by the reactants. Additionally, the pore size of support material can be used to maximize a catalyst's selectivity. The most common support species are metal oxides or active carbon which makes them, in most cases, more affordable than catalysts consisting out of pure active components. Combined catalysts can be further improved by the addition of promoters. Their application can lead to a wide variety of different effects [12]. The preparation of supported catalysts relies on different approaches. Either can an existing support structure be impregnated with an active species containing solution, or the active species are introduced on the support species by a (co-)precipitation [12].

The properties of a catalyst are therefore not only functions of their composition but depend strongly on their structure. Accessibility and dispersion of the active species; as well as a large surface area, depend strongly on the catalyst preparation. Small deviations in procedures or preparation conditions can lead to significant differences in structure and local compositions, resulting in different catalyst performances. Additionally, catalysts must endure the reaction conditions as well as unfavorable presence of disturbing species for a long time for them to be suitable for industrial applications. Reasons for catalyst deactivation can be aging (caused by high temperature sintering), fouling (blockage of active sites) or poisoning. For the comparison of catalysts, knowledge about reaction conditions is required. The performance of a catalyst is often described in different quantities. In addition to the conversion of reactants at operating conditions, the selectivity of a catalyst for a certain product is of interest. The selectivity hereby describes the share of limiting reactants, which have converted into the desired products in case of the occurrence of concurrence reactions.

$$s = \frac{n_{P,out}/v_P}{(n_{A,0} - n_{A,out})/|v_A|} * 100 \text{ [mol\%]} \quad (21)$$

For the definition of the operating conditions, temperature and pressure, as well as knowledge about the feed stream is required. Hence, the volumetric flow rates, as well as the molar feed compositions, are needed. The activity of a catalyst can be described by the rate of reaction or the turn-over frequency (TOF). As these parameters are often complicated to determine or difficult to compare for different catalysts, simpler approaches are used in practice [6, 10, 16]:

- Conversion at constant reaction conditions
- Space velocity for a certain conversion
- Space-time yield

- Temperature and time to reach a certain conversion

The catalyst mass can be linked to the feed stream via a space-time velocity ( $v_{space}$ ). Additionally, the gas hourly space velocity ( $GHSV$ ) is often used to link the feed stream to the used catalyst volume.

$$v_{space} = \frac{\dot{V}_{feed}}{m_{cat}} \quad (22)$$

$$GHSV = \frac{\dot{V}_{feed}}{V_{cat}} \quad (23)$$

The space-time yield ( $STY$ ) connects the amount of formed products to the catalyst volume.

$$STY = \frac{\dot{n}_p}{V_{cat}} \quad (24)$$

For the development and optimization of new catalysts, a considerable amount of experiments has to be performed. Additional to a long time to market (which expands over several years/decades [10]) comes the financial risk of failure. Nevertheless, a lot of different research on new or existing catalysts is performed. Such research aims either on optimizing catalysts for existing processes or to develop catalysts, needed for an economic large-scale implementation of promising processes, such as the methanol synthesis from carbon dioxide.



## 3 Methanol synthesis

With a world production of over 90 million tons, methanol is one of the most important single feedstocks for a large variety of chemicals and alternative fuels. Regarding its use as a feedstock for chemical synthesis, formaldehyde and methanol-to-olefins (MTO) production are the largest methanol consumer, as both combined require almost half of the world's methanol production. Formaldehyde is often used in the production of polymers, as well as for paints or in pharmaceutical applications. MTO processes can be used for the synthesis of polyethylene as well as propylene, which are the largest volume chemicals [6]. Other large consumers which use methanol as a feedstock for chemicals are the production of methyl tertiary-butyl ether (MTBE) and acetic acid. MTBE is mostly used as a fuel additive for the optimization of their knock resistance, while acetic acid finds its use as a preservative in the food industry and as a feedstock for further synthesis. In addition to these products, other intermediates produced from methanol such as, for example, methyl chlorides, are visualized in *Figure 4*. As mentioned before, methanol is not only suitable as a feedstock for chemicals or fuels, but can also be used directly as a fuel. Here, the sector with the biggest annual growth over the past years is the production of biodiesel [17]. Gas turbines have been tested successfully to run on methanol, which allows to provide electricity in remote regions as well as the use of methanol as a marine fuel [18].

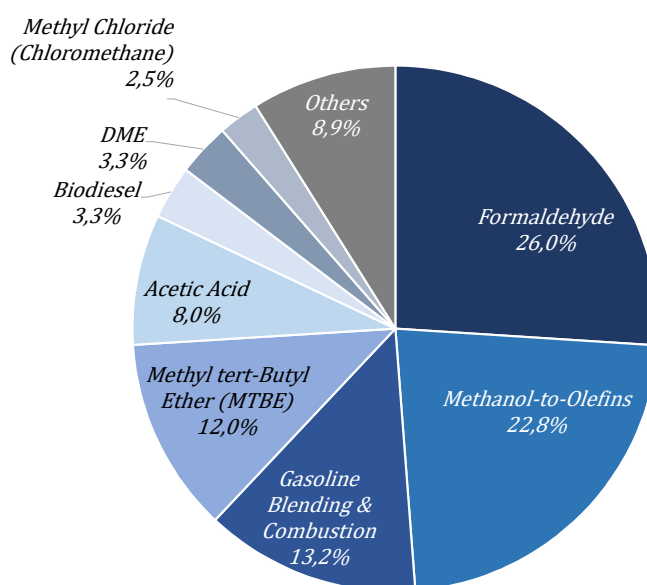


**Figure 4:** An overview of the world's main consumers of methanol in the year 2018 [27]

For the synthesis of methanol, a variety of different approaches have been investigated, although most of them are of no industrial relevance. Some of them are listed below:

- Oxidation of methane
- Pyrolysis of methane and hydrogenation of  $CO_2$
- The capture and hydrogenation of  $CO_2$
- Enzymatically from methane
- From synthesis gas (syngas), generated by hydrolysis of biomass as feedstock
- From syngas, generated from fossil fuels

Due to the fact that the, in this work followed, approach of the hydrogenation of  $CO_2$  has not been implemented in an industrial scale (yet), the state-of-the-art methanol production will be discussed first.

### 3.1 Methanol from syngas

Today, the dominating process for methanol production is its catalytic synthesis from syngas at pressures between 50 – 100 *bar* and temperatures near 250 °C [6, 10, 16]. Therefore, three steps have to be performed:

- The generation of synthesis gas
- The synthesis of methanol
- The purification of the crude methanol

#### 3.1.1 Syngas preparation

For the generation of syngas, a broad variety of feedstocks can be used, ranging from classic fossil fuels such as natural gas or crude oil to organic matter [4]. Depending on the available feedstock, either natural gas or gasification of coal (most commonly in South Africa and the People's Republic of China [11, 19, 20]) are used. The availability of a cheap feedstock has a huge impact on the overall production cost. Furthermore, the selection of the right reforming technology is of utter importance, since typically 60% of the investment must be made for syngas preparation and compression [11]. Four different reformer processes are common:

- Steam reforming STR
- Two-step reforming
- Autothermal reforming ATR

- Partial oxidation POX

All of them have the purpose to convert the gaseous feedstock into hydrogen and carbon oxides. For catalytic steam reforming, catalyst poisons such as sulphur have to be removed from the feed stream [20]. Steam is then added, the mixture heated to about 600 °C and fed to a reactor. The reactor hereby consists out of up to 1000, with *Ni*-catalyst filled tubes for the through passing stream, which are heated on their outside. Here, different burner arrangements are possible. If methane is used as a feed gas, conversions of 85 to 90 % can be reached. Regarding the produced syngas properties, a so-called module *M* is introduced:

$$M = \frac{n_{H_2} - n_{CO_2}}{n_{CO} + n_{CO_2}} \quad (25)$$

Under ideal conditions module *M* should be equal to 2 [6, 11] for methanol synthesis. The product stream of a steam reformer with natural gas as feed stream leads to  $M \cong 2.8 - 3.0$ , which implies that the process can benefit from adding  $CO_2$ . Another way to shift *M* towards the desired value of two is the extension of conventional steam reforming to a two-step reformer. Hereby, steam reforming is used to partially reform the feed stream, while in a second step the residual feed is reformed by combusting oxygen, similar to an ATR. In reformers that use oxygen, module values lower 2 are usually achieved [6, 11]. The combination of the steam and oxygen-reformers allows the manipulation of the overall module *M* to the desired value while being able to provide large quantities of syngas [11]. The autothermal reformer (ATR) combines partial oxidation with a steam reformer in one compact unit. Therefore, steam is added to the feed stream which enters the reactor from its top. Here, the stream is mixed with oxygen and partial oxidation occurs. In the following catalyst bed, steam reforming takes place and the equilibria are reached. Syngas from ATR has often a module under two, which can be shifted by adding  $H_2$  or by removing  $CO_2$ . POX allows the generation of syngas from heavy refinery residues and other liquid and/or solid containing low-value organic matter. In case of the availability of cheap oxygen, POX can be used for generating value from residuals [6]. A more detailed investigation of the catalysts, reactors, and processes, used in the reforming of natural gas, has been performed by *Aasberg-Petersen et al* [5].

According to *Air liquide* [19], conventional steam reforming is suited to supply small and medium methanol plants with a capacity of 3000 t/d. Two-step reforming is suited for plants with capacities between 2500 and 7000 t/d while being the most economically reforming

technology in this range. For higher capacities, ATR is considered as the most suitable reforming process if light natural gas is available.

### 3.1.2 Reactor systems

On an industrial scale, the synthesis of methanol from syngas is performed in solid catalyst-containing reactors. Commercial catalysts, applied in low- pressure methanol synthesis, use copper as their active compound and varying compositions of zinc and aluminum phases as support [6]. Other approaches, based on noble metals such as Pd were never considered for industrial applications because of their, compared to copper catalysts, high costs. In the catalyst containing reactors, the water gas shift reaction (WGS) (Equation (26)) as well as the hydrogenation of  $CO$  and  $CO_2$  to  $CH_3OH$  (Equation (27) and (28)) take place.



Since the synthesis reaction of methanol from syngas is an exothermic process, a main focus of the reactor development lies in the removal of excess heat and temperature control. All industrial processes are based on (variations of) a few different reactor principles:

- Adiabatic reactors (as quench reactors or in series)
- Boiling water reactors (BWR)
- Gas-cooled reactors (GCR)

Adiabatic reactors are either built as one reactor, containing several catalyst beds, or as a series of adiabatic reactors. In the first case, up to five layers of catalyst are mounted in one reactor, while several (cold) feed streams are entering between the catalyst stages. This setup is no longer state of the art [11]. The usage of adiabatic reactors is implemented in serial arrangement of two to four reactors. Between the different stages, indirect cooling takes place. The excess heat is often used for the pre-heating of saturator water or the generation of medium pressure steam [6]. Cascades of adiabatic reactors with intermediate cooling can (theoretically) be upscaled as single line arrangement of more than 10000  $t/d$ . [6, 11]

Even better temperature control resulting in (quasi) isothermal conditions can be achieved in boiling water reactors. BWR use the principle of cooling with a liquid at its boiling point. The syngas feed stream is entering the reactor from above, from which it flows through several catalyst-filled pipes downwards, where it exits the reactor. Around the catalyst containing pipes, boiling water is circulated in a shell. The temperature of the boiling water can be influenced by the pressure in the cooling system, allowing nearly isothermal conditions. Since reaction temperatures of about 250 °C are usual, medium pressure steam is generated, which can be used in other process parts. BWR are limited in size, because of their relatively complicated and therefore expensive design. Temperature profiles in a series of fixed bed reactors and in a BWR can be seen in *Figure 5*.

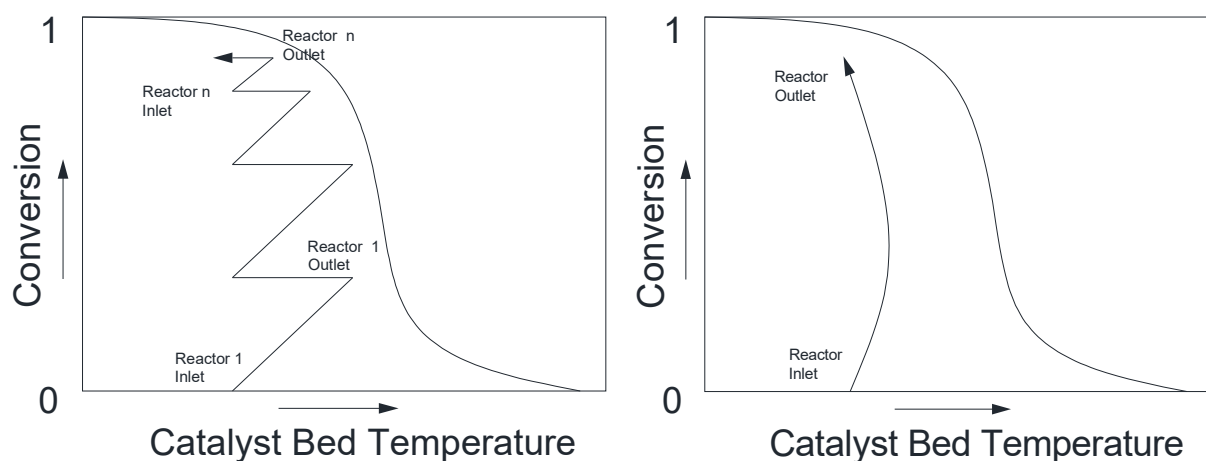


**Figure 5:** Schematic representation of conversion profiles to reach a certain conversion for a series of fixed bed reactors with intermediate cooling (left) and a single tubular boiling water reactor (right) in which the S-shaped curve represents a symbolic equilibrium conversion

Gas-cooled reactors are similar to a BWR in their construction but obviously vary in their cooling media. The usage of gases instead of boiling water leads to minor cooling capabilities but significant cost reductions. Additionally, the cooling media is here present on the tube side, while the feed and product gases are present on the shell side.

The different reactor types are often combined in practice, either by the external serial arrangement or by the inclusion of different reactor principles in one unit. Adiabatic reactors can be used to bring the feed stream on the desired reaction temperature, before entering a BWR. The integration of such an adiabatic top layer section in a BWR leads to a reduced total catalyst volume and a decrease in synthesis costs of 15 – 25 % while increasing the reactor's capacity of up to 20 % [11]. *Air Liquide* uses a combination of a BWR and a GCR to minimize the size of the expansive BWR in its *Lurgi MegaMethanol™* process. Therefore, the GCR is

used to preheat the syngas feed stream before entering the BWR. The very reactive feed gas is partially converted into the quasi isothermal BWR. In the following GCR, another reaction step takes place, while the temperature of the through flowing gas is constantly decreased, which favors the formation of methanol [6]. Today, a lot of different suppliers and therefore also processes, as well as reactor combinations, are available on the market. Some of them do only provide (parts of) process solutions and licensing (which includes the syngas preparation, as well as the methanol purification), while other manufacturers, such as *Haldor Topsøe* [6, 11] do their own catalyst development as well.

Apart from the separation of the liquid product from the gas stream, an effort has to be done in the following purification steps to remove water and other byproducts. The therefore needed number of distillation columns depends on the desired methanol grade (fuel grade or AA grade) [11, 19]. A more sophisticated and detailed overview of many processes such as the *Lurgi MegaMethanol™*, the *Haldor Topsoe-* or one of *Casales-* processes can be found in literature [6, 11, 19, 21].

### 3.2 Methanol from $CO_2$

The direct hydrogenation of  $CO_2$  to methanol seems to be a promising way to encounter two main problems of modern society: the search for an alternative to the limited availability of fossil fuels and the necessity to minimize  $CO_2$  emissions to stop global warming.

A basic requirement for the switch in a  $CO_2$  based industry is the availability of cheap  $H_2$  and  $CO_2$ . Capturing  $CO_2$  from flue gas streams is necessary for the production of “green” methanol. The  $CO_2$ , available on today’s market, is mostly a byproduct of industrial processes such as hydrogen production from natural gas steam reforming [22]. There are three different approaches available for carbon capture: pre-, oxyfuel- and post-combustion. These strategies differ in their complexity, necessary unit operations, the composition of their output streams, the used capture technology, and many more. Possible capture technologies are Absorption, adsorption, membranes and cryogenic technics among others [2].

Considering the largest emitters of  $CO_2$ , visualized in *Figure 6*, the huge potential in the energy sector seems obvious. Here, post-combustion technology can be applied, since it is retrofittable in existing power plants. Studies have shown, that the integration of a post-combustion unit in a new powerplant will increase the electricity cost up to 85 % [2]. As mentioned before, large quantities of  $H_2$  are these days provided by steam reforming of natural

gas. To avoid the usage of fossils, alternatives such as water electrolysis using renewable electricity sources or reforming of biogas must be promoted [23].

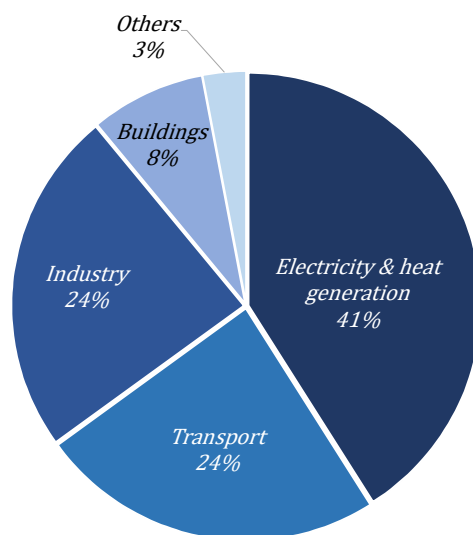


**Figure 6:** Overview of the global  $CO_2$  emissions from fuel combustion in the year 2017, sorted by sector [21]

The first research in the hydrogenation of  $CO_2$  has been conducted in the 1960s [20]. Scientists concluded that small amounts of  $CO_2$  are beneficial for the conventional methanol synthesis from  $CO$  and  $H_2$  on conventional  $Cu/ZnO/Al_2O_3$  catalysts. Since then, many different catalysts, reactor concepts, and feed compositions have been investigated.

### 3.2.1 Hydrogenation of $CO_2$

The thermodynamic stability and inertness of  $CO_2$  ( $\Delta G_F^0 = -394.38 \text{ kJ/mol}$ ) make it very difficult to activate. In addition to the unfavorable activatability, kinetic limitations result in the need for well-suited catalysts. The hydrogenation of  $CO_2$  can not be described as a stand-alone reaction. The presence of the RWGS (Reversed watergas shift reaction) must be taken into account. The hydrogenation of carbon dioxide, as well as the hydrogenation of carbon monoxide, are exothermic reactions (see equation (27) and (28)), which are promoted by lower temperatures. Low temperatures are also favorable to prevent the formation of unwanted water, produced by the RWGS reaction. Its endothermic character (described by the reverse reaction of Equation (26)), recognizable by the positive enthalpy of reaction  $\Delta H_R$ , results in a shift of the equilibrium composition to the, in this case undesired, product side. Nevertheless, a minimum temperature is required to overcome the  $CO_2$ 's inactivity. Furthermore, Equation (27) and (28) show a decrease in volume, due to the changing number of moles on the reactant and on the product side. Therefore, increasing pressure is favorable for the equilibrium

of these reactions, or the yield maximization of the desired product methanol. The need for temperature and pressure variation results in the thermodynamic equilibrium of the hydrogenation of  $CO_2$ , which is rather unfavorable, and the inertness of  $CO_2$ . The link between equilibrium conversion and temperature and pressure can be seen in *Figure 7*.

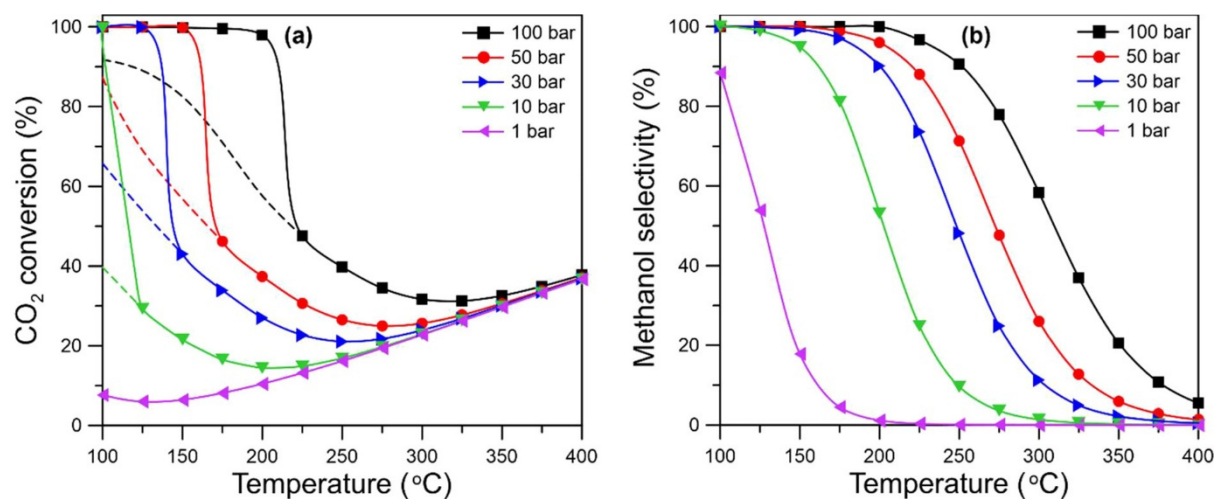


**Figure 7:** Conversion of  $CO_2$  and selectivity for  $CH_3OH$  as functions of temperature and pressure, calculated with Aspen; Reprinted with permission from Stangeland et. al. [30]

When comparing the hydrogenation of pure  $CO_2$  with the synthesis of methanol from syngas, differences in the exothermicity and the formation of water arise. When methanol is formed from  $CO$ , more heat, compared to the hydrogenation of  $CO_2$ , is generated. The heat leads to a drastic increase in temperature, ending in the need of BWR for adequate temperature control (see chapter 3.1.2). Furthermore, the exothermicity of  $CO$  hydrogenation can lead to hotspots which lead to catalyst sintering and/or the formation of other byproducts, therefore minimizing the selectivity of the catalyst. The hydrogenation of  $CO_2$  (exothermic), as well as the occurring RWGS (endothermic), results in less heat which needs to be expelled. This allows the usage of simpler and cheaper tube-cooled reactors. Lower temperatures due to the absence of hotspots in direct  $CO_2$  hydrogenation result in less formation of byproducts such as ethanol or other hydrocarbons [24]. A disadvantage of direct methanol formation from  $CO_2$  arises when considering the amount of formed water [25]. As water is a strong oxidant at elevated temperature, oxidation of the active zero valent form of metal and therefore deactivation of catalysts is favored by its presence [26].

Regarding the reaction mechanism, different approaches are known today. For the hydrogenation of  $CO_2$  on a  $Cu/ZnO$  catalyst, two mechanisms are mostly accepted:



- A RWGS & CO hydrogenation pathway
- A formate pathway

The RWGS pathway assumes a formation reaction of CO, which then is hydrogenated via formyl and formaldehyde intermediates to methanol. The formate pathway includes several intermediate products as visible in Figure 8. At this point, literature is discussing if dioxomethylene ( $H_2COO$ ) or hydroxycarboxyl ( $HCOOH$ ) is forming from formate [27, 28]. Regarding the dominating pathway, it has been shown, that the conversion of  $CO_2$  via the formate way [29] is the dominating one. This stands in contradiction to one's expectation since the RWGS is faster than the formation of methanol over the formate pathway. The explanation for this behavior is expected to route in the influence of the  $CO_2$  presence. Too much  $CO_2$  results in a decrease in the reaction rate of syngas [6] (caused by the negative influence of forming water).

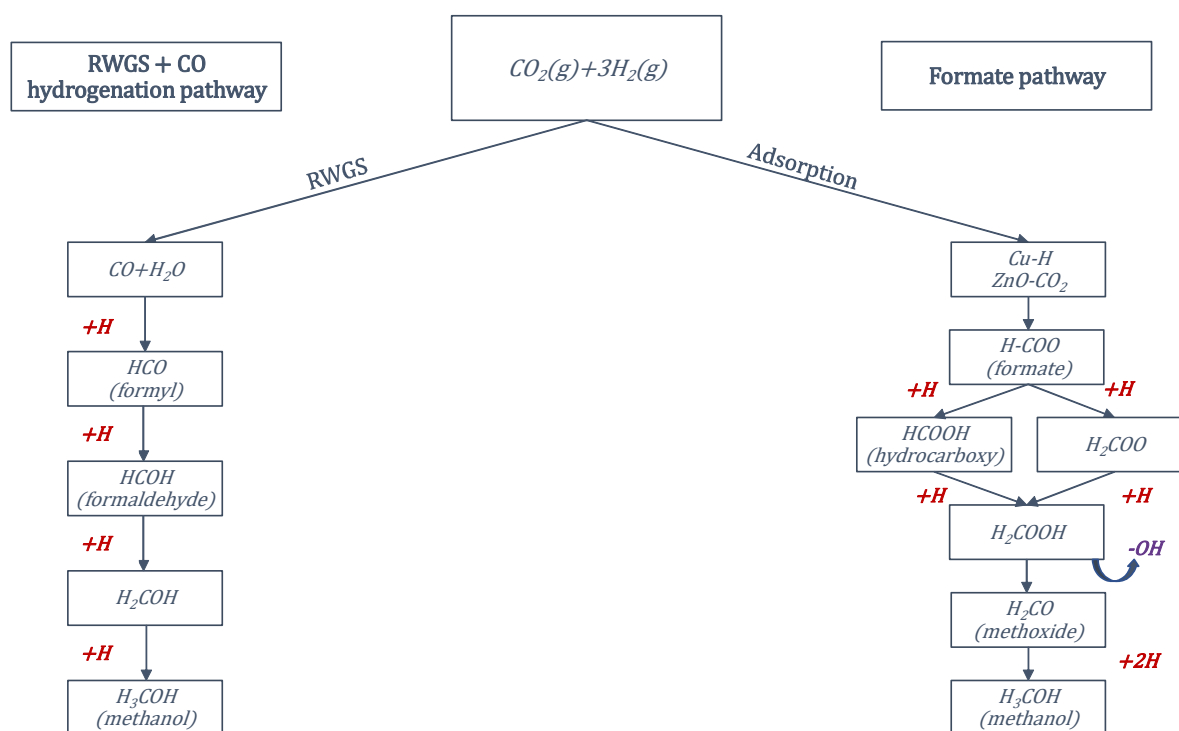


**Figure 8:** Two possible pathways for the hydrogenation of  $CO_2$  to methanol, adapted from [16]

### 3.2.2 Current research

The development of suitable catalysts for the hydrogenation of  $CO_2$  has been a growing field of research ever since but is especially growing in the last ten years (see Figure 9). Because of the similarities with classic syngas hydrogenation, their catalysts have been the basis for  $CO_2$  hydrogenation. Adapted/optimized catalysts must be more resistant to the influence of

water such as oxidation or blocking of unsaturated sites, leading to highly active catalysts with a long life span [6]. While first efforts were mainly focused on the improvement of existing *Cu*-based catalysts, already used in the hydrogenation of syngas, other aspects are now of interest as well. New supports, promoters, and other active species than copper are tested. Additionally, the influence of catalyst preparation and activation is of interest. Furthermore, alternatives in the existing reactor- and process-concepts, the catalyst systems as well as reaction conditions and feed compositions are investigated.

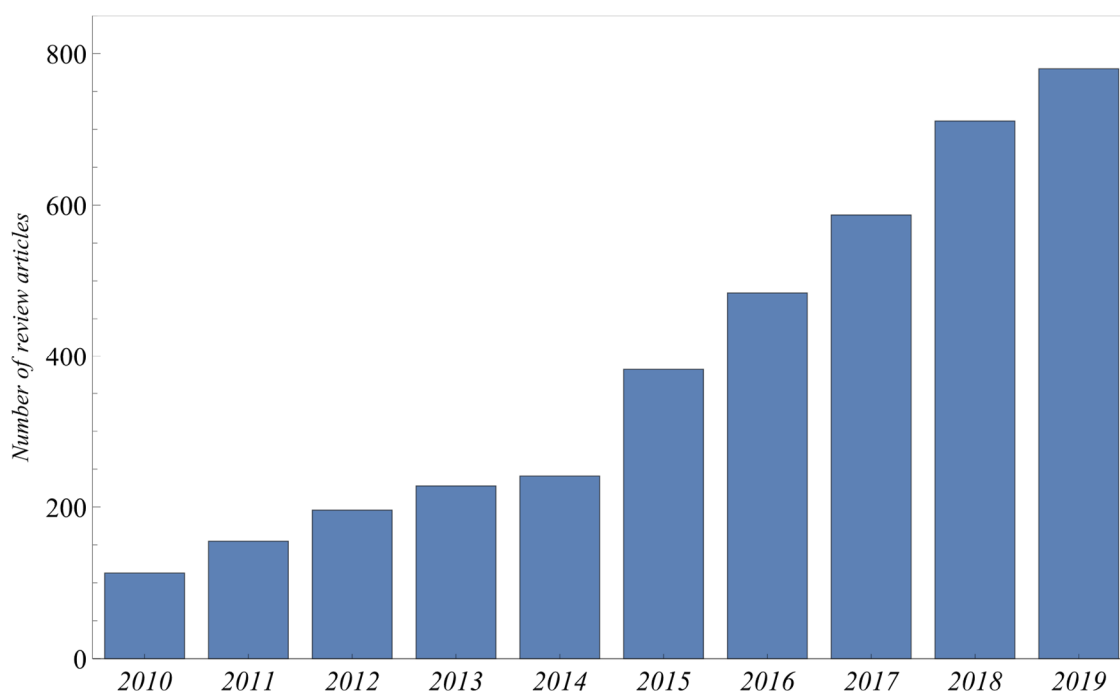


**Figure 9:** Number of review articles listed on ScienceDirect containing all of the following keywords over the years 2010 to 2019:  $CO_2$ , methanol, hydrogenation, catalyst

### 3.2.2.1 Catalyst research

Classic  $Cu/ZnO/Al_2O_3$  catalysts, respectively modified versions, are still the main focus of  $CO_2$  hydrogenation research. The presence of  $ZnO$  is assumed to be beneficial in the dispersion of the  $Cu$  particles and additionally promotes the adsorption of  $CO_2$ .  $Al_2O_3$  is used to further improve the thermal- as well as the pressure-stability and promote dispersion of the active copper sites [30]. For the addition of promoters to the mentioned catalyst, two different approaches have been studied:

- The modification of the  $Cu$  active site with noble metals
- The addition of promoters to interact with alumina

Studies regarding the first approach resulted in increased activities when adding noble metals such as *Pt, Pd, Rh* or *Au*. At this time, this approach is considered as not justifiable because of their (comparable) high price and the unsolved question regarding the recycling of these catalysts [6, 31].

Studies on the second approach do mostly focus on zirconium *Zr*, Gallium *Ga* and fluoride *F*. Decreasing contents of *Al* in favor of *Zr* results in an increase of  $CO_2$  conversion and methanol selectivity up to a ratio of *Al:Zr* of 2.33 [32]. The addition of *Zr* is considered to be beneficial because of its effect on the formation process during precipitation, the stabilization of *Cu* and the effect of increasing the catalyst's basicity. Studies have also been performed with *Ga* or *F* instead of *Zr*. A limited addition of *Ga* can increase the methanol yield and  $CO_x$  conversion while the addition of *F* has been proven to promote  $CO_2$  adsorption [33].

Another approach to the addition of promoters to conventional *Cu/ZnO/Al<sub>2</sub>O<sub>3</sub>* catalysts is the combination of *Cu/ZnO* with other supports. A replacement of the *Al*- with a *Zr*-support leads to higher conversions, which stands in contrast to previous results [32, 34]. This implies that the combination of both species results in synergetic effects, leading to higher catalyst performance.

Research regarding the effect of alkaline earth metals as a third component in *Cu/x/Al<sub>2</sub>O<sub>3</sub>* has been carried out. Hereby the addition of *MgO* and *SrO* leads to a higher *Cu*-metallic surface area than the classic system which contains *ZnO*. While all tested alkaline earth metals lead to higher basicity than the conventional system, the one containing *MgO* shows the best result. Furthermore, at the tested conditions (20 bar and 250 °C), this catalyst shows higher activities and turnover frequency's than *Lurgi* and *HF* reference catalysts [35].

Alternative approaches to catalyze the  $CO_2$  hydrogenation have been performed as well. They range from including more exotic combinations, such as the combination of different transition metals on molybdenum carbide, noble metals on classic supports (e.g. highly selective *Au/ZnO* catalysts), to homogenous catalysis instead of heterogeneous catalysis. At this time, none of them are even close to usage in a pilot plant [6].

### 3.2.2.2 Processes, pilot plants and reactor improvements

The first (semi-)commercial pilot plant has been presented by *Lurgi* (today owned by *Air Liquide* renamed as *Air Liquide Global E&C Solutions Germany GmbH*), using a

$Cu/ZnO/Al_2O_3$  catalyst, provided by *Süd-Chemie* (today part of *Clariant*). Their process uses a combination of two reactor types. In a first adiabatic reactor (operated at 80 bar and 240 – 280 °C) mostly  $CO_2$  hydrogenation and *RWGS* reaction take place. Consequently, the following BWR (operated at 78 bar and 270 °C) and the therefore needed recycling loop can be built 80% smaller. The liquid product of this process is a mixture of 63.9 wt% methanol and water [6].

A similar approach has been implemented in the *CAMERE* process. It includes two loops, each containing a reactor and a separator. The first reactor is operated at 500 °C and 10.13 bar, strongly promoting the endothermic *RWGS* reaction and therefore minimizing the volumetric feed stream for the second loop. Additionally, unwanted water is separated and excluded from the process, which promotes the activity in the second reactor. In contrast to the *Lurgi* process, a  $Cu/ZnO/ZrO_2/Ga_2O_3$  catalyst was developed to better address the high  $CO_2$  concentrations. The combination of the *RWGS* reactor (operated at 30.4 bar and 250 °C) loop to the following methanol synthesis loop, lead to an increase in overall carbon conversion from 69 to 89%. The strongly promoted *RWGS* is increasing the need for cheap and green  $H_2$  for the process to be economically relevant [6, 36].

Other pilot plants that are known today include the *Mitsui's Process*, which uses a  $Cu/Zn/Al/Zr/Si$  catalyst, or the *CRI Iceland* demonstration plant, which uses the patented *ETL* process and aims at the production of methanol as a marine fuel from geogenic  $CO_2$  and renewable  $H_2$ . [6, 25] Additionally, *CRI* has built a second pilot plant in cooperation with *RWE POWER* and *Mitsubishi Hitachi Power Systems Europe*, which uses 1.5 t/d of captured  $CO_2$  from a lignite powerplant (Niederhaußen, Germany) and  $H_2$ , produced from renewable electricity [37]. A much larger  $CO_2$  to valuables plant with an investment volume of 90 million dollars for a capacity of 180000 t/y of methanol and liquified natural gas is expected to be commissioned at the end of 2021 in the province of Henan, China [38]. Austria's mineral oil company *OMV AG* has announced to investigate the feasibility of a 40 MW "green"  $CO_2$  to methanol pilot plant in 2018, but has not published any further information yet [39].

Regarding advances in the reactor technology, membranes have been tested to separate the forming water in-situ. *Duponts Nafion-*, as well as a *Si/Al*-membrane, showed promising results by being faster permeable by methanol and water than the feed gases, increasing a fixed-bed reactor's methanol yield by 50%. Nevertheless, it must be kept in mind that these

membranes cannot be used at optimum synthesis conditions (for the catalyst), leading to lower methanol yields than conventional reactors at optimum conditions [6].

### 3.2.2.3 Catalyst preparation techniques

Catalysts are usually prepared either by impregnation or by (co-)precipitation, followed by calcination and a reduction step [6, 12]. For coprecipitation methods, different precipitator agents are known. In a classical carbonate coprecipitation (used in the industrial preparation of  $Cu/ZnO/Al_2O_3$  catalysts), the desired composition of active-, support- and promotor-metals is achieved by dissolving their metal-nitrate-salts  $M(NO_3)_x$  in deionized water. This happens under heavy stirring. Studies have shown, that longer aging times are beneficial for the BET surface area as well as the  $CO_2$  conversion and the methanol selectivity [6]. The precipitation itself is introduced by the addition of  $Na_2CO_3$  solution, while the pH, as well as the temperature, must be controlled. Depending on the pH either nitrate or carbonate is present in the precipitate [12], while elevated temperatures can lead to a decrease in catalyst activity [6]. Residual nitrate and carbonate are removed by thoroughly washing and the following drying and calcination steps. While the (co-)precipitation is assumed to define the mesostructure of a catalyst, calcination is assumed to highly influence its nanostructure [33]. Other coprecipitation methods, which lead to more active catalysts, are known in research but aren't relevant on a commercial scale at this point.

Impregnated catalysts are prepared by adding an impregnation solution and support species. Hereby dry impregnation, as well as wet impregnation, are possible, depending on the volume of impregnation solution. Dry impregnation means that less volume of impregnation solution is used than the support pores can contain. While the amount of impregnated species can be better determined in dry impregnation, wet impregnation allows a more evenly distribution of the catalytically active species. Furthermore, wet impregnation allows (limited) control about the penetration of the active species in the support material. This allows the preparation of catalysts according to the limiting steps. If pore diffusion is limiting in a reaction, no active species is needed on the inside of the support, while catalyst presence is crucial if the reaction rate is the limiting step. Impregnation is considered to be especially suitable for catalysts with very expensive components since only a little amount of the valuable substance is needed. Impregnated catalysts have to be dried carefully, preventing out-blowing of active species due to vapor formation in the pores [6, 12].

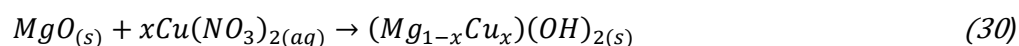
### 3.3 Catalyst of interest

As seen in chapter 3.2.2.1, many different catalyst compositions and variations for methanol synthesis are investigated in research to address the challenges of  $CO_2$  hydrogenation. The catalyst of interest, proposed in this work, uses  $Cu$  as the active species in combination with a support of  $MgO$ .  $Ni/MgO$  catalysts have shown great results in the hydrogenation of  $CO_2$  to methane, resulting in a selectivity for methane  $> 99\%$  and  $CO_2$  conversions of  $87\%$  [7, 8]. Furthermore, the addition of  $MgO$  to  $Al_2O_3$  based  $Cu$  catalyst has been proved to be beneficial (see chapter 3.2.2.1).

The preparation procedure of the new magnesia-copper catalyst is based on a wet impregnation, similar to the one proposed by *Loder et. al* [8]. Therefore, different steps are executed:

1. The calcination of the magnesia carbonate-tri hydrate in a muffle furnace
2. The impregnation of the formed  $MgO$  with  $Cu(NO_3)_2$
3. Filtration and washing
4. Drying
5. Calcination
6. Milling and sieving
7. Reduction/Activation in  $H_2$  stream

For the calcination step, a defined amount of *Sigma-Aldrich's*  $MgCO_3 \cdot 3H_2O$  (the desired molar ratio of one mole  $Cu$  to three moles  $Mg$  must be fulfilled), placed in a suitable ceramic container, is put into a muffle furnace. During the calcination step magnesium carbonate, beginning at  $400\text{ }^\circ C$  [40], is burned to magnesium oxide (a powder of white color) and carbon dioxide as described by Equation (29). The furnace therefore runs a defined temperature over time program, as shown in *Figure 10*.



The  $Cu(NO_3)_2 \cdot 3H_2O$  (*Sigma-Aldrich* 99.5% purity) is diluted with distilled water in a beaker, which results in a clear blue color (see *Figure 12*). The beaker itself is placed in a water bath, to compensate a potential change in temperature. A predefined amount of produced  $MgO$  is added stepwise, while the mixture is agitated and aged for two hours. This addition of  $MgO$

results in the formation of the catalyst precursor, described by Equation (30), which leads to a change of color to turquoise.

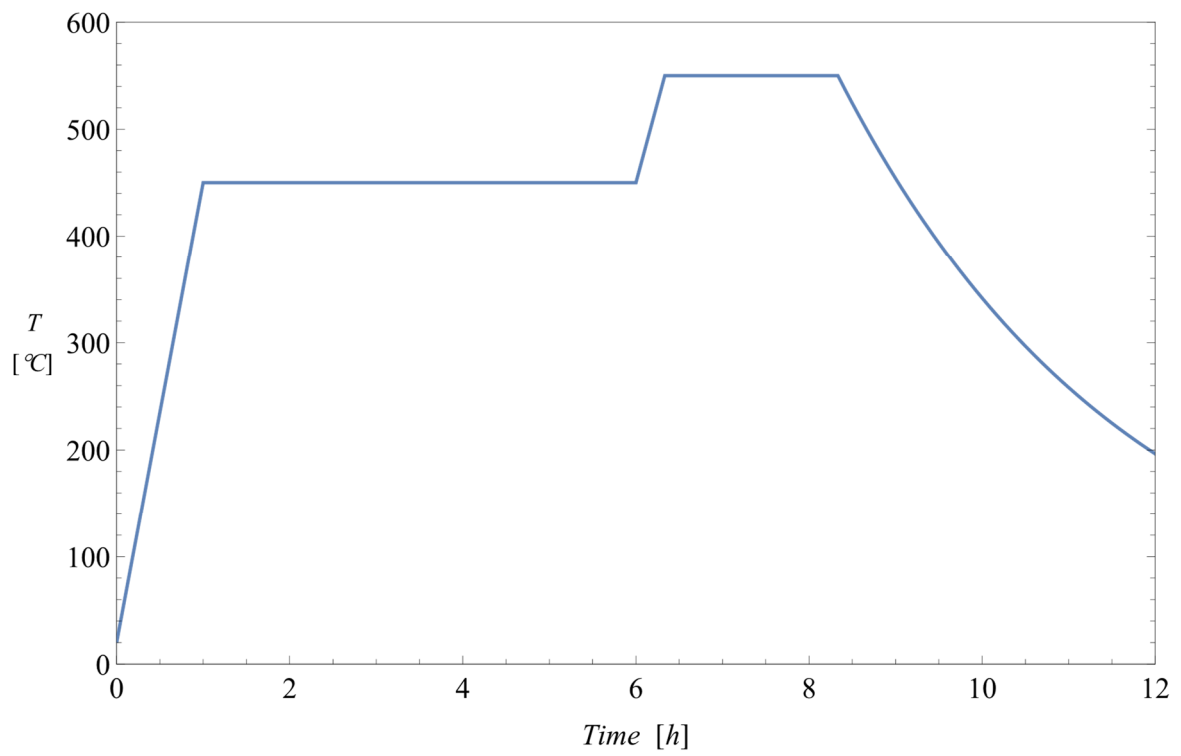


**Figure 10:** Temperature profile during the calcination of  $MgCO_3$  to  $MgO$

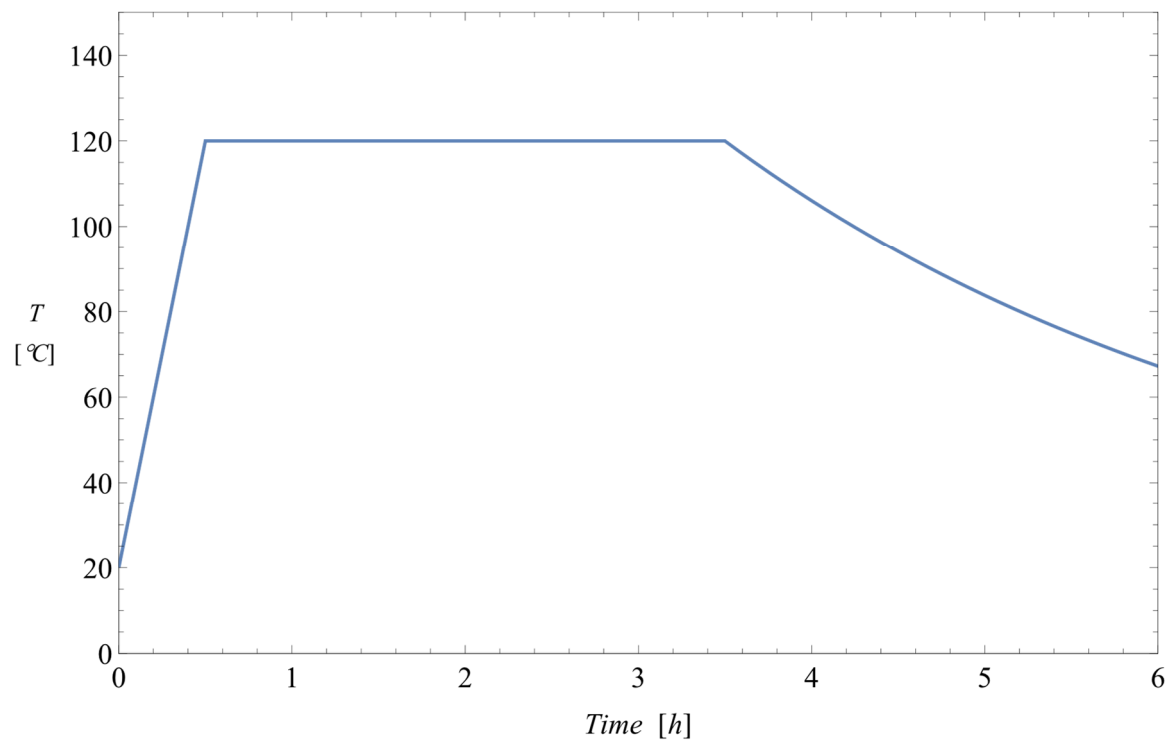


**Figure 11:** Temperature profile during the drying of the filtered and washed catalyst

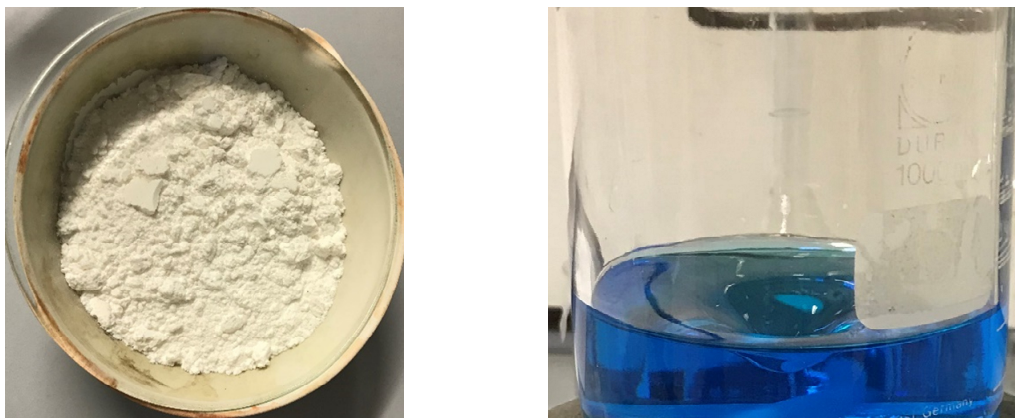


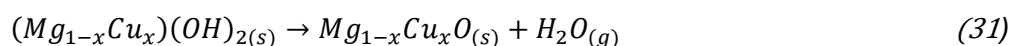
**Figure 12:** The figure shows the white  $MgO$  powder (left) and the blue  $Cu(NO_3)_2$  solution before the  $MgO$  is added.

Afterwards, the suspension is washed and filtered using a filter flask in combination with a vacuum pump. In order to prevent the cake from drying and to prevent channel formation, the suspension is added uniformly. As shown in *Figure 11*, the formed filter cake is then dried for three hours in a kiln at  $120\text{ }^\circ\text{C}$ , which results in a paler color (see *Figure 13*).



**Figure 13:** The picture on the left shows the turquoise catalyst precursor filter cake, while the right picture shows it after the drying process.

The dried cake is transferred to the furnace once more to perform the last calcination step (see *Figure 14*). This second calcination step assures that both metals, copper and magnesium, are present in their oxidized state [41]. Additionally, gaseous byproducts such as nitrogen oxides and other oxides are removed [6]. The decomposition of the catalyst precursor during the second calcination step can be described by Equation (31). The color of the powder changes during this step from pale turquoise to black (see *Figure 15*).





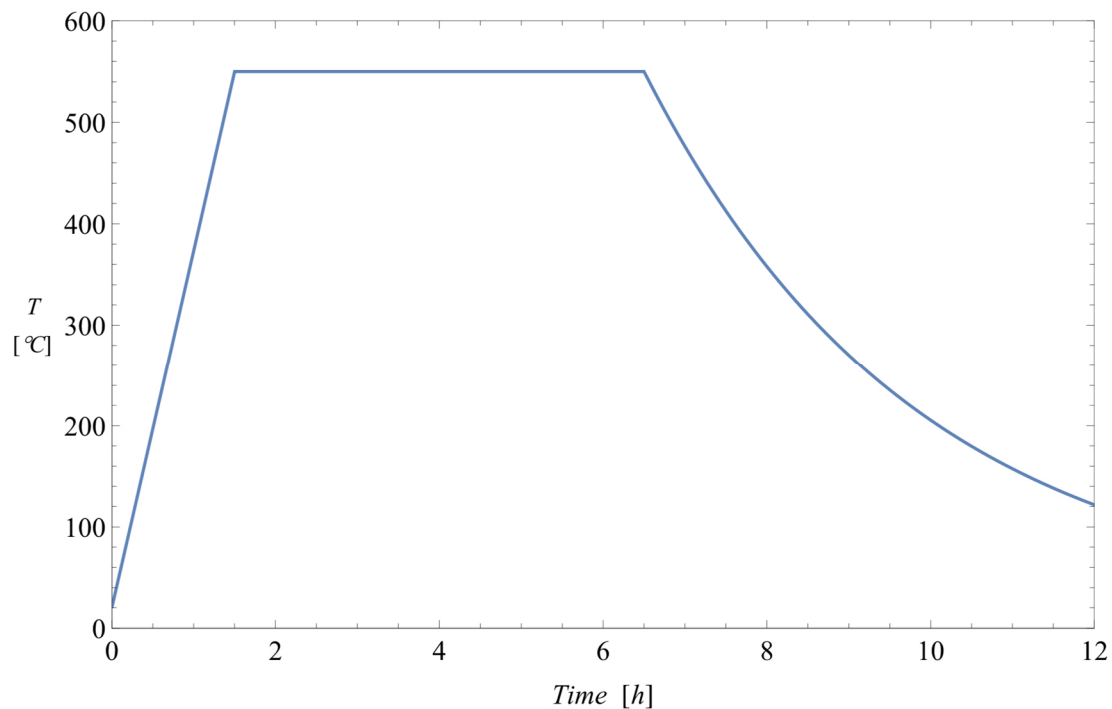
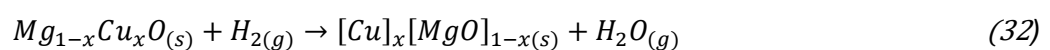


**Figure 14:** Temperature profile during the final calcination step



**Figure 15:** The figure shows the catalyst after the calcination step. The previously turquoise particles have become black.

The finalization of the catalyst, namely its exothermic reduction (the reduction of  $CuO$  to  $Cu$  with  $H_2$  results in a  $\Delta H_R = -120 \text{ kJ/mol}$  at  $T = 300^\circ\text{C}$  and  $p = 1.013 \text{ bar}$ ), is performed after milling and sieving of the calcined catalyst. The description of the occurring reaction can be found in Equation (32). The catalyst is therefore installed in the reactor, where a  $H_2$  flow is established under increasing temperature and pressure ( $T_{max} \cong 300^\circ\text{C}$  and  $p_{max} \cong 50 \text{ bar}$ ). The reduction of copper oxide results in a color change to a copper-red color. A more detailed description about the activation procedure can be found in chapter 4.2.4.2.



## 4 Process design

For testing purposes of the catalyst of interest, lab scale plants are needed. Therefore, two different approaches are followed: a DSTR batch operated plant and a continuous PFR. The lab scale PFR plant is evaluated using the self-prepared  $Cu/MgO$  catalyst (see chapter 3.3). Meanwhile a  $Cu/ZnO/Al_2O_3$ , of which the functionality is proven [42], is used for the validation of the DSTR lab scale plant. Each plant has four main equipment parts:

- The gas supply via the mass flow controllers
- A reactor
- A condenser
- A product vessel

For both plants the same gas supply, condenser and product vessel (in different arrangements) are used. Since pressures between 50 and 60 *bar* must be realized, stainless steel pipes, fittings and vessels have to be installed. As feed gases hydrogen ( $H_2$ ), nitrogen ( $N_2$ ) and carbon dioxide ( $CO_2$ ) are used. To assure an adequate tightness of the lab scale plants, pressure tests are carried out before the actual experiments can be performed. In this context, it must be mentioned that tightness has to be defined as a leaking rate, at which the risk, caused by the leaking gases, can be controlled. These gases are supplied by different gas flasks. Regarding the utilities, compressed air as well as different cooling liquids are supplied.

### 4.1 Standard equipment

As already mentioned, some equipment is used for both plants. Furthermore, many components, identical in their construction, have been installed. This chapter aims therefore to give a short overview of these parts and their properties.

#### 4.1.1 Fittings and piping

In both plants three types of piping/hoses are used, which variate in their material, pressure rating, as well as in their usage:

- Inflexible steel piping
- Flexible, metal housed hoses
- Flexible PTFE hoses

As standard piping for permanent installations, mostly 1/4" stainless steel of the type SS316 pipes with a wall thickness of 0.049" are used. For some applications, other diameters/sizes, such as M6, are installed. SS316 pipes are designed for pressures of about 517 bar, while being able to resist corrosion. In applications where a certain flexibility at high system pressures is necessary, 1/4" metal housed hoses are used. The need for flexibility can arise where pipes must be simply moveable, or where dynamic burden can occur. These conditions do occur at the connections between the gas flasks and the trailer, on which the mass flow controllers are mounted. Flexible piping is also used for the exhaust lines, leading from the lab scale plants to the vent. Furthermore, flexible hoses are used for utilities such as cooling liquid or compressed air. Since these lines are not operated under high pressures, lines in form of PTFE hoses are installed. All three types of piping are connected to each other and to various types of fittings with union nuts and ferules.

Regarding the needed fittings for the assembly of both lab scale plants, mostly imperial fittings of the manufacturer Swagelok are used. The diameter of the fittings corresponds mostly to those of the piping, namely 1/4", 1/2" and M6. For the connection of a pipe with any kind of vessel, reactor or even to some valves, connectors are needed. These connectors use conical NPT thread which need sealant (e.g. Teflon tape), while standard threads, which connect any kind of fitting with a tube, do not need any sealant due to the self-sealing ability of the ferules. For further information regarding correct bending of pipes, their installation as well as the right handling of fittings, "Swagelok® tube fitter's manual" can be consulted.

#### 4.1.2 Valves

For the control of the fluid paths in the lab scale plants, four types of valves are used:

- Needle/control valves
- Ball valves
- Three-way valves
- Check valves

The installed needle valves are used as control valves and allow the regulation of the fluid flow, which passes between the needle and the socket of the valve. Two different versions can be found, a straight and a 90° one. While the straight one can be considered the standard valve, the 90° version is mounted only in the bypass line. For high temperature applications special

control valves of the manufacturer *BüchiGlassUster*<sup>®</sup> which can withstand temperatures up to 450 °C are available. In comparison to control valves, which serve the purpose of regulating a fluid flow, ball valves are designed to either close or open a path for the fluid. Three-way valves are installed in positions where fluid streams, depending on the current task, must be directed to a certain path. One example of application is the vent system, where the gas stream, leaving the mass flow controllers, must be switchable either to the reactor or the vent. To assure that no unwanted fluid flow, respectively back rinsing, occurs, check valves are installed.

#### 4.1.3 Mass flow controllers

The gas feed streams are controlled by three mass flow controllers (MFC). As noted in *Table 2*, two thermal and one coriolis mass flow controller are used. Since mass flow controllers are calibrated and therefore restricted to a certain volumetric flow, bypass piping in combination with control valves are installed. This allows manual control of all gas streams, as well as depressurization in case of failure (MFCs are standard closed).

**Table 2:** Overview of the used MFCs and their properties

Tag	MFC-01	MFC-02	MFC-03
Media	$H_2$	$N_2$	$CO_2$
Product Nr.	<i>F-231M-AAD-22-V</i>	<i>F-231M-AAD-22-V</i>	<i>M13-AGD-33-0-S</i>
$V_{max}$ [Nml/min]	<i>30</i>	<i>15</i>	<i>10</i>
Ø	<i>1/4 "</i>	<i>1/4 "</i>	<i>1/4 "</i>
Actuator type	<i>electric</i>	<i>electric</i>	<i>pneumatic</i>
Meas. principle	<i>thermal</i>	<i>thermal</i>	<i>coriolis</i>

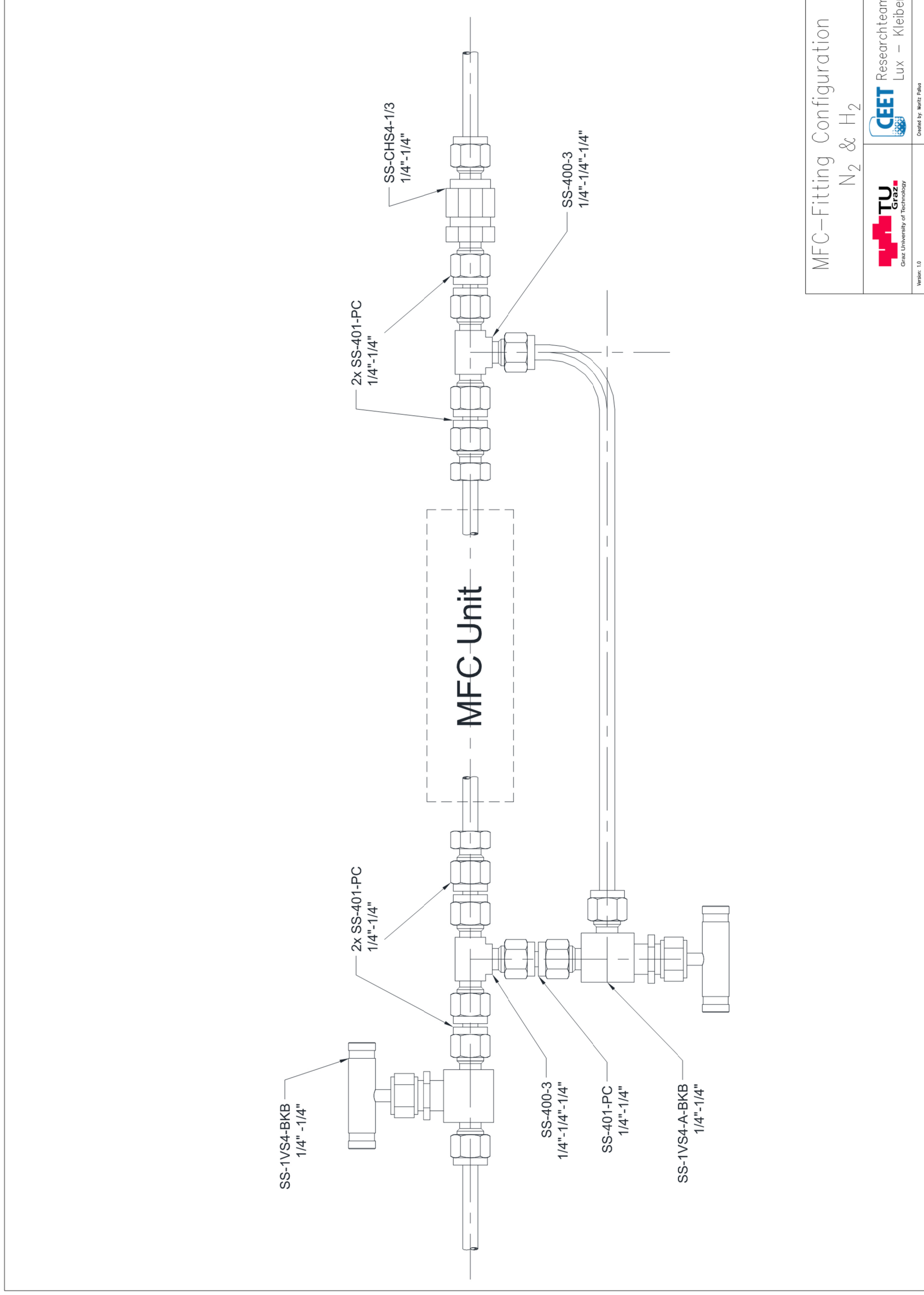
The thermal MFCs regulate the nitrogen and hydrogen streams. To prevent the MFC from clogging and malfunction, a unit comes with a preinstalled filter element, positioned before the actual controller. The Thermal Mass Flow Controllers themselves consist of a laminar flow element, a bypass (with integrated heater and two thermo-sensors), a control valve as well as the therefore needed electrics. Their working principle is based on a temperature measurement, or rather the change in temperature of the media in a bypass stream. Two temperature sensors are placed in series with a heating element between them. Without a gas flow, the two sensors show the same temperature. While with gas flow, cold gas arrives at sensor one, and thereby decreases its temperature, warm gases, heated by the heating element, arrive at the second sensor, leading to an increase in temperature there. This

temperature gradient, in combination with the law of energy conservation, allows the calculation of the mass stream flowing through the bypass. The laminar flow element assures a proportional flow through the bypass element. Therefore, when knowing the diameter of the bypass and the main supply line, the calculation of the overall mass flow is an ease. A typical assembly for a thermal MFC, the corresponding bypass piping and control valves, can be seen in *Figure 16*.

The Coriolis Mass Flow Controller Unit consists of the Coriolis Mass Flow Meter (MFM) itself and the check valve, needed for regulation of the gas stream. In comparison to a thermal MFC unit, no filter element is preinstalled. Therefore, a third-party filter with a mesh size of  $7\mu\text{m}$  is installed. In the MFM, two actuators are used to cause vibration in a small tube. An optical sensor measures the vibration. When fluid flow is applied, the tube twists and the vibration changes. This change in vibration and the therefore caused phase shift is measured by an optical sensor in the MFM, allowing the calculation of an actual fluid mass. The check valve acts according to the result of the comparison between the measured and the set value. Compressed air from the main supply line, in combination with a pressure reducer, is used to power the check valve's actuator.

#### 4.1.4 Condenser

For the condensation of all substances in the vaporous phase, a stainless-steel double jacket condenser is used. The diameter of the outer pipe is  $3/4"$  while the diameter of the inner pipe is manufactured as  $3/8"$ . A static mixer on the inside of the inner tube assures introduction of turbulence, which assures a high heat transfer. Regarding the connection of the cooling media, two hose connectors are available. The media itself enters the cooler in countercurrent flow direction and is provided by a cryostat *ECO 1050* of the company *LAUDA-Brinkmann, LP*. Isopropanol is used as a cooling media. Compared with water, isopropanol allows lower set-temperatures due to its lower freezing point. Nevertheless, the setpoint is usually defined as  $T_{Cooler,Set} = 2\text{ }^{\circ}\text{C}$ . All connection hoses, as well as the cooler itself, are isolated with *DURAFLEX*<sup>®</sup> insulation foam to minimize heat transfer from the surrounding to the equipment or the cooling liquid.



MFC-Fitting Configuration  
N<sub>2</sub> & H<sub>2</sub>



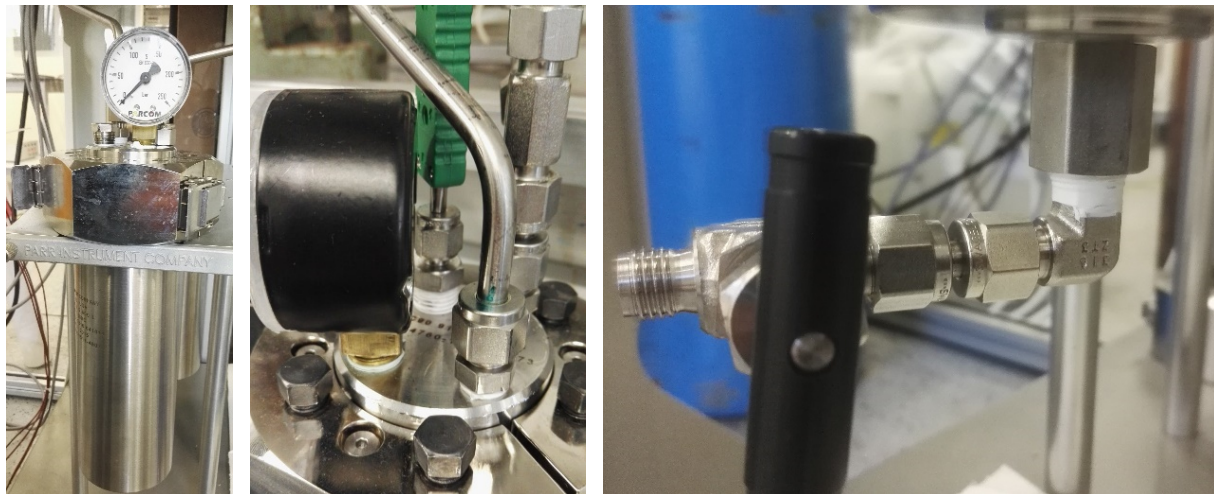
 <p>TU Graz Graz University of Technology</p>	 <p>CEET Researchteam Lux - Kleiber</p>
<p>Version: 1.0</p>	<p>Created by: Martin Pöschl</p>

Figure 16: An example for an MFC assembly including the bypass piping, as well as all needed valves

#### 4.1.5 Product vessel

The product vessel (PV), originally only used in the plug flow reactor setup, is a stainless steel SS316 vessel of the manufacturer *Parr Instrument*<sup>®</sup>. The vessel itself has a volume of 0,6 l and is rated for 200 bar at 350 °C. Between the lower cylindrical part and the lid, a PTFE gasket is mounted in a groove. The lid is mounted on the product vessel by a clamp system in combination with nuts, needed for the establishment of a sufficient clamping force. For the purpose of product collection, simpler handling and therefore quantification, a glass or steel beaker is positioned in the vessel. Regarding the product vessel's connections, it offers four openings on the lid and one at the bottom. In both lab scale plants, one lid connection is always used for an analog pressure indicator and one for an inlet pipe. The inlet pipe is designed as a vertical pipe, which reaches through the lid into the reactor, ending only a few centimeters over the bottom of the pre-placed beaker. A third lid connection is in both lab scale plant's used for an exit pipe, allowing a fluid stream out of the vessel. In addition, the batch plant's exit pipe is equipped with a pressure transmitter. While the fourth lid connection is plugged in the PFR setup, a thermocouple type K is installed in the DSTR setup, allowing a temperature measurement in the product vessel. At the bottom of the vessel another connection is available. The product vessel and all its connections can be seen in *Figure 17*.



**Figure 17:** PV installed in the PFR setup, a detail photo of the lid connections (when installed in the DSTR setup) and the bottom connection

#### 4.1.6 Safety equipment

Since high pressures and temperatures in combination with explosive gases are used, different safety features are installed:

- Rupture discs to avoid high pressures (*Figure 18*)
- A solenoid valve to limit the hydrogen feed (*Figure 18*)
- Gas sensors
- High temperature safety switches and alarms
- Adequate ventilation



**Figure 18:** Solenoid valve UV-001, installed in the hydrogen stream and the installed rupture disc SE-001

To prevent high pressures, rupture disks are installed. Rupture disc SE – 001 is located near the MFCs and can therefore be used in both lab scale plants. At a temperature of 22 °C it is designed to introduce a pressure relief at 206 bar. Since a part lab scale batch plant, respectively its reactor and pressure vessel, are disconnected from the rest of the system after pressurization has occurred, additional pressure relief equipment is needed. Therefore, another rupture disc is installed on one of the reactor connections. Since the reactor as well as its heating jacket are located in the near surrounding of the rupture disc, respectively its piping, an M10 exhaust pipe is installed, connecting the rupture disc to the exhaust vent system.

In case of emergency, such as a blackout or a major gas leakage, the solenoid valve UV – 001 assures that no more hydrogen is fed to the system. It is therefore installed in the piping between the gas cabinet and the hydrogen MFC and electrically connected to the general gas



alarm of the laboratory. If a gas alarm is triggered by a hydrogen leakage, the electric power is shut off, resulting in a closure of the solenoid valve, since its standard position is closed.

Both reactor systems are built in separate lab boxes, which are equipped with their own ventilation system. The permanent ventilation fulfills two purposes:

- Hinder the formation of an explosive atmosphere in case of leakage
- Remove a potentially explosive atmosphere

The first case can occur during normal operation since fittings and screwed connections are not always 100% gas-tight (especially when  $H_2$  is used). The second task can occur if a connection is not tightened correctly, which can result in huge  $H_2$  streams. Since the  $H_2$  gas flask, as well as all *MFCs*, can be controlled from outside the box, the feed stream can be shut without the need for a person to enter the danger zone. The potentially explosive atmosphere, present at the beginning, can be controlled and diluted by the ventilation, since it will not leave the reactor box. To assure the functionality of the ventilation, measurements have been performed, resulting in a volumetric flow for the batch ventilation of  $\dot{V}_{DSTR,vent} = 222 \text{ m}^3/h$  and for the PFR ventilation  $\dot{V}_{PFR,vent} = 122 \text{ m}^3/h$ . This equals  $C_{DSTR} \cong 150$  and  $C_{PFR} \cong 30$  air changes per hour. The exact calculations and measurements can be found in the appendix.

## 4.2 PFR plant

The following chapter includes the documentation of the first lab scale plant. This setup is built around a plug flow reactor and is not only validated for its functionality but furthermore used for the validation of the *Cu/MgO* catalyst of interest.

### 4.2.1 Working principle and build up

The PFR lab scale plant is based on a *Parr Instrument*<sup>®</sup> tubular reactor system. This lab scale plant aims on a continuous production/operating mode. For its validation the catalyst of interest, namely a self-made *Cu/MgO* catalyst as described in chapter 3.3, will be used. Therefore, gases, or rather a mixture of gases, are fed continuously to a catalyst packed, heated reactor where reactions take place. The vaporous reaction products are then condensed in a condenser. The formed liquids, methanol and water, are separated from the gas stream in the product vessel acting as a liquid separator, more specifically in a beaker, placed in the product vessel. The remaining gases leave the vessel over a back-pressure

regulator. Liquid samples are taken discontinuously from the product vessel and analyzed with a gas chromatography (GC). Gas sampling will be possible in future experiments with GC-vials and a micro GC.

The complete piping and instrumentational setup, or rather its P&ID, can be seen in *Figure 19*. Regarding its main equipment, the lab scale plant consists of a gas supply, the actual reactor with its heating jacket, a condenser with a subsequently connected product vessel, as well as a pressure maintaining valve.

The gases, hydrogen, nitrogen and carbon dioxide, are supplied via 1/4" stainless steel tubing to three mass flow controllers (see chapter 4.1.3). The gas stream, of which the desired composition is controlled via the MFCs, has two possible paths available. Using the three-way valve, it can either be sent to the gas sampling and exhaust vent, or to the reactor, which it is entering from its top. For the reactor, a stainless-steel pipe with a diameter of 1/2" and a length of 52 cm is used. The reactor is packed with a bed of catalyst powder (See chapter 4.2.4.1), which is surrounding a thermo-sensor. This sensor allows the measurement of three temperatures at different axial positions in the reactor. The electrical heating jacket which surrounds the reactor and of which the temperature is also measured, is used to modify the temperature conditions in the reactor. In addition to these temperature measurements, an analogue pressure indicator, as well as a pressure transmitter, are available for pressure measurement and monitoring. The mixture of gases flows through the packed catalyst bed, where different reactions, depending on the composition of the gases, occur. For the activation, a combination of large  $H_2$  and a very low  $N_2$  stream is fed to the reactor, while for the synthesis reaction a mixture of  $H_2$ ,  $CO_2$  and  $N_2$  is used.

The hot gas stream, potentially containing vaporous products, leaves the reactor at its bottom, entering a condenser. The condenser consists of an inner tube with a static mixer and an outer tube. Hot gases and vapor stream through the inner pipe, condensing on the outer walls, which are cooled by a cooling liquid flowing through the outer pipe. The cooling liquid, namely isopropanol, is supplied by a cryostat (see chapter 4.1.4) with an inlet temperature of 2 °C and passes through the condenser in countercurrent flow direction. Formed liquid is then separated from the two-phase fluid stream due to gravitational force. Exiting a dip tube, leading from the condenser to the product vessel, liquid trickles in a beaker while the gas stream rises and exits the product vessel through a pipe in its lid. For pressure measurement in the product vessel

and therefore after the catalyst, which acts as a flow resistor, an analogue pressure indicator is installed.

After the product vessel, a back-pressure regulator assures that the desired pressure is held in the system. A bypass piping in combination with a control valve is installed for depressurization of the lab scale plant without a change in position of the back-pressure valve. To avoid fine solid particles from interfering or blocking the control or back pressure valve, a filter with a porosity of  $7 \mu m$  is installed.

The sampling of the formed liquid at this time is performed discontinuously. Therefore, the lab scale plant must be depressurized and the product vessel dismantled. As mentioned before, liquid is collected in a beaker from which now the liquid samples can be taken. The product vessel is equipped with a bottom outlet, which theoretically could be used for liquid sampling. Therefore, more liquid product and consequently higher feed flow rates are needed. In the future, gas sampling and analyzation will either be possible continuously or discontinuously. A continuous solution would be the installation of gas analytics. Discontinuous sampling could be realized by filling vials (as proposed in the P&ID, visualized in *Figure 19*) and evaluating their content using a GC.

#### 4.2.2 Process control

All electric sensors, seen in the P&ID in *Figure 19*, are of no use without an appropriate device for visualization, monitoring and controlling of the parameters of interest. Therefore, a *Parr Instrument*<sup>®</sup> *Process Controller 4871* in combination with a *4875 Power Controller* are available. All temperature sensors, namely the one in the heating jacket ( $T_j$ ) and the three positions measuring sensor in the reactor ( $T_1$ ,  $T_2$  and  $T_3$ ), as well as the pressure transmitter, located before the reactor, are connected to the named process controller. In addition to the temperature and pressure data, the controller is also used for the control of the mass flow controllers, as well as the heater. A list of the installed instruments can be found in *Table 3*.

The mentioned temperature sensor in the reactor allows a temperature measurement in its top section ( $T_3$ ), in (or just below/under) the catalyst bed ( $T_2$ ) and below the catalyst bed ( $T_1$ ). Usually,  $T_2$  is defined as the temperature which has to be controlled (in such experiments  $T_R$  is  $T_2$ ).

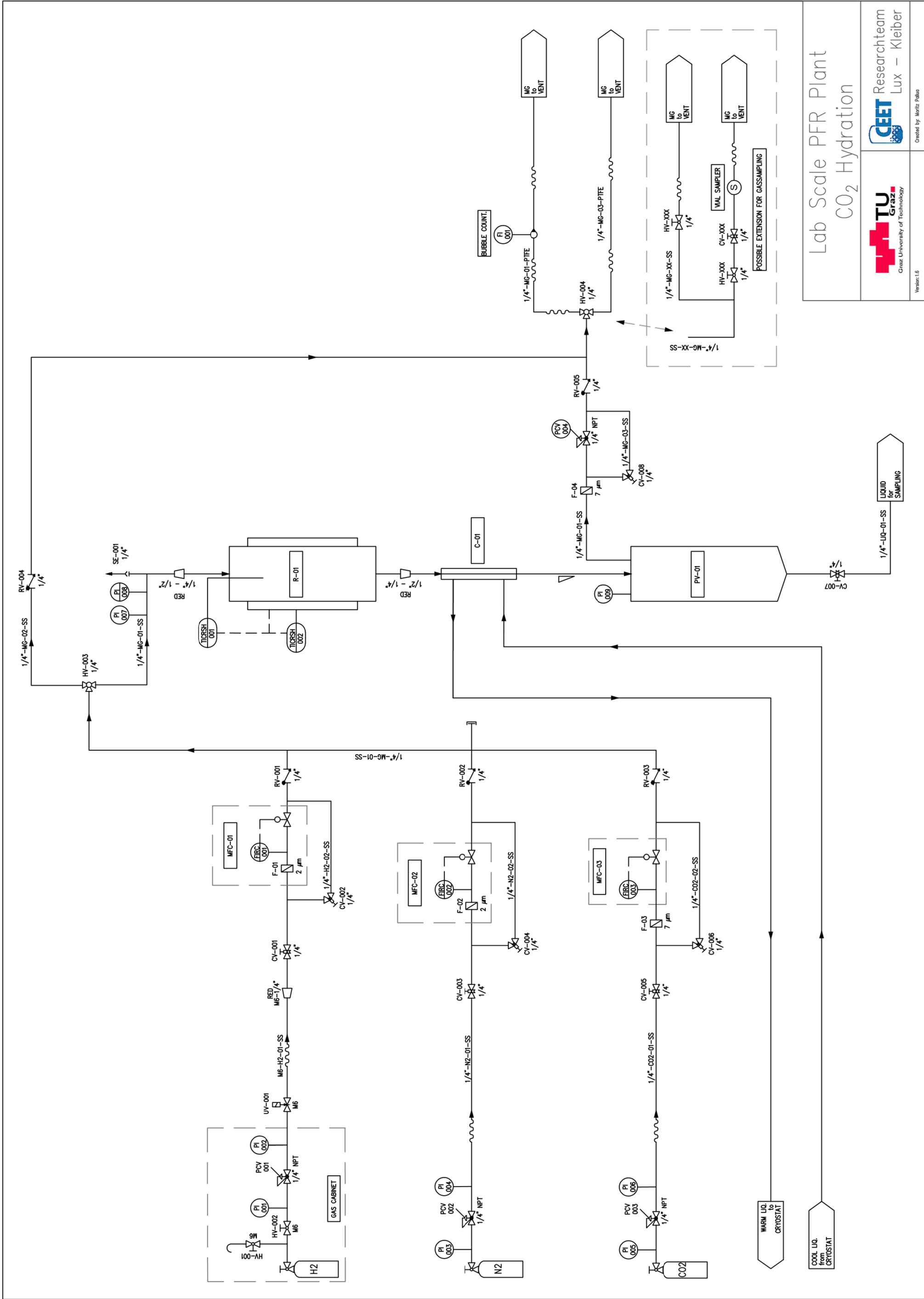


Figure 19: P&ID of the lab scale PFR setup including all sensors, equipment as well as a proposal for an extension for a batch wise gas sampling station.

**Table 3:** List of installed instruments which are connected to the process controller

Tag	Type	Function	Position
FIRC-001	<i>MFC</i>	<i>H<sub>2</sub> volumetric flow measurement and control</i>	<i>H<sub>2</sub> Feedline</i>
FIRC-002	<i>MFC</i>	<i>N<sub>2</sub> volumetric flow measurement and control</i>	<i>N<sub>2</sub> Feedline</i>
FIRC-003	<i>MFC</i>	<i>CO<sub>2</sub> volumetric flow measurement and control</i>	<i>CO<sub>2</sub> Feedline</i>
PI-008	<i>Pressure transmitter</i>	<i>Logging pressure</i>	<i>Before the reactor</i>
TICRSH-001	<i>Temperature transmitter</i>	<i>Reactor temperature at 3 axial positions; Usable as safety switch high</i>	<i>In reactor</i>
TICRSH-002	<i>Temperature transmitter</i>	<i>Jacket temperature Usable as safety switch high</i>	<i>Reactor jacket</i>

For the visualization and manipulation of the measured data, the software "SpecView" is used. In its main window, the actual temperatures, the reactor pressure and the heater's status can be seen. With the "PV Selection" option, the reference temperature for the set temperature can be defined. The set temperature value, which the controller tries to reach by heating the electric heating jacket, is also defined in this window. Recorded temperatures and pressure data are visualized in two separate charts. An alarm setpoint can be defined for each temperature as well as the pressure. If such an alarm setpoint is reached or exceeded, an acoustic signal sounds and the power controller's fuse switch is tripped. As a result, to avoid even higher, potentially dangerous temperatures and pressures, the electric heating jacket is no longer heated.

In addition to the pressure measurement and the temperature control via the heater, the software allows the control of the MFCs. The window "FlowControl" shows the actual measured volume streams (in *Nml/min*), the total amount integrated over time, as well as the defined operating points. In case of emergency, the submenu "Utilities" provides a button "Pop Breakers", which allows to manually trip the heaters fuse switch.

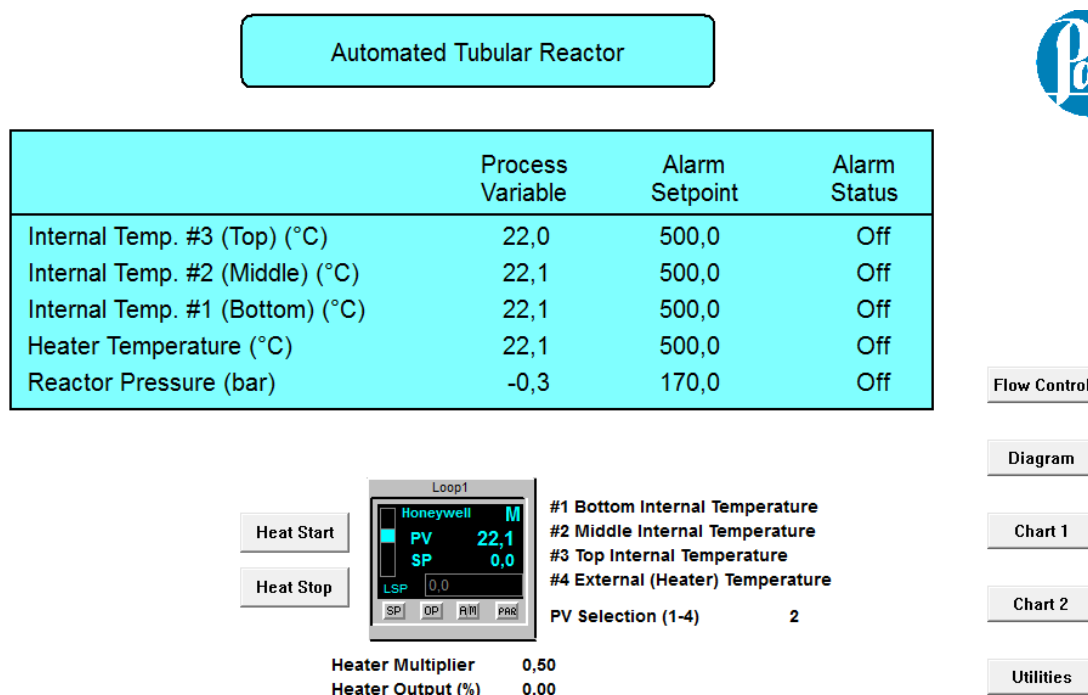


**Figure 20:** Screenshot of Parr Instrument<sup>®</sup>'s software Spec View, used for monitoring and control of the lab scale PFR system

#### 4.2.3 Pressure test

To assure gas tightness or an acceptable gas leaking rate, several pressure tests, each at over 50 *bar*, are executed. This results in three different tests:

- $N_2$  at ambient temperature
- $H_2$  at ambient temperature
- $H_2$  at reaction temperature

Since Hydrogen is a potentially flammable and explosive media, the first pressure test is performed using pure  $N_2$  at ambient temperature. A second pressure test is performed with  $H_2$  at ambient temperature and a third pressure test uses  $H_2$  at reaction conditions. For leakage detection, soapy water, as well as a hydrogen sensor are used. In this chapter, only a nitrogen pressure test at ambient temperature is shown and evaluated in *Figure 21*. At the beginning of the pressure test, rather low pressure is established to check for untightened connections or open valves. Different pressure levels are then established, and the system left for about 15 *min* to check for leakages. After the final pressure is established (here 55 *bar*), pressure data is logged for several hours (here 5 *h*) which can later be used to calculate the pressure drop and the leakage rate. As a result, an average pressure drop of 0.045 *bar/h* can be

calculated, resulting in a leakage of  $\dot{V}_{PFR,Leakage} = 0.1 \text{ ml/min}$ . Such a small leakage will not result in a dangerous explosive atmosphere. Nevertheless, pressure tests have to be performed even after the system is approved as gas-tight for the first time. The need roots in the necessity of removing the reactor for the catalyst filling process. Therefore, two connections have to be loosened, which must be controlled afterwards for tightness.

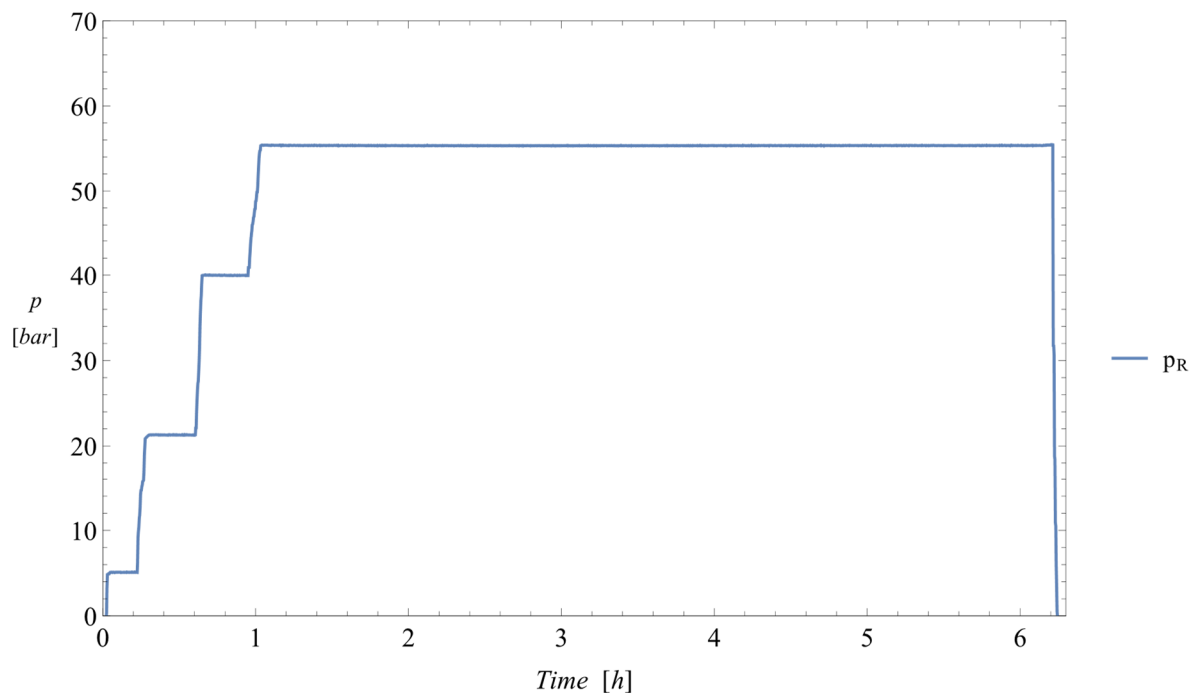


**Figure 21:** Pressure test with  $N_2$  at ambient temperature

The interested reader can find an exemplary, but detailed documentation of all three tests as well as their graphical evaluation and a risk assessment for the batch reactor system in chapter 4.3.3.

#### 4.2.4 Experiments

The validation of the PFR and as a consequence the self-prepared  $Cu/MgO$  catalyst requires different experiments and preparations. The preparation of the catalyst bed is followed by the activation of the catalyst, which is necessary for the functionality of the catalyst. Once the catalyst is activated, the actual validation by hydrogenating  $CO_2$  to methanol can be performed.

##### 4.2.4.1 Preparation of the catalyst bed

Before any kind of experiment can be performed in the PFR-lab scale plant, a way to fix the catalyst in the reactor must be found. Since the catalyst is available as a powder of small

particles only ( $d_{p,m} < 600 \mu m$ ) and not as a porous solid, additional resources are needed to solve the two main problems. These problems are the following:

- The formation of a stable packed bed
- Its axial position in the reactor and the filling process

To prevent powder from following the fluid flow, glass wool, which acts as a kind of filter cloth, is used. Furthermore, the layer of glass wool gives the packed bed more stability. This stability is needed since pressure drop across the packed bed (similar as for a filter cake) increases with the flow rate.

The axial position of the packed bed in the reactor is connected inseparably with the filling process. As visualized in *Figure 22*, a temperature sensor is installed in the radial center of the reactor. Since a packed bed of catalyst is too dense for the temperature probe to stick through, the catalyst bed must be filled when the probe is already installed. As mentioned in chapter 4.2.2, temperatures in the reactor are measured at different axial positions. Therefore, the axial position of the catalyst bed must be known to allow reproduceable and comparable experiments. Since only a small volume of the reactor shall be filled with catalyst, support elements are needed. Looking at the top section of the reactor in *Figure 22*, it can be noted that the installed temperature sensor requires the installation of a T-piece. This T-piece is unfavorable for the filling process, since filling cannot be performed from the top opening of the reactor. Filling the reactor from its bottom results in the need of additional non stiff support elements during the filling process. Since these support elements shall be removed afterwards to avoid unnecessary flow resistance and weight on the catalyst bed,  $SiO_2$  spheres with a diameter of 2 mm are chosen. The reactor is turned on its top, the T-piece closed, and spheres are poured in. The height of the  $SiO_2$  spheres and therefore the axial position of the packed bed is assured by measuring the depth from the bottom edge of the reactor to the level of glass spheres. When the desired height is reached, a small amount of glass wool is inserted, which assures that no catalyst will fall through. The exact amount, needed for a certain volume of catalyst bed, can be estimated using the powder's bulk density. This density is determined by filling a measured amount in a graduated measuring cylinder. The resulting volume in combination with the mass of the used catalyst allows the calculation of a bulk density. After inserting the pre weighed amount of catalyst, another layer of glass wool is applied, and the reactor filled up with  $SiO_2$  spheres.



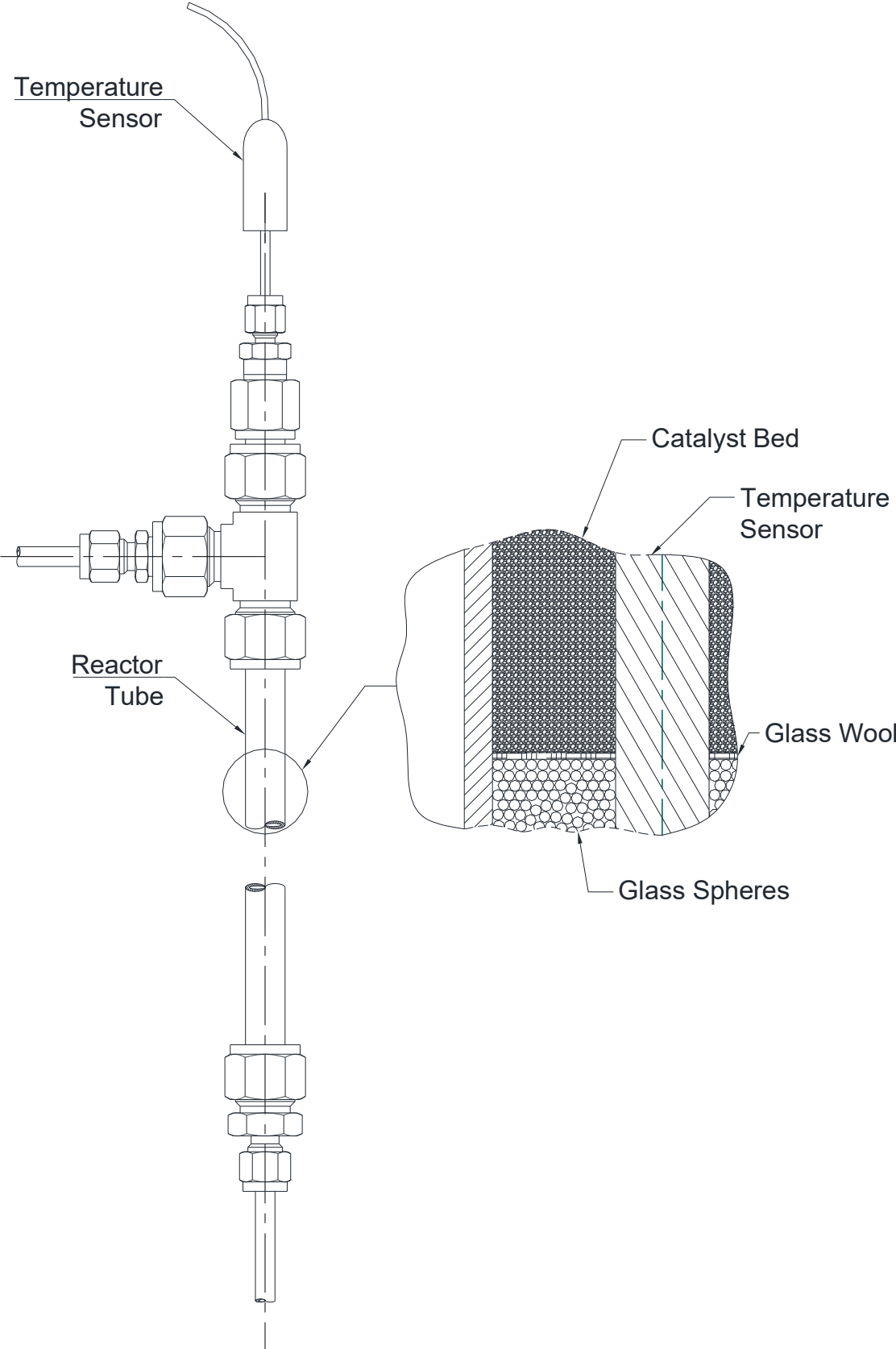


**Figure 22:** Schematic drawing of the PFR unit, including the temperature sensor and the connected tubing. Additionally, a detail of a sectional drawing is shown to demonstrate the structure of the catalyst bed and its support.

At last a metallic sieve with a mesh size much smaller than  $2\text{ mm}$ , which blocks the spheres from falling out of the reactor, is inserted and fixed due to the mounting of a reducing fitting. Since the catalyst bed is established and fixed in its axial position, the no longer needed spheres in the reactors top section can be emptied through the previously closed T-piece.

#### 4.2.4.2 Catalyst activation

For the activation of the catalyst, a predefined amount of catalyst powder is used to establish a packed bed, according to the procedure described in chapter 4.2.4.1. The activation itself is carried out in the reactor, where afterwards the actual synthesis experiment will be performed. The activation of the catalyst is needed to assure that the *Cu*-oxides in the catalyst are present in their reduced, metallic form. The catalyst of interest, a *Cu/MgO* catalyst pre-sieved to a particle diameter which is lower than  $600\ \mu\text{m}$ , is used. A mass of  $m_{\text{Cu/MgO}} = 2.03\ \text{g}$ , which equals a volume of about  $V_{\text{CuMgO}} = 8,25\ \text{ml}$  is forming the packed catalyst bed. Regarding the glass wool,  $m_{\text{gw,top}} = 0.14\ \text{g}$  and  $m_{\text{gw,bottom}} = 0.13\ \text{g}$  are inserted in the reactor. The temperatures and the pressure present during the whole activation process can be seen in *Figure 23*.

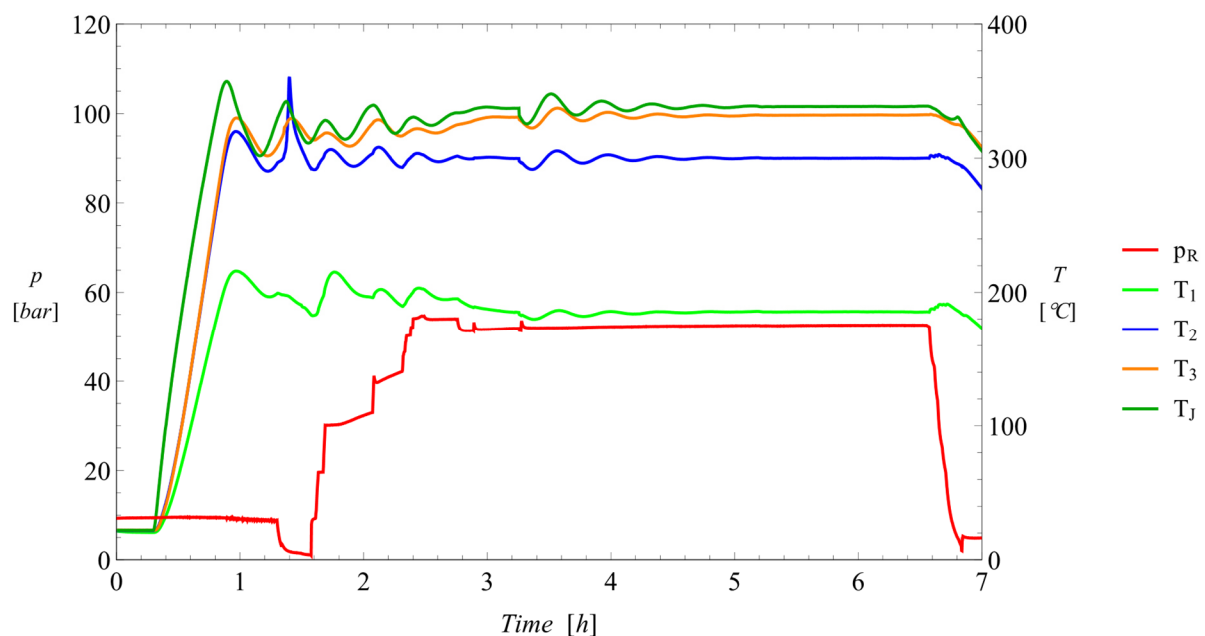


**Figure 23:** Temperatures and pressure data during the activation experiment. The activation itself can be seen as an increase of the temperature  $T_2$  (which represents  $T_R$ ), resulting in a steep spike. The experiment is carried on assuring complete activation under the actual validation conditions of  $T_R \cong 300\ \text{°C}$  and  $p_R \cong 50\ \text{bar}$ .

After the packed bed reactor is installed and all EMSR-equipment is connected to the process controller, the system is manually rinsed with nitrogen. Rinsing is performed to assure that no unwanted impurity remains in the plant. A pure nitrogen atmosphere goes hand in hand with the absence of oxygen, which would be necessary for an explosive mixture. Therefore, hydrogen's upper explosion limit of 78.5 vol% [43] will always be lower than the actual hydrogen concentration. The manual control of the nitrogen stream, which is flowing through the  $N_2$ -MFC's bypass, allows much higher volume flows compared to the  $N_2$ -MFCs. Such a high flow decreases the needed rinsing time but results in an increase of pressure. Such an increase can be seen in the beginning of *Figure 23*, where the red line shows the pressure. During the rinsing process, the set-temperature is set to  $T_{2,set} = 300\text{ }^\circ\text{C}$  to preheat the reactor and the temperatures begin to rise. After 70 minutes, rinsing is complete and the bypass, or rather the control valve, is closed, an immediate pressure drop is noticeable. A hydrogen flow  $\dot{V}_{H_2} = 30\text{ Nml/min}$  as well as a nitrogen flow of  $\dot{V}_{N_2} = 10\text{ Nml/min}$  are established. The falling pressure indicates that the packed catalyst bed is porous enough for the small fluid flow to pass through, without resulting in huge pressure gradients at this volumetric flow rate. Looking at the temperatures, a vast increase, resulting in a sharp peak with a maximum of  $T_{2,Max} = 360\text{ }^\circ\text{C}$ , can be noted shortly after the hydrogen flow is switched on. The increase in temperature indicates the presence of the activation reaction, which is exothermic. To assure that the whole catalyst is activated, the system pressure is manually increased step-wise to over 50 bar by opening the hydrogen streams bypass control valve. Since two nuts had to be removed for catalyst insertion in the reactor, these two connections must be tested for gas leakage throughout the pressurization process. As a result of the before mentioned temperature peak, the heating power (noticeable from the heater's temperature) is decreasing, since the controller aims to control  $T_2$  to  $300\text{ }^\circ\text{C}$ . Because of the influenced heating power, the reactor's bottom temperature  $T_1$  drops to a minimum. During the pressurization the manually controlled volume flow is not constant which may contribute to the swinging temperatures. The decrease of pressure after the maximum of  $p_{max} \cong 53\text{ bar}$  is again caused by the modified feed stream. The hydrogen bypass control valve is shut and the volume flow is set to  $\dot{V}_{H_2} = 30\text{ Nml/min}$ , using the MFC. Compared to the previous flow rate, which was controlled by the bypass check valve, the now established volumetric flow is much smaller. Regarding the temperatures, a stabilization can be noticed due to the constant volumetric flows. After the pressure drops to  $p \cong 51\text{ bar}$ , it remains constant before it rises once again. Two peaks, similar in magnitude and time interval, as well as a continuous pressure increase, occur. The pressure

peaks could result from a fast clogging and opening of the catalyst bed, while the continuous pressure increase suggests that the whole catalyst bed is being compressed over time. Only a few minutes before the second pressure peak occurs, a short power outage, in *Figure 24* visible as step-like values of the temperature, introduces instabilities. These instabilities flatten out after another hour. Since pressure and temperatures reach constant operating conditions and therefore no further reduction of the catalyst is occurring, the activation experiment is finished after a total of five and a half hours. All inlet stream valves as well as the outlet valves are closed to hinder other gases from entering the system.

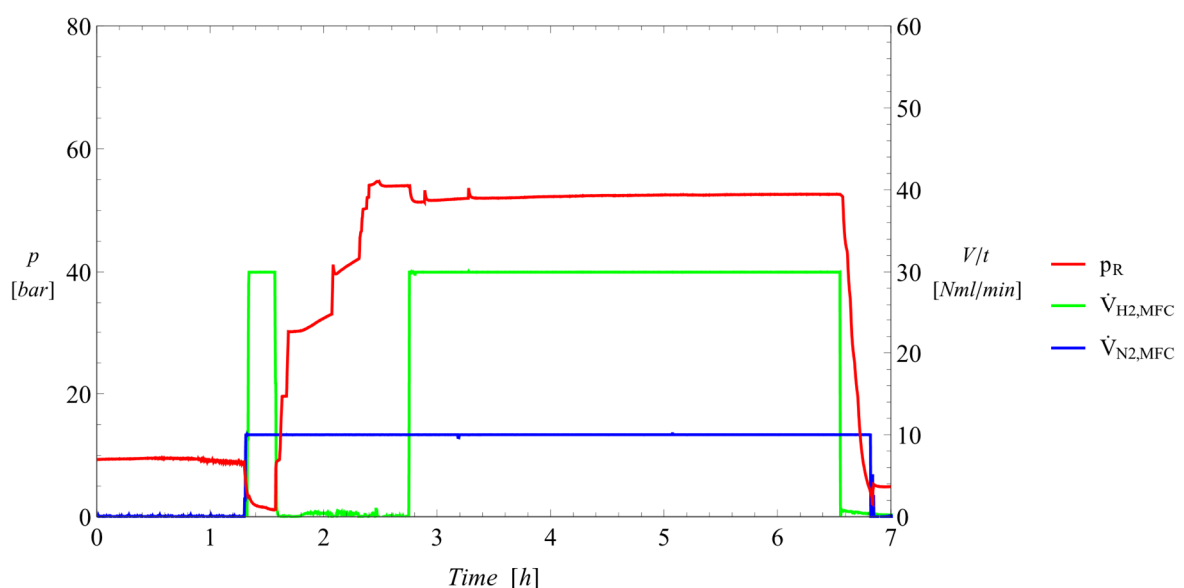


**Figure 24:** Volumetric flow rates and pressure data during the activation experiment. Note that fluid streams, introduced by a manual opening of the bypasses, or their magnitudes, are not shown in this figure. The manually introduced gas streams are a hydrogen stream at the beginning, resulting in a pressure of 9 bar and a hydrogen stream used for pressurization of the system.

The so preserved hydrogen atmosphere in the plant and therefore around the catalyst, visible as the remaining pressure at the end of the depressurization in *Figure 24*, aims to avoid a re-oxidation and therefore inactivation of the catalyst.

#### 4.2.4.3 Validation

For a positive validation result, regarding the functionality of the lab scale plant and the catalyst of interest, methanol must be synthesized. Therefore, the lab scale plant containing the pre-activated catalyst is used. Regarding the catalyst properties, this experiment does not aim at a quantitative but on a qualitative statement, so if the catalyst as well as the lab scale plant

work at all. Since the used catalyst has not been characterized, the exact amount of liquid, produced during activation and still present in the product vessel's beaker, is not known. As a consequence, no quantitative statement will be possible, since the exact amount of liquid in the metal beaker, produced during the activation experiment, cannot be distinguished from produced liquids during the validation experiment.

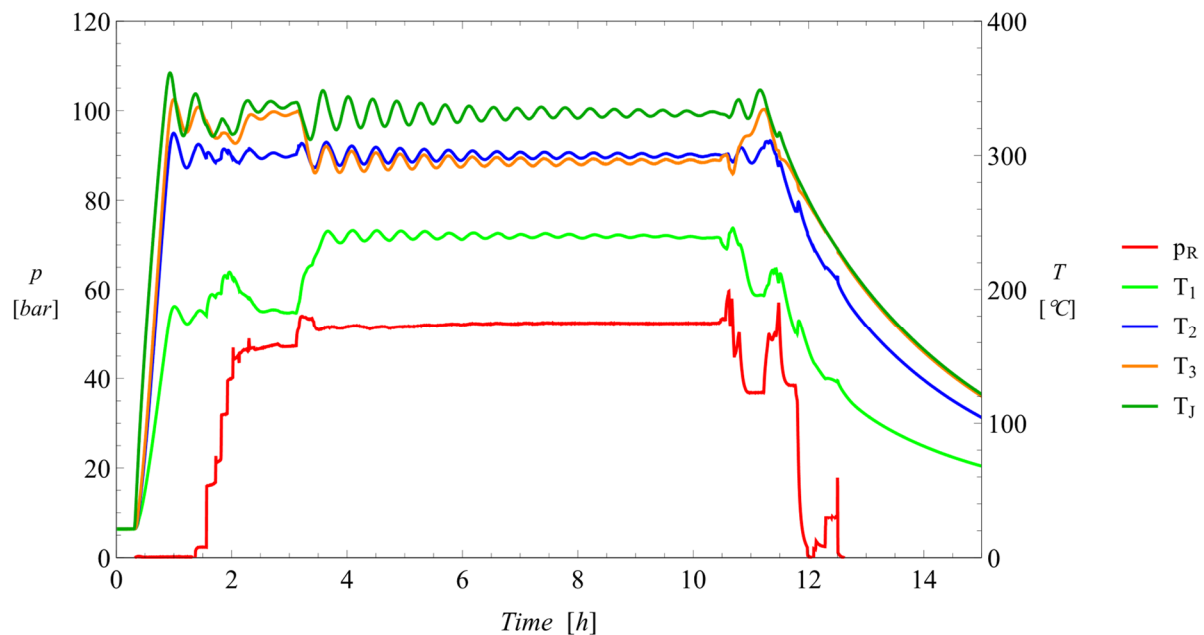


**Figure 25:** Temperature and pressure data of the validation experiment. Preheating of the system is followed by pressurization with hydrogen. As  $\text{CO}_2$  is added to the feed stream, the final pressure and temperatures establish. After several hours the catalyst bed clogs and the experiment has to be terminated.

To assure a preferably pure hydrogen atmosphere in the plant and to test the permeability of the catalyst bed, a hydrogen flow of  $\dot{V}_{\text{H}_2} = 15 \text{ Nml/min}$  is established. Similar to the activation process, the set-temperature is adjusted to  $T_{2,\text{Set}} = 300 \text{ }^\circ\text{C}$  and the heating process begins. After  $T_2$  reaches  $T_{2,\text{Set}}$ , the MFC controlled hydrogen flow is shut off and the bypass valve opened to pressurize the system. During pressurization, an increase of  $T_1$  can be observed, although the heater temperature  $T_{\text{Heat}}$  is not increasing. From now on, only hydrogen is present in the system and an activation of catalyst particles, which were not activated before, seem possible, while a synthesis reaction can be excluded due to the lack of carbon dioxide. Furthermore, the temperature increase might be caused due to the increased volumetric flow rate, bringing more hot gases from the areas of  $T_2$ , respectively  $T_3$  to the temperature sensor which measures  $T_1$ . After the control valve is closed, a hydrogen flow of  $\dot{V}_{\text{H}_2} = 30 \text{ Nml/min}$  is established. As the pressure levels out at  $p \cong 47 \text{ bar}$ ,  $T_1$  drops while  $T_3$  rises. This might be

the result of the changed volumetric flow rates. Less fresh and respectively colder fluid in the top section allows its temperature ( $T_3$ ) to increase, while at the same time a smaller flow of hot gases decreases the reactors bottom temperature  $T_1$ . The controlled temperature  $T_2$  is held constant by the process controller, respectively the controlled heater power. After approximately 40 minutes the synthetization is started by adding a  $CO_2$  flow  $\dot{V}_{CO_2} = 10 \text{ Nml/min}$  as well as a nitrogen flow  $\dot{V}_{N_2} = 5 \text{ Nml/min}$ . Pressure rises rapidly, caused by the increased flow resistance of the catalyst bed due to the increased volumetric flow, stagnating at  $p \cong 53 \text{ bar}$ . Since it seems likely that high pressures increase the compression of the catalyst bed, the pressure retaining valve (PCV – 004) is opened slightly to lower the pressure to  $p \cong 51 \text{ bar}$ . Meanwhile, the  $CO_2$  MFC is struggling to support the desired volumetric flow, which can be solved by increasing its pre-pressure. The increased bottom temperature, compared to the temperature during activation, is rising at the same moment as the other gas streams (namely  $N_2$  and  $CO_2$ ) are added to the system, implying causality between the two events. The increase might be, at least partly, a result of the exothermic synthesis reaction (see equation (28)). The contemporarily happening decrease in the reactors top sections temperature might be caused by the increased volumetric flow rate of fresh, respectively cold gases. As the temperatures in the reactor have not yet reached a steady state, a three times repeating increase and decrease in pressure can be noted. After the third node the catalyst bed resistance seems to increase slowly, although the volumetric flow rates have not changed.

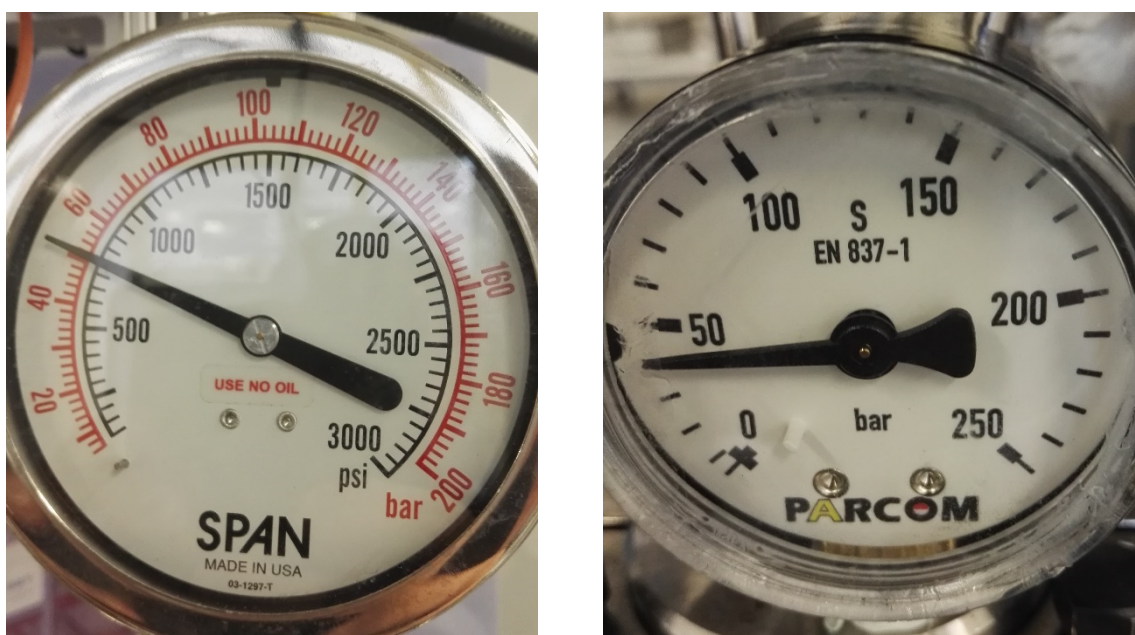


**Figure 26:** Pressures, measured before the reactor (left) and after the reactor (right). The difference results mainly out of the pressure drop across the packed catalyst bed.

After a reaction time of approximately 7.5 hours, a slight increase in pressure, followed by a drastic one, occurs. To prevent a further increase in pressure and a therefore unwanted compression of the catalyst bed, the gas flows are shut off. As the pressure drops immediately, another attempt with lower volumetric flow rates, which results again in a rapid rise of pressure, is conducted. With all MFCs shut, the system stabilizes at a pressure of  $p \cong 36.8 \text{ bar}$ . Since the pressure after the catalyst bed is now smaller compared to previous synthesis conditions, another attempt is made. The idea is that a decreased pressure in combination with a more compressed catalyst bed, and a therefore higher-pressure resistance, will lead to similar total pressures. As the volumetric flows are set with the MFCs, constant pressure of  $p \cong 50 \text{ bar}$  seems to establish. After  $t \cong 8 \text{ min}$  the pressure increases once more to a maximum of  $p \cong 56 \text{ bar}$ . The MFCs as well as the heater unit are shut off and the expansion of the system is initialized. After depressurization is finished, the system is left to cool down.

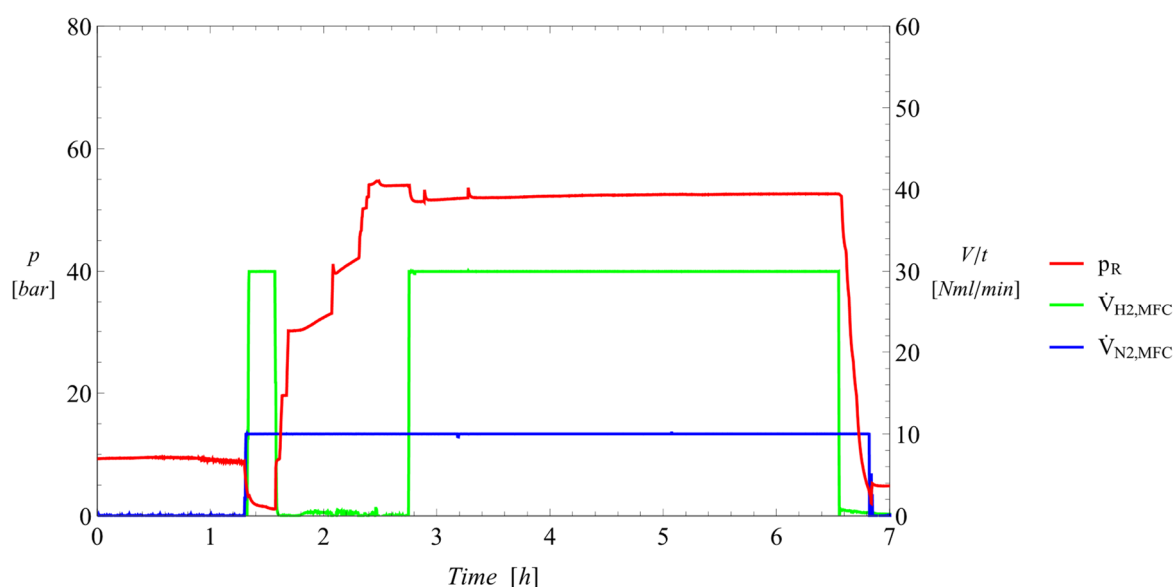


**Figure 27:** Rinsing is followed by manual pressurization.  $\text{CO}_2$  and  $\text{N}_2$  are added, synthesis is started, and the system is left approaching steady conditions. At  $t \cong 11 \text{ h}$  clogging of the catalyst bed occurs. A second attempt results also in clogging and the experiment is terminated.

Prior to the opening of the product vessel, the system is rinsed with  $\text{N}_2$  to displace all  $\text{H}_2$ . The pipes, connected to the product vessel, are disconnected and the vessel opened. The condenser is disconnected as well and flushed with nitrogen, in order to assure that the entire liquid will be collected. On the ground of the beaker a small amount of liquid, from which samples are taken using a syringe, is found. The liquid samples are analyzed in a GC-2010 Plus of the manufacturer Shimadzu, using a Zebron ZV-WAXplus™ column.



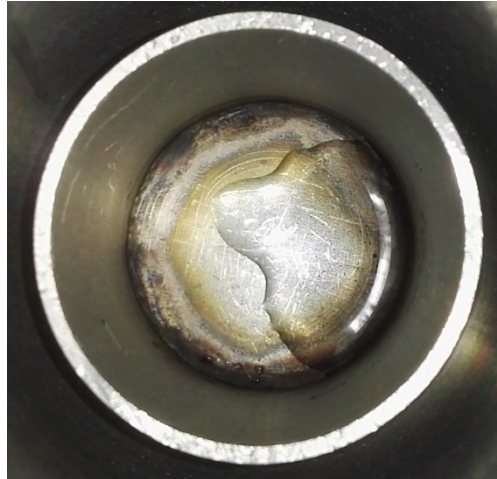


**Figure 28:** Metal beaker with formed liquids in the product vessel, opened after the end of the validation experiment

At the time at which the produced liquid is analyzed in the GC, no calibration curve for such a small concentration range is available and therefore only a quantitative evidence according to the detected peaks can be made. The PFR lab scale plant as well as the self-made  $Cu/MgO$  catalyst, respectively their function, are therefore proven, laying the basis for future investigations.

#### 4.2.5 Optimization and future improvements

The lab scale PFR plant is a proofed platform for future experiments but different modifications and improvements seem reasonable. Before catalyst research can be performed on the validated lab scale PFR plant, different improvements have to be implemented. These improvements include:

- Catalyst characterization
- Reproducible experiments with quantitative balancing
- Minimization of the needed time for each experiment

For the comparison of experimental data, gained from different experiments, the used catalysts must be characterized. Such a characterization includes different parameters. Its chemical composition as well as the oxidation state of the present metal must be determined using a suited analysis method such as X-ray diffraction. Performing such an analysis before and after the activation of the catalyst, the amount of reduced metal and as a result, the produced amount of water can be calculated. The knowledge about the so determined amount of water is crucial for the determination of the actual methanol yield in the liquid products. X-ray



diffraction can also be used to evaluate the impact of longer experiments on the catalyst's composition. In addition to its chemical composition, further properties are of interest. The catalyst's porosity and bulk density must be determined. A simple method which allows the calculation of the bulk density is to weigh a cylinder of known volume, fill it with the coarse catalyst and weigh it again. From the known volume and the mass difference, respectively the catalyst mass, the bulk density can be calculated as:

$$\rho_{Bulk} = \frac{m_{Cat}}{V_{Cylinder}} \quad (33)$$

For the determination of the catalyst porosity as well as its specific surface area,  $N_2$  physisorption must be performed [12]. By implying the simplification that the volumetric flow rate is not changing and known, since the volumetric feed stream is set by the *MFCs* another important parameter, the residence time  $\tau$ , can be calculated.

$$\tau = \frac{m_{Cat} * \varepsilon}{\rho_{Bulk} * \dot{V}_{Feed}} \quad (34)$$

Prior to these measurements, the upper and lower limit of catalyst's particle size must be defined. Here two different thoughts must be kept in mind. On one side, small particles are desired, resulting in a very large specific surface area, on the other side, small particles will clog the catalyst bed. Clogging of the catalyst bed goes hand in hand with a drastic pressure increase, prior to the catalyst, finally leading to a breakthrough, destroying the catalyst bed. The destroyed catalyst bed, respectively the catalyst particles, contaminate the downstream section including the produced liquids and disable their usability for analysis. Too large particles on the other hand result in a smaller specific surface area but bigger bulk porosity, which is favorable for the fluid flow through the catalyst bed, but unfavorable for the synthesis reaction. By performing experimental series with different upper and lower particle size diameter boundaries, a suited size must be determined. The flow resistance of the then installed catalyst bed can be monitored by installing an additional pressure transmitter in the product vessel. Comparing the measured signals of both pressure transmitters at constant volumetric flow rates, respectively the measured difference in pressure, clogging behavior of the catalyst can be monitored.

Regarding the control of the experiments, respectively its reproducibility, consistent catalyst bed arrangement is obligatory. Therefore, the filling process, as described in chapter 4.2.4.1

must be followed and complemented. Amounts of  $SiO_2$  spheres as well as the catalyst, respectively their axial extension must be standardized by measuring their distance from the bottom of the reactor, which will be used as the reference point. This assures constant distances, respectively points of temperature measurement, relative to the position of the catalyst bed. Constancy of those positions is crucial when experiments, respectively the measured temperatures shall be compared. Regarding the glass wool, used for catalyst bed fixation, an amount of  $m_{gw} = 0,14 \text{ g}$  is advised. Contemporarily, the market can be screened for an alternative to the glass wool such as some kind of cloth. Such a cloth provides a more evenly support over the whole reactor cross section, minimizing the risk of breakthrough. Furthermore, the proposed modifications for a batch wise operated gas analysis (see *Figure 19*) must be pointed out, since knowledge about the exhaust gas composition is required to determine the steady state of an ongoing reaction. If sufficient funding is available, an upgrade to a (semi-)continuously measuring gas analysis should be considered. The installation of an electronically controlled pressure control valve would be beneficial for the setups handling and the reproducibility of experiments. At last, the collection of formed liquid should not be performed batch-wise (for a whole experiment) in a beaker, but in constant intervals by opening the valve at the bottom of the product vessel. Hereby water, which is formed during the catalyst activation, could be removed prior to the actual experiment.

As only little liquid was found after an experimental time of over 11 h, the feed stream seems to be quite low at this point. To improve the amount of liquid products while minimizing the time, needed for an experiment, the *MFCs* should be recalibrated for higher throughputs. In addition, higher volumetric flow rates allow a reproducible, computer-aided pressurization process, making the manual pressurization obsolete. A higher frequency of experiments is necessary in order to generate enough data for comprehensive comparisons.

### 4.3 DSTR plant

The second lab scale plant uses a discontinuous stirred tank reactor and is validated using a  $Cu/ZnO/Al_2O_3$  catalyst. In addition to the performed validation experiments and the documentation of the plant, optimization experiment data can be found in this chapter.

#### 4.3.1 Working principle and build up

As a second lab scale plant, a batch wise operated reactor system is built. The present lab scale plant, which is an extended version of a classic DSTR reactor, aims on manipulating the

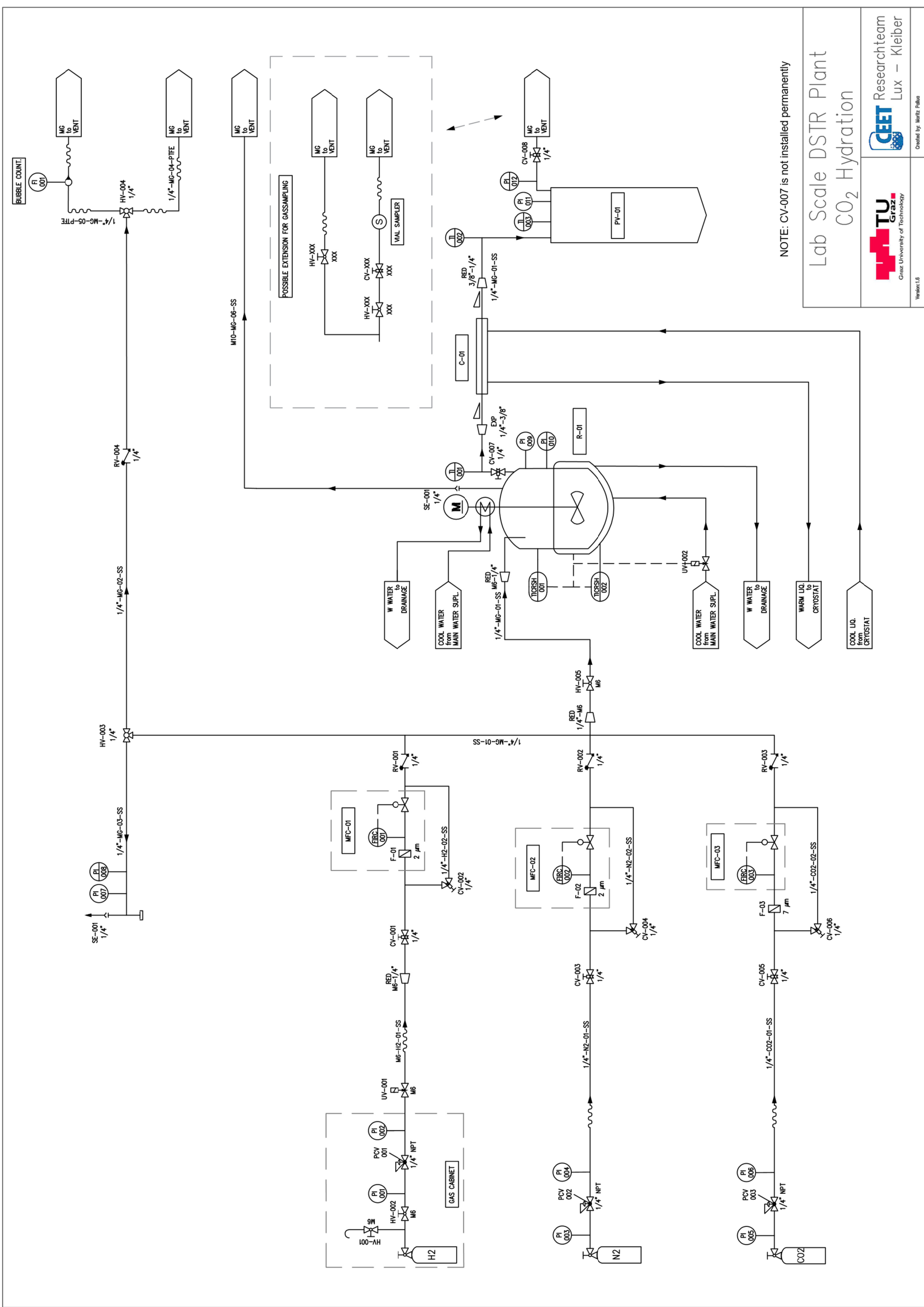
formation of the reaction equilibria. This is done by the removal of products, introduced due to a vaporous product flow from the reactor to the condenser in combination with the permanently present gas diffusion. The convective gas flow originates in the volume contraction due to condensation, as well as common diffusion. The catalyst containing DSTR is pressurized with gases, heated and stirred. Vaporous products, formed by the reactions on the catalysts surface, rise through the rising pipe and condensate in a condenser. The liquid is separated from the gas stream in the following product vessel. Gases leave the product vessel through a top positioned valve to the exhaust fan. Formed liquid, present in the product vessel, is analyzed in a GC. The implementation of a system to analyze the exhaust gases, or rather their composition, is an optional possibility for future work. All piping and instrumentation used for the lab scale batch plant, can be seen in the P&ID in *Figure 29*. Similar to the PFR-plant, the system's main parts are the gas supply, the reactor, a condenser and a product vessel.

Regarding the batch plant's gas support, the same flasks and MFC's as for the PFR lab scale plant are used. Since both plants are placed in different experimental boxes, slight differences regarding the gas supply are present. The gases, supplied in 1/4" piping from the gas flasks, can either be sent through MFCs or via their bypass piping. The batch plant does not aim at a continuous operation mode. Therefore, pressurization of the system is the most important task for the gas supply. As the MFCs do only support small volumetric flow rates, the bypass control valves are used for pressurization. Gases leaving the MFC/bypass section can either be sent in vents' direction or out of the PFRs to the batch plant's box, using the three-way valve *HV – 003*. Gases sent to the vent can then either flow through a dip tube to visualize the gas flow, or, in case of high gas flows, directly to the exhaust vent. A pressure indicator and the transmitter allow pressure measurement in those parts of the system, which are located in the PFR's box. Furthermore, a rupture disc is installed as a safety measure. The piping, leading to the batch plant, can be interrupted using an installed ball valve. A *BüchiGlassUster®*'s Limbo, in combination with an electrical heating jacket, is used as a stirred tank reactor. Here activation, as well as the methanol synthesis reaction, are performed. Therefore, the catalyst is placed in the reactor, the system is pressurized with gas and finally heated to reaction temperature. Depending on the type of experiment (activation or synthesis), either pure hydrogen or hydrogen as well as carbon dioxide are used. To improve the contact between gases and catalyst surface, a turbine stirrer in combination with a hollow axel is installed in the reactor. While the turbine stirrer pushes fluid in radial direction, an under-pressure is noticeable

at the outlets of the hollow axel. Fluid is therefore sucked from the reactor to the upper inlets of the hollow axel, through its inner down to the outlets and again out into the reactor. Since conventional mechanical coupling is not possible due to high system pressures and the need of gas tightness, magnetic coupling is used. The magnetic coupling is cooled with tap water, to avoid the magnets from exceeding their designed operating temperature. This would result in a decrease, or in the worst case in the irreversible demagnetization of the magnetic coupling. In the reactor the temperature is measured, which can be increased using the electric heating jacket. For cooling and prevention of thermal runaway, the water cooling, which is integrated in the heating jacket, is used. Products, formed on the catalyst surface, rise as vapor through the rising pipe to the condenser. The rising pipe is necessary to establish a sufficient slope of the condenser, allowing the condensed liquid to flow to the product vessel. As mentioned in chapter 4.1.4, a jacket tube cooler with an inner diameter of 3/8" and an outer diameter of 3/4", manufactured in SS316, is used. The cooling liquid isopropanol is re-cooled by the cryostat to 2 °C. In the product vessel, liquid flows through a vertical tube into a beaker. To depressurize the system and to therefore avoid high gas streams, the control valve CV – 008 is carefully manually opened. Regarding the quantification of formed products, the whole batch scale plant must be dismantled. The condenser and other tubing are disconnected from the product vessel. The vessel, as well as the reactor, have to be opened and liquid samples can be taken using a syringe.

#### 4.3.2 Process control

Regarding the monitoring and control of the batch scale plant, different instruments are used. Gas feeds can be added to the system by using the same software and process controller as described in chapter 4.2.2. The DSTR's process controller is supplied by the same manufacturer as the reactor itself. It consists of two controller sub units, one for the temperature control and one for the stirrer's control. The temperature control unit *btc 02* has three temperature sensor inlets at its disposal. One sensor, *TICRSH – 001*, measures the temperature in the reactor  $T_R$ , while the second sensor, *TICRSH – 002*, is placed in the inside of the reactor's heating jacket and is further noted as  $T_J$ . The last sensor is a safety temperature sensor, used to avoid too high temperatures and is also located in the heating jacket. A list of all sensors can be found in *Table 4*.



NOTE: CV-007 is not installed permanently

Lab Scale DSTR Plant  
CO<sub>2</sub> Hydration



Researchteam  
Lux – Kleiber

Created by: Moritz Pfaller

Figure 29: P&ID of the lab scale DSTR setup.

**Table 4:** List of all instruments which are either connected to the Parr Instrument's® process controller, the BüchiGlassUster® process controller or to the National Instruments® hardware. The MFC arrangement is the same as for the PFR plant and they are therefore not listed again.

Tag	Type	Function	Position
PI-008	Pressure transmitter	Logging pressure	Before the reactor
PI-010	Pressure transmitter	Logging pressure	In reactor
PI-012	Pressure transmitter	Logging pressure	In product vessel
TICRSH-001	Temperature transmitter	Reactor temperature Usable as safety switch high	In reactor
TICRSH-002	Temperature transmitter	Jacket temperature Usable as safety switch high	In reactor jacket
TI-003	Temperature transmitter	Logging temperature	Product vessel

For the temperature control, two different measures are situated in the reactor's jacket, an electric heater and a cooling water loop. For temperature manipulation, a set temperature  $T_{set}$  can be defined directly at the temperature controller. If the temperature shall be increased, the electric heater is supplied with power until the reference temperature reaches  $T_{set}$ . As reference temperature either  $T_R$  or  $T_J$  can be defined. Setting  $T_R$  as reference temperature increases the system's stability with the current controller parameter. If the investigated temperature exceeds the set temperature, cooling water can be sent through the cooling water loop. Therefore, the controller can open the solenoid valve  $UV - 002$ , allowing tap water to flow. In addition to the water cooling, other safety features are available. The process controller *btc 02* allows the definition of maximum allowable temperature deviations, which can be set for  $T_R$ , as well as  $T_J$ . If a measured temperature exceeds or falls below this interval, an acoustic signal sounds. Regarding overheating protection, a maximum allowable temperature can be defined. If this temperature is exceeded, an alarm sounds, an error message is displayed, and

the heating power is switched off. The second controller unit is used to set a rotational speed of the stirrer. It can be varied in a range from 0 to 3000 *rpm*.

To measure and monitor the pressure, two analog manometers and two digital pressure transmitters are available. The pressure transmitter *PI – 009* logs the pressure in the reactor, while *PI – 011* logs it in the product vessel. Both are combined with analog manometers to visualize the pressure present in those vessels on site. In contrast to the previously mentioned temperatures, the pressure instruments are not connected to the process controller but to different *National Instruments*<sup>®</sup> devices. In addition to the pressure transmitters, thermo couples can therefore be installed. A Type-K thermo couple is used to monitor the temperature in the product vessel. Optional thermocouples can be installed if needed: One thermocouple in the top of the reactor's rising pipe for monitoring the temperature of rising fluids, and one thermocouple before and after the condenser to assure that the cooling power is sufficient to cool the through passing fluid streams.

All measured data is logged with a *National Instruments*<sup>®</sup> instrument. A *NI – 9211* module allows the connection of thermo couples and a *NI – 9207* module allows the connection of the pressure transmitter sensors, as well as the collection of signals coming from *btc 02*. Both modules are installed on a *cDAQ – 9188* board, which allows visualization in a customized *LabVIEW*<sup>®</sup> program. The logged data is exportable in form of a .xls file which can be used for evaluation.

### 4.3.3 Pressure test

As mentioned in chapter 4, tightness, or an acceptable leaking rate, must be assured. Therefore, three different approaches are followed:

- $N_2$  test at room temperature
- $H_2$  test at room temperature
- $H_2$  test at elevated temperatures

Note that pressure transmitter data is used to evaluate all pressure tests. Furthermore, local leaks of  $N_2$  can be detected with soapy water, while  $H_2$  leaks are localized using a  $H_2$  gas sensor.

As a first test, the system is pressurized stepwise with nitrogen to pressures over at least 50 *bar*. Therefore, an optional high temperature check valve can be installed after the reactor. The ball valve *HV* – 005 before the reactor, the high temperature check valve *CV* – 007 after the reactor, and the check valve *CV* – 008 after the product vessel are closed. Closing these valves in combination with the pressure measurements in the reactor and the product vessel allows a differentiated statement about the tightness of each equipment. After the valves are closed, a certain time is needed for the system to stabilize. This stabilization can be seen in *Figure 30* as maximum peaks, which decrease to more constant values. Furthermore, *Figure 30* allows a statement about the tightness of the reactor and the product vessel. The different slopes of both pressure curves suggest that in this pressurization experiment the product vessel, or rather the piping between the auxiliary valve *CV* – 007 and the product vessel, was more leaking than the reactor.

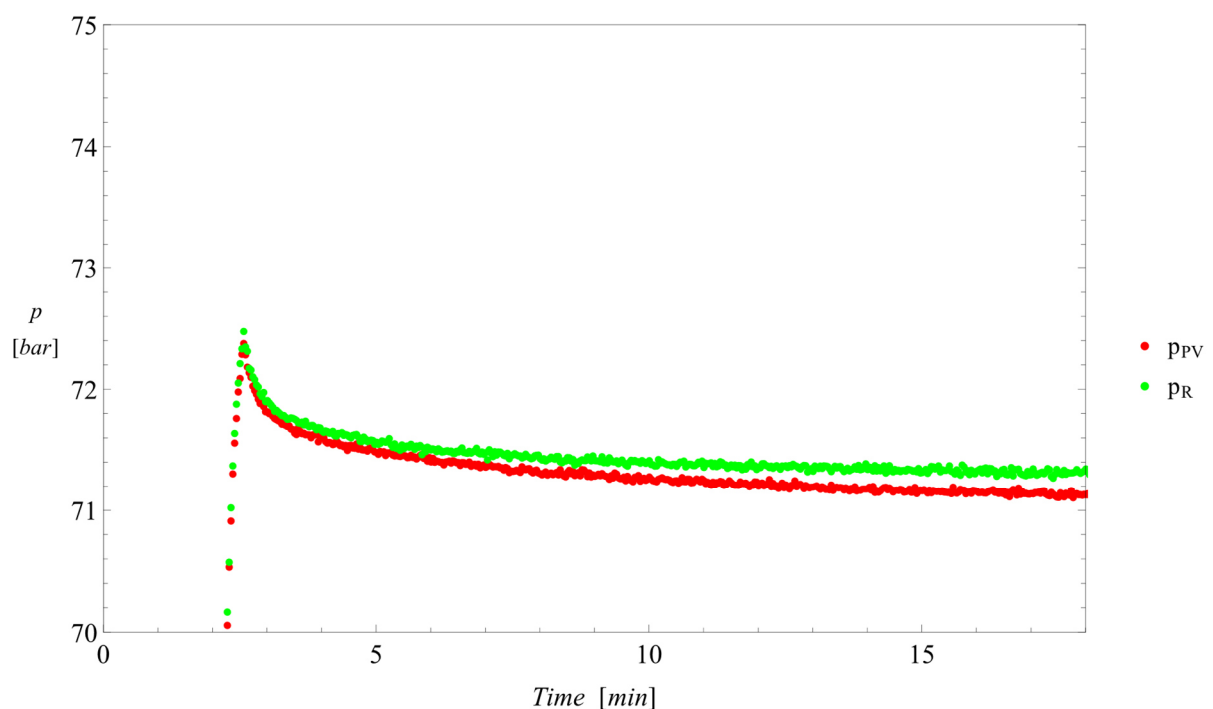


**Figure 30:** Pressure peak after pressurization with different slopes of the reactor- ( $p_R$ ) respectively the product vessel-pressure ( $p_{PV}$ )

Since heavy leaking is very unfavorable, only small pressures are applied at the beginning of a pressure test. If heavy leaking occurs, it can be seen in the pressure over time diagrams. To localize the gas leakage, screwed connections are sprayed with soapy water. If gas leaking occurs, bubbles, as shown in *Figure 31*, are forming.





**Figure 31:** Bubbles of soapy water, caused by leaking gas

As a countermeasure, the connections can be tightened while the system is under pressure. If this measure does not lead to the desired result, the system must be depressurized, the connection unscrewed, cleaned and re-screwed/connected. Since the tightness or the gas flow out of the system are a function of the applied pressure, the pressure is increased stepwise. At each step, every potential leaking spot is tested with soapy water. If the desired maximum pressure is achieved and no significant change in pressure is noted, the system is left under these conditions for several hours, while the pressures are logged over time. Pressure values at different times are noted for an estimation of the leaking gas rates. Knowing the volume of the reactor and the product vessel, including the volume of the connection piping and the condenser, the pre-filled moles of nitrogen can be calculated using *Equation (35)*. For a first estimation regarding the leaking rates the ideal gas law is used. This assumption is a simplification but can be justified, since all calculations are performed at ambient temperatures and moderate pressure. Furthermore, the assumption is made that the system's temperature does not change over time and therefore can be evaluated at room temperature.

$$n_i = \frac{p_i * V_{system}}{R * T_{t_i}} \quad (35)$$

$$V_{t_i} = n_i * V_m(T_{t_i}) \quad (36)$$

$$\dot{V} = \frac{\Delta V}{\Delta t} = \frac{(V_{t_{i-1}} - V_{t_i})}{(t_i - t_{i-1})} \quad (37)$$

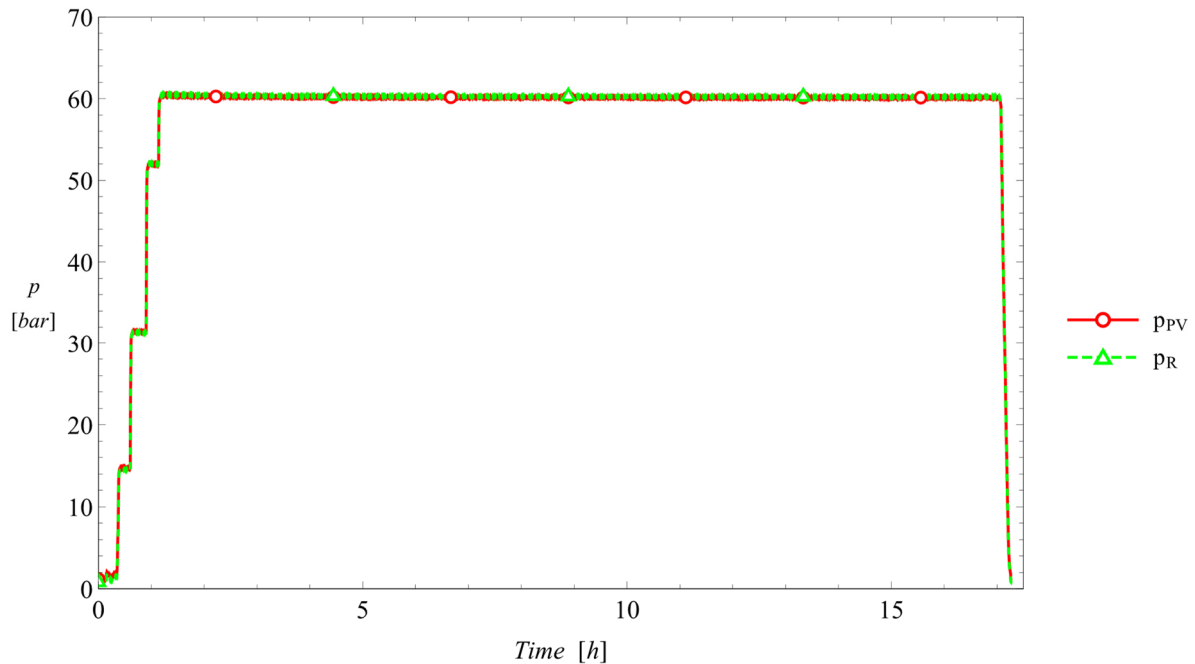


**Figure 32:** Pressure over time curves for a whole pressurization test, using nitrogen

A whole pressure test with all phases, namely the pressurization, the stabilization and pressure test as well as the depressurization can be seen in *Figure 32*. In this pressure test no high temperature valve is installed. Therefore, the evaluation is performed for the product vessel only. As the pressurization is finished, the maximum in pressure is used as the reference point for the pressure test. The initial fast decrease in pressure, as mentioned before, can be observed. After two hours the system seems to have stabilized. Comparing the pressure peak with the pressure before depressurization, a total pressure drop of  $\Delta p_{15h} = 0.2944 \text{ bar}$  in  $15 \text{ h}$  can be observed.

Assuming constant leaking, a pressure drop of  $\Delta p/t = 0.02 \text{ bar/h}$  results in a volumetric flow rate of  $\dot{V}_{leak,0-15h} = 0.36 \text{ mL/min}$  which can be calculated by combining equation (37), (36), and (35). Looking at *Figure 33* in which the product vessel pressure is plotted, the huge decrease at the beginning can be noticed. Afterwards, the pressure is stabilizing and therefore only slightly decreasing.

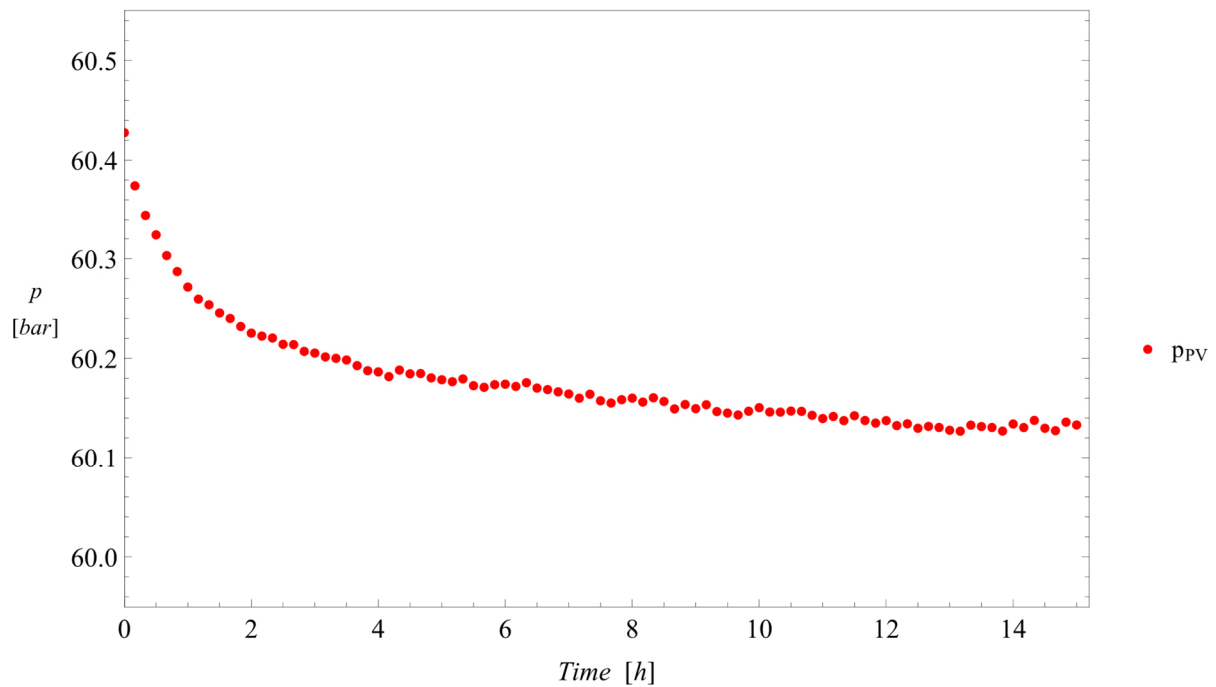


**Figure 33:** Pressure decrease during pressure test with nitrogen including a fast decrease at the beginning and constant decrease after two hours

By plotting the pressure difference, respectively the resulting volumetric flow after every thirty minutes, as visualized in *Figure 34*, one can see that in only 2 hours a drop from  $\dot{V}_{leak,0} = 3.81 \text{ ml/min}$  to  $\dot{V}_{leak,2h} = 0.74 \text{ ml/min}$  is occurring. Assuming that the decrease in pressure until two hours after the valves are shut can be seen as a decrease, occurring during a settling phase, the total pressure difference in the remaining thirteen hours equals  $\Delta p_{2-15h} = 0.1 \text{ bar}$ .

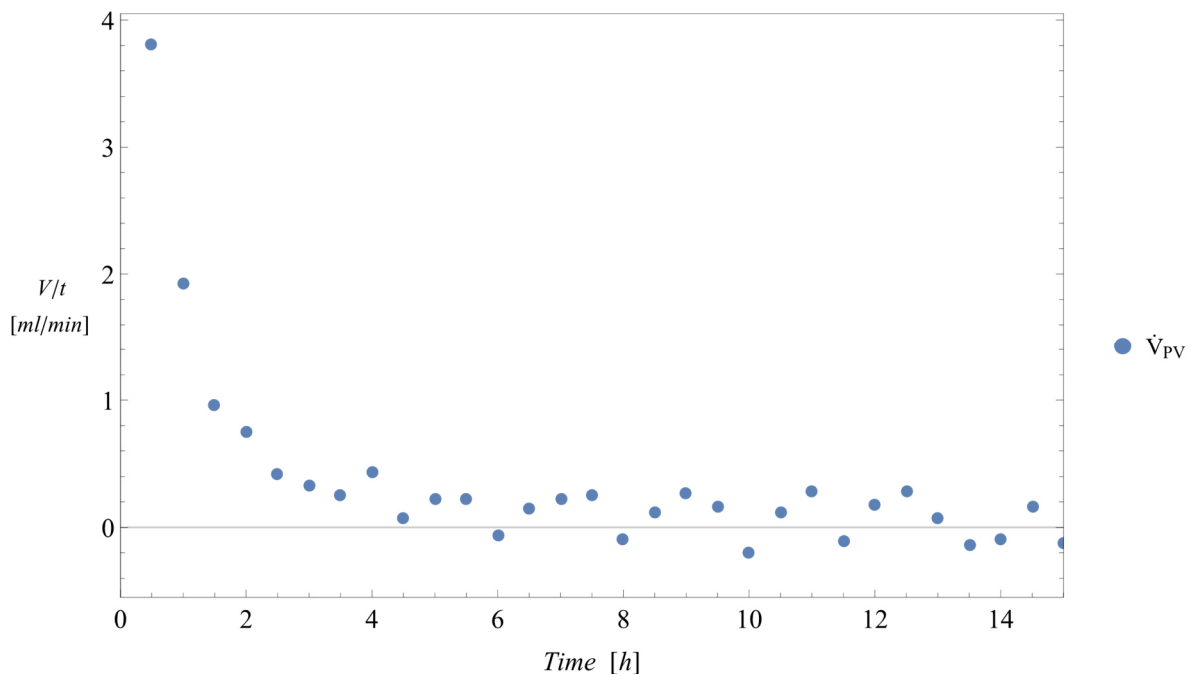


**Figure 34:** Volumetric flow rates calculated from measured pressure data

Such a pressure drop, occurring over 13 hours, equals a volumetric flow rate of  $\dot{V}_{leak,2-15h} = 0.14 \text{ ml/min}$ .

As a next pressure test, the system is pressurized with hydrogen. First, the system is again pressured stepwise to a pressure of at least 50 bar. It is then checked for leakages with a hydrogen sensor and left to rest for several hours as visible in *Figure 35*. Evaluating the mentioned figure, a total pressure drop of  $\Delta p_{21.5h} = 0.249 \text{ bar}$  in 21.5 h can be observed. Such a pressure drop results in a volumetric flow rate of 0.213 ml/min.

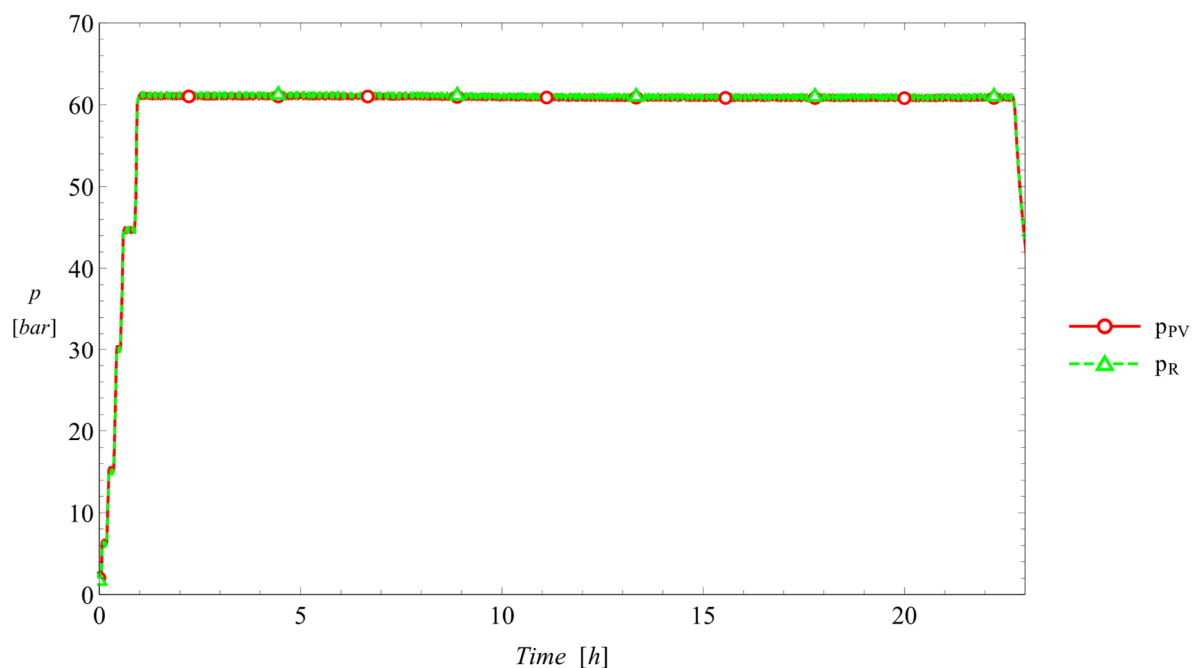


**Figure 35:** Pressure test using hydrogen without heating

As the reactor's top section is united with the bottom section in the same way as a flange, increased temperatures, or rather their influence on the material's properties, must be considered. Therefore, the same temperatures as during activation and the actual experiments are established. At the beginning a hydrogen atmosphere with a pressure of about 41.5 bar is established for the last pressure test. Then the temperature is increased stepwise. The first two steps equal  $\Delta T_{Set} = 100 \text{ }^\circ\text{C}$  while the latter two are smaller, namely  $\Delta T_{Set} = 50 \text{ }^\circ\text{C}$ . With increasing temperature, the pressure rises. At each  $T_{Set}$ , the reactor temperature is left to stabilize and the whole system is tested with the hydrogen sensor. As no leakage could be found, the pressure test is finished after about two hours, the system is depressurized and flushed with nitrogen.

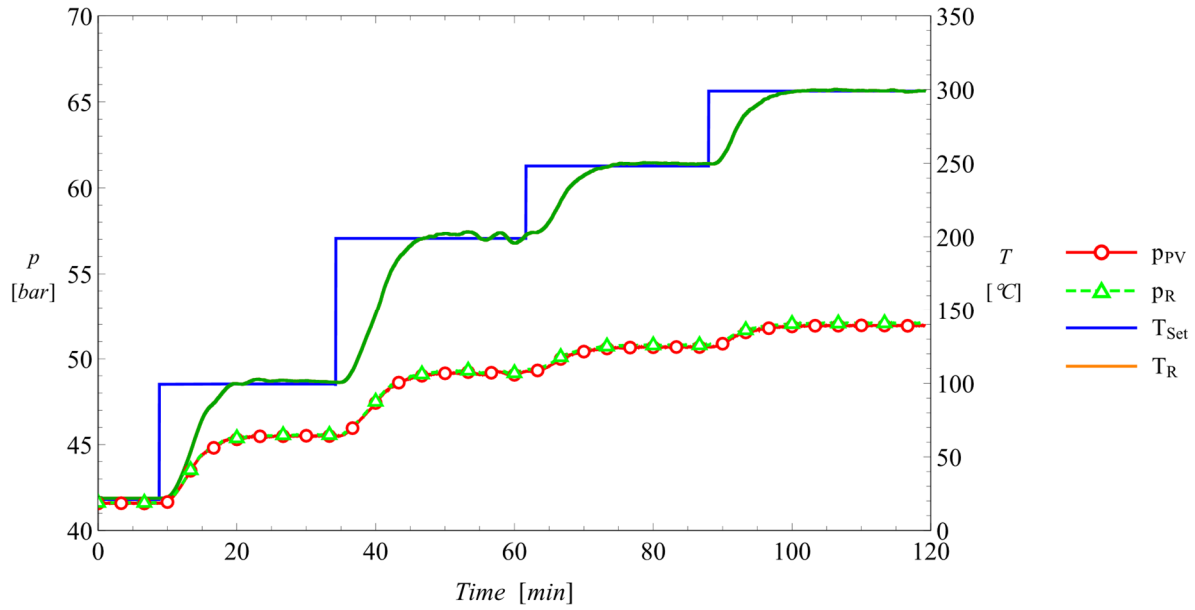


**Figure 36:** Pressure test under increased temperatures using hydrogen. The tightness of the system is tested periodically using a hydrogen sensor.

#### 4.3.4 Risk assessment

For a better understanding of different leaking rate scenarios, area classification, according to EN-60079-10 (2009), is performed. Therefore, data from the pressure test with nitrogen, as described in chapter 4.2.3, is investigated. By rearranging and combining Equation (35), (36), and (37) to Equation (38), the measured pressure drop, shown as  $\Delta p$ , can be used to calculate the volumetric flow rates of each case.

$$\dot{V}_{leak} = V_m * \Delta n = V_m * \frac{\Delta p * V_{system}}{R * T} \quad (38)$$

Note that in equation (38) the molar volume  $V_{m(25^\circ C), H_2} = 24.464 \text{ l/mol}$ ,  $R = 8.314 \text{ J/(mol * K)}$  and the total volume of the system  $V_{system} = 1.1 \text{ l}^1$ . To dilute such a leakage, the amount of needed fresh air respectively the minimum volumetric flow rate can be calculated using Equation (39).

$$\dot{V}_{fresh, min} = \frac{\hat{G} * T}{k_s * LEL * 293} \quad (39)$$

Where  $\hat{G}$  is the maximum leaking rate in the considered time window,  $T = 298.15 \text{ K}$  and the  $LEL$  (lower explosion limit) in  $\text{kg/m}^3$ . The safety factor  $k_s$  is set constant to 0.25, since in these

<sup>1</sup> The calculation of the system's total volume  $V_{system}$  can be seen in the appendix

considerations the case of a standard occurring leakage, which results in a primary release, is investigated.  $\dot{G}$  represents the leaking flow as a mass flow, which can be calculated from the volumetric flow using equation

$$\dot{G} = \dot{V}_{leak} * \rho_{H_2}(25^\circ C; 1.013 \text{ bar}), \quad (40)$$

where  $\rho_{H_2}(25^\circ C; 1.013 \text{ bar}) = 0.08 \text{ kg/m}^3$ . Furthermore, the *LEL* limit for hydrogen must be calculated, using equation (41)

$$LEL \left[ \frac{\text{kg}}{\text{m}^3} \right] = 0.416 * 10^{-3} * M_{H_2} * LEL [\text{vol}\%]. \quad (41)$$

Using the minimum volumetric flow rate, calculated in Equation (39) in combination with the air changes  $C$  in the experimental box per minute, known from chapter 4.1.6, an effective volume  $V_{zEff}$  of potentially explosive atmosphere can be calculated. A correction factor  $f$ , with values from one to five, considers nonidealities.  $f = 1$  assumes ideal flow conditions of fresh air, resulting at the point of leakage in a homogenous and instantaneous mixing with the leaking gases. For the following calculations  $f = 5$  is chosen, which considers an impeded air flow, caused by piping and equipment in the experimental box.

$$V_{zEff} = \frac{\dot{V}_{fresh,min} * f}{C} \quad (42)$$

The first column in *Table 5* assumes constant leaking over the first two hours, the second column represents the case of constant leaking over the whole time, and column number three assumes constant leaking between  $t = 120 \text{ min}$  and  $t_{end} = 900 \text{ min}$ . In the last column, the maximum leaking rate, namely at the beginning of the recording, is used as the basis for all calculations. Comparing the resulting volumes, huge deviations between the different scenarios can be seen. While constant leakage during the first two hours results in a volume of  $352.67 \text{ ml}$ , a minimized explosive atmosphere of only  $24.75 \text{ ml}$  can be observed during the rest of the experiment. Assuming a constant pressure drop over the whole experiment leads to an explosive atmosphere volume of  $68.47 \text{ ml}$ , which is less than a tenth of the volume resulting out of the maximum leakage rate and represented in the last column. The shape of the zone EN 60079-10-1 suggests a sphere shape for gases at high pressures, for which the release direction is unknown. This applies to the lab scale batch apparatus, since the exact position of the leakage is not known. In case of a leak at the top of the reactor or the product

vessel, a hemisphere shape must be considered. The therefore resulting radii allow a better imagination of how small the potential explosive atmospheres are.

**Table 5:** Measured pressure differences, calculated leaking rates and the expansion of potentially explosive atmospheres for different leakage scenarios

	$t_0$ to $t_{120}$	$t_0$ to $t_{900}$	$t_{120}$ to $t_{900}$	$t_0$ to $t_{30}$
$\Delta p$ [bar]	-0.20	-0.29	-0.09	-0.10
$\dot{V}_{leak}$ [ml/min]	1.86	0.36	0.14	3.81
$\dot{G}$ [kg/min]	1.49E-07	2.89E-08	1.04E-08	3.05E-07
$\dot{V}_{fresh,min}$ [m <sup>3</sup> /min]	1.81E-04	3.51E-05	1.27E-05	3.70E-04
$\dot{V}_{fresh,min}$ [ml/min]	180.62	35.07	12.67	369.96
$V_{z,Theo}$ [m <sup>3</sup> ]	7.05E-05	1.37E-05	4.95E-06	1.44E-04
$V_{z,Theo}$ [ml]	70.53	13.69	4.95	144.47
$V_{z,Eff}$ [ml]	352.67	68.47	24.75	722.35
$r_{hemisphere}$ [cm]	5.52	3.20	2.28	7.01
$r_{sphere}$ [cm]	4.38	2.54	1.81	5.57

An estimation of the required time needed to lower an initial concentration to the *LEL* can be performed using the following equation:

$$t = -\frac{f}{C} * \ln \left[ \frac{LEL * k_s}{X_0} \right] \quad (43)$$

Using equation (43) with the previous parameters and hydrogens *UEL* of 78.5 vol% as the initial concentration  $X_0$ , a needed time of  $t \cong 9$  min can be calculated. According to the *Berufsgenossenschaft Rohstoffe und chemische Industrie (BG RCI)* [44] an explosive atmosphere is considered to be highly dangerous if  $V_{z,Eff} > 10$  l, which, however, none of the above scenarios fulfill. Nevertheless, an explosion might harm people in the near surrounding. Polycarbonate windows are therefore installed to hinder people from being in the nearest surrounding of the reactor. Regarding the area classification, a primary release is defined, since the small leakages are similar to a leakage of a pumps shaft. The availability of the ventilation is taken into account as good, since continuous ventilation is present. Another

consideration regarding the ventilation, is the effectiveness of the ventilation going from low dilution over medium dilution to high dilution. Since leaking gas can be controlled resulting in a stable situation and potentially explosive atmospheres are not persistent for a long time after the end of release, medium dilution can be determined. Evaluating the so determined parameters, a Zone 1 can be determined. The extent of this zone varies from  $r_{Hemisphere} = 2.28 \text{ cm}$  and  $r_{Sphere} = 1.81 \text{ cm}$  for the most favorable scenario to  $r_{Hemisphere} = 7.01 \text{ cm}$  and  $r_{Sphere} = 5.57 \text{ cm}$  for the least favorable scenario. As the zone concept includes restrictions regarding the maximum allowable temperatures in a zone, heat sources must be investigated. For the present Zone 1, the maximum allowable temperature is 80% of the hydrogen's autoignition temperature ( $T_{Auto} = 560 \text{ }^\circ\text{C}$ ), and therefore  $T_{Max} = 448 \text{ }^\circ\text{C}$ . In normal operation, the reactor's heating jacket should be the only source of heat in this setup. As mentioned in chapter 4.3.2, temperature restrictions can be set by using the controller to avoid too high temperatures, and thereby excluding the heater as a possible source of ignition.

#### 4.3.5 Experiments

Before the actual validation of the DSTR based setup can be performed, the  $\text{Cu/ZnO/Al}_2\text{O}_3$  catalyst must be activated. This chapter contains the documentation of all these experiments.

##### 4.3.5.1 Catalyst activation

As described in chapter 4.3.1, catalysts are activated before the actual synthesis experiment can be performed. The unit operation itself is carried out in the same reactor in which later the synthesis reaction will be performed. After the activation of the catalyst, copper oxides should be reduced to pure copper. A catalyst mass  $m_{cat} = 17.17 \text{ g}$  is inserted in the reactor by pouring it through a 1/4" threaded pipe connection at the top of the reactor. Afterwards, the pipe connection is closed using a plug.

The actual measured temperatures and pressures, as well as the defined set temperature (visible in blue) over time for such an experiment, can be seen in *Figure 37*. Pure hydrogen is therefore used for pressurization of the stirred reactor. After a certain pressure is established, all valves are closed and leakage detection, using a hydrogen sensor, as well as monitoring of the pressure over time, is performed. Since the system shows an acceptable tightness at these conditions, the heater is switched on with a set-temperature of  $T_{Set} = 200 \text{ }^\circ\text{C}$ . At the beginning of the heating process, the controller is set to control the jacket temperature rather than the reactor temperature. As mentioned in chapter 4.3.2, overheating of the jacket temperature



triggers an electrical fuse in the controller, leading to interruptions and inconsistencies in the experiment, especially undesirable for data logging and the stability of the controlled temperatures.

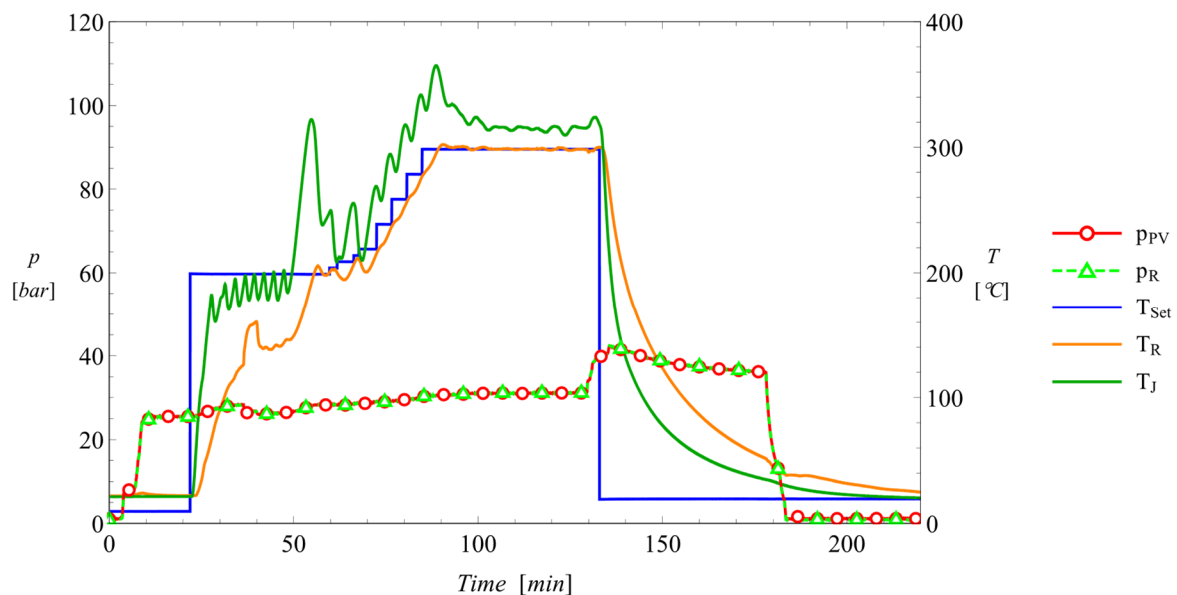


**Figure 37:** First activation experiment using  $\text{Cu/ZnO/Al}_2\text{O}_3$  catalyst. At  $t \cong 40$  min a temperature increase of  $T_R$ , indicating the exothermic activation reaction, can be seen. The Activation experiment is terminated due to a hydrogen leakage after a second pressurization at  $t \cong 133$  min.

With the increase of temperature, a slight increase in pressure can be observed. At  $T_R \cong 130$  °C a spontaneous and fast increase in temperature can be observed. This increase in temperature is an indicator for the presence of an exothermic reaction. As mentioned in 3.3, the reduction of copper oxide with hydrogen is exothermic, leading to the conclusion that this peak shows the actual activation of the catalyst. Since the reactor temperature is stagnating and the jacket temperature oscillates at approximately  $190$  °C  $\pm$   $10$  °C, the target temperature for the controller is changed to the reactor temperature. This event is visible in *Figure 37* as a rapid increase of  $T_j$  at  $t \cong 55$  min. After the system has reached the set-temperature of  $200$  °C, the controller fails to adjust a constant value. The reason for such a behavior could route in the disturbance of the heating process due to the changed target temperature, and the insufficient time given to the system to reach steady state before increasing the set-temperature once more. Strong heating followed by heavy cooling can be observed after the new target temperature is defined, probably leading to an overshoot of the reactor temperature compared to the set-temperature. Such an overshoot can induce instabilities. To deal with the imposed instability and for the salvation of the experiment, the set-temperature is step-wise increased

to the final desired  $300\text{ }^{\circ}\text{C}$ , which can be achieved after another 30 minutes. With the temperature also the pressure levels out at approximately  $31\text{ bar}$ . To assure that no further activation will be carried out through the actual experiment, the pressure is increased by a flow of fresh hydrogen. During this step of the experiment, heavy leaking around the reactor's flange is detected at  $p \cong 42\text{ bar}$  with the hydrogen sensor. Since tightening off the flange and therefore increasing the force on the trapezoidal gasket is not possible while the reactor is installed, the experiment is aborted to prevent further leakage of hydrogen. The reactor is cooled down and opened up to remove the activated catalyst, which is then stored in an airtight container. Solvents are used for cleaning the reactor and the metallic sealing, or rather their sealing surfaces which are then polished. Before the actual validation/methanol synthesis can be performed, complete activation of the catalyst must be assured. Therefore, a second activation experiment, as shown in *Figure 38* is carried out in the pre-pressure tested batch system.

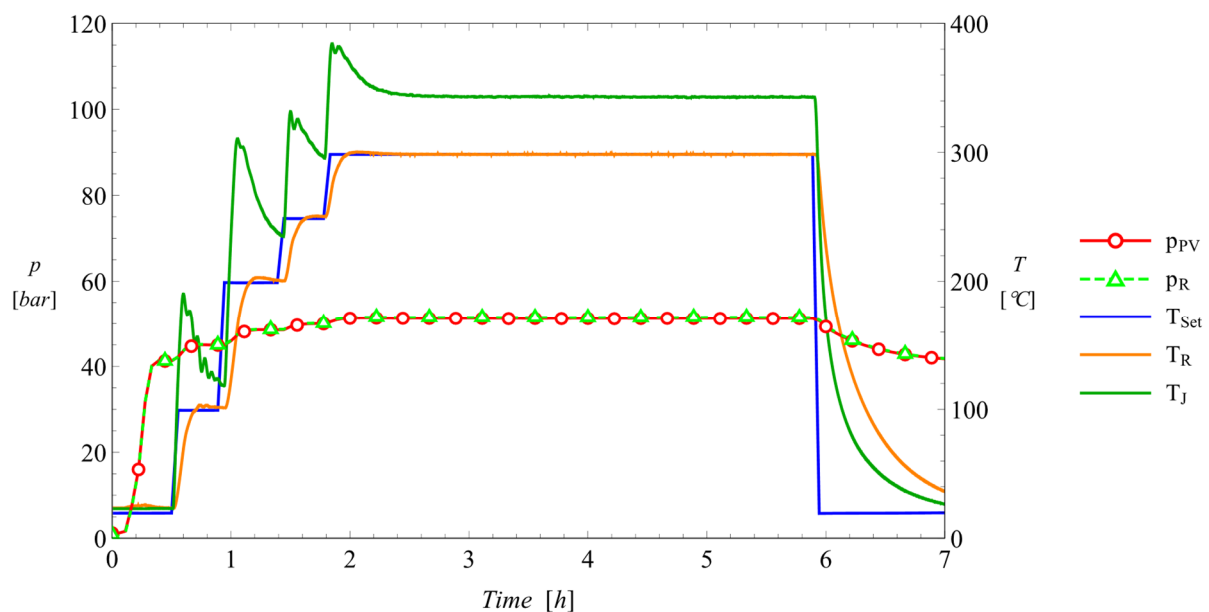


**Figure 38:** Second activation of the  $\text{Cu}/\text{ZnO}/\text{Al}_2\text{O}_3$  catalyst to assure a complete activation

After the catalyst is reinserted in the reactor, the system is pressurized with hydrogen to  $p \cong 41\text{ bar}$  while no heating is applied. Compared to the first activation experiment, the established pressure level at ambient temperature is now higher. This assures that no valve must be opened, respectively no pressurization has to be performed during the heating process, since no more hydrogen is needed. After approximately 20 minutes, in which no remarkable change

in pressure or leakage using the hydrogen sensor is detected, the heating process is initialized. To prevent instabilities in the temperature profile over time, two new approaches are followed:

- The target temperature is always defined as  $T_R$
- The first set temperature is defined as  $T_{set} = 100\text{ }^\circ\text{C}$  instead of  $200\text{ }^\circ\text{C}$

As seen in *Figure 38*, the implemented approaches allow stable heating of the system to the final desired  $300\text{ }^\circ\text{C}$ . With the increase in temperature, also the pressure is rising. Since no rapid or unforeseen rise in temperature occurs, it can be noted that the entire catalyst must have been activated during the first activation attempt. Comparing the temperatures, especially  $T_j$ , to those from the first activation experiment, a more stable heating process can be noted. To minimize the risk of product loss and to ensure that the catalyst remains activated until the actual validation experiment is performed, the system's hydrogen atmosphere with a pressure of  $p \cong 41\text{ bar}$  is untouched and the reactor is not opened.

#### 4.3.5.2 Validation

To validate the functionality of the built batch reactor, methanol must be synthesized. This can be proven by a qualitative analysis of potentially formed products. Therefore, the activated catalyst, as described in the previous chapter, is used in combination with a gas atmosphere, consisting of  $H_2$  and  $CO_2$ . The gases are therefore present in a molar ratio of  $n_{H_2}/n_{CO_2}$  which is approximately three to one. *Figure 41* shows the timeline of all variables of interest. The synthesis experiment's procedure is described in chapter 4.3.1. To assure that liquid reaction products are not evaporated and therefore lost, a small amount of distilled water is pre-filled in a metal beaker, located in the product vessel. Since the system is not opened between the activation experiment and the actual validation, the liquid must be preplaced in the product vessel prior to the activation experiment. As the actual composition of the catalyst, and as a consequence, the amount of water produced during activation, as well as the amount of pre-filled liquid, still present in the vessel after the validation experiment, are unknown, quantitative balancing of the final liquid products is not possible. Furthermore, probable methanol contents, determined with the gas chromatography, can not be corrected, since dilutions are unknown.

At the beginning of the recorded data, the system is still pressurized with hydrogen ( $p \cong 41\text{ bar}$ ) from the previous catalyst activation. For the reaction, a molar ratio of three parts  $H_2$

to one part  $CO_2$  is desired. To simplify the experiment's handling and to minimize the risk of a blow out of the catalyst or the product, the reactor is not completely depressurized. As the control valve is opened to initiate expansion, the temperature in the reactor decreases. The carbon dioxide is then added to the system, pressurizing it to  $p \cong 41 \text{ bar}$  as visible in *Figure 40*. The molar ratio will not be exactly three to one, since the hydrogen atmosphere has already been used in the activation experiment. Furthermore, the manual pressurization is not suitable to adjust precise pressures.

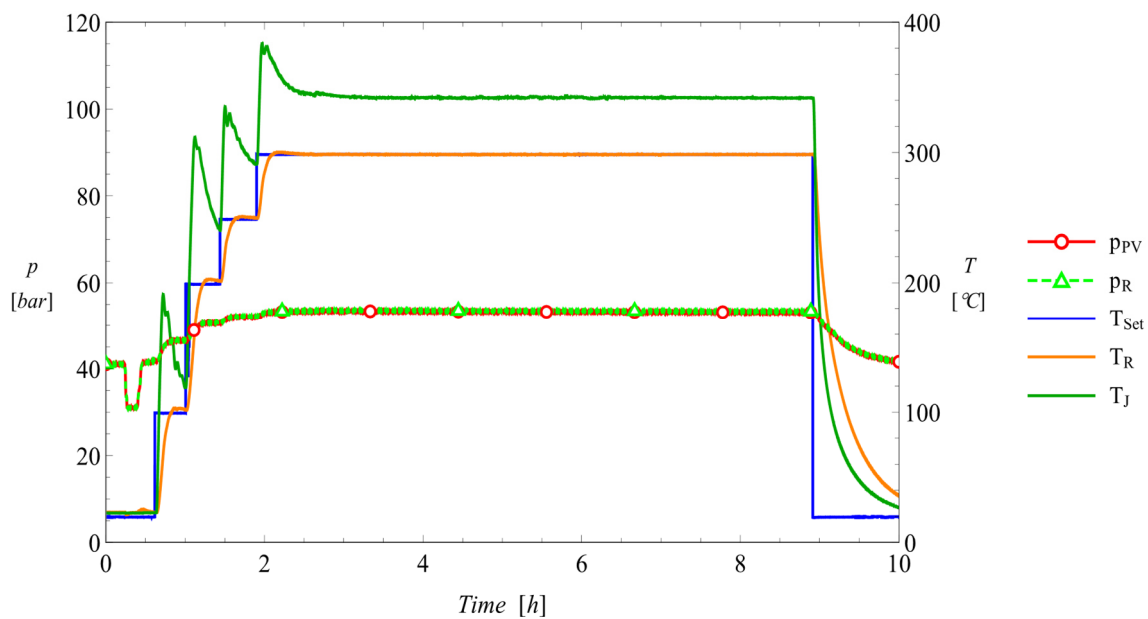


**Figure 39:** Validation experiment data of day one including the molar ratio adjustment, prior to the actual experiment

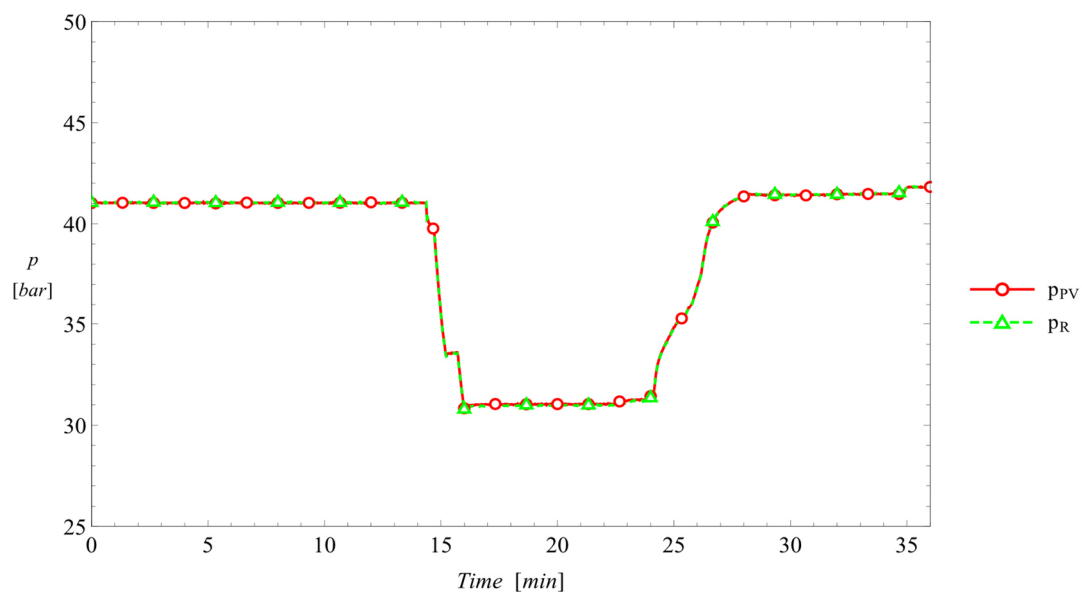


**Figure 40:** Adjustment of the desired molar ratio of  $n_{H_2}/n_{CO_2} = 3/1$  by depressurization, respectively repressurization with  $CO_2$

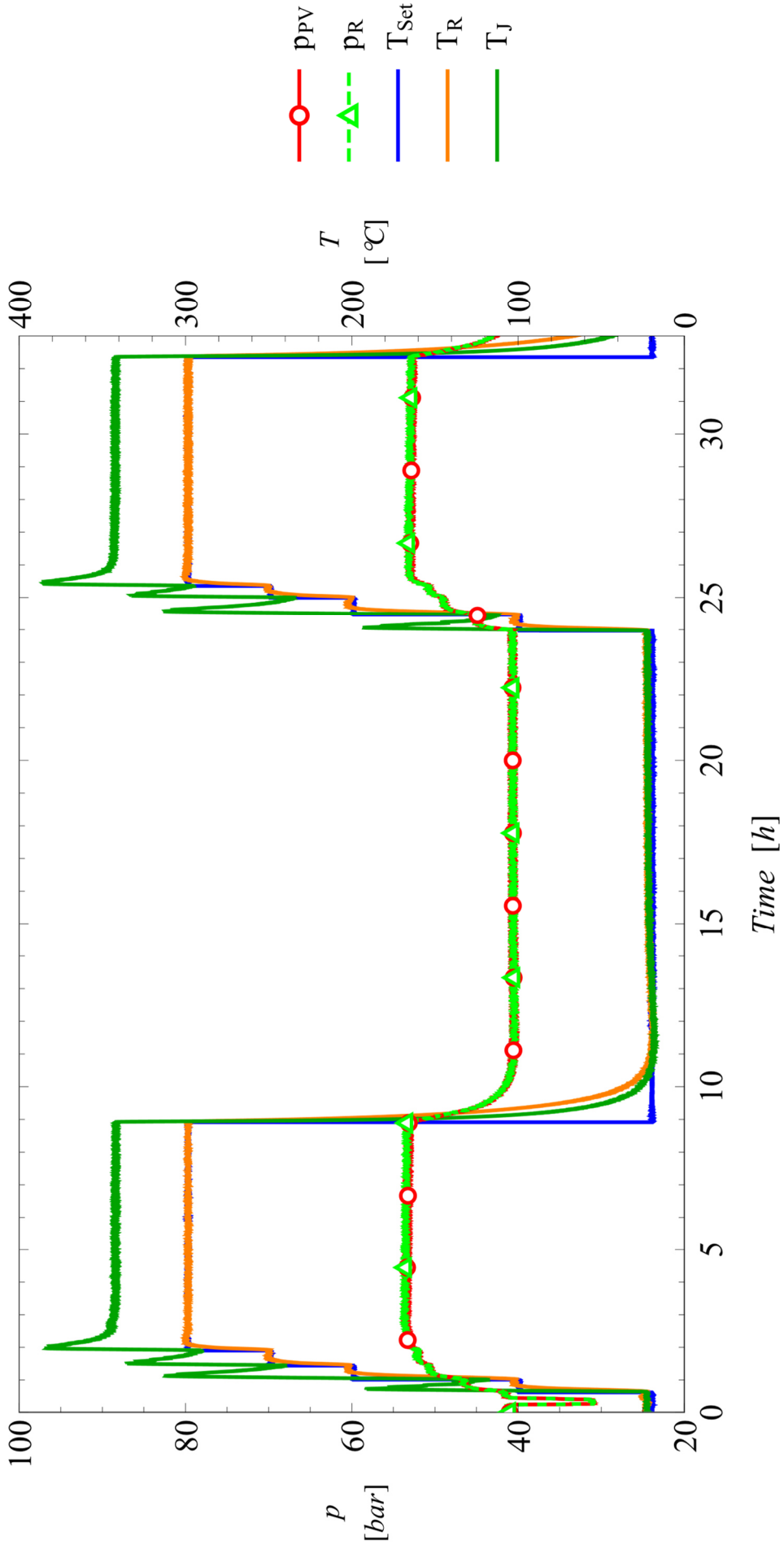


Figure 41: Validation experiment over two days using the Cu/ZnO/Al<sub>2</sub>O<sub>3</sub> catalyst

With stabilized conditions in the lab scale plant, the heating process is performed, using the same procedure as for the activation experiment. As the desired  $T_{R,Set} = 300\text{ }^{\circ}\text{C}$  is reached, the pressure of the system is  $p \cong 53\text{ bar}$ . It is left under these conditions for several hours, allowing the reaction to take place. As described in chapter 4.3.1 the stirrer assures circulation of the gases in the reactor, increasing the mass transfer to and from the catalyst. In the evening, after a reaction time of  $t_{Reaction} \cong 7\text{ h}$ , the water cooler of the reactor is activated by changing the set temperature to  $T_{R,Set} = 20\text{ }^{\circ}\text{C}$ . To prevent unwanted leakage the cooling water is shut off over night, while the cryostat and therefore the support of cooling liquid for the condenser remains on. On the next day in the morning the heater is reactivated, and the same heating procedure performed. The lab scale plant is again left under reaction conditions for  $t_{Reaction} \cong 6.25\text{ h}$ . Afterwards, the system is cooled down and left still until the following morning. The lab scale batch plant is depressurized by opening the control valve  $CV - 008$ , mounted on the product vessel. After depressurization, the condenser is disconnected from the reactor and flushed with nitrogen to ensure that all liquid, present as condensate in the condenser, is found in the product vessel. Opening the product vessel, a small amount of liquid, as well as catalyst particles, can be found. Note that this liquid contains deionized water, placed in the product vessel before the experiments, in order to assure that produced methanol is not evaporating immediately. To separate the solid catalyst particles from the liquid reaction products, a centrifuge is used. Congruent to the sampling during the PFR-validation, the collection of liquid and sample preparation for the GC is performed using a syringe.



**Figure 42:** Humid catalyst particles, coating the stirrer with a thin layer

When opening the reactor, more liquid can be found on the stirrer itself. Furthermore, the catalyst on the bottom of the reactor seems to be moist, probably caused by any liquid, either dropped down from the stirrer or the rising pipe which connects the reactor to the condenser. The walls of the reactor, as well as the stirrer, are coated with a thin layer of very fine catalyst particles. Looking at *Figure 42*, fine particles have accumulated at the stirrer wings. Since the dry catalyst does not stick together, such a behavior implies that the adhered catalyst contains a certain moisture. The catalyst, collected from the reactor, shows a red color, typical for copper. As the nut, which fixes the stirrer in its axial position and divides the reactor from the bearing room is removed, catalyst trickles out. The bearing room contains a considerable amount of finest, moist catalyst powder, which are also coating parts of the axel as well as its plain bearings. It seems likely that a possible secondary flow, introduced by the stirrer in combination with the hollow axel, has pumped fluid as well as particles in the bearing room. Vaporous products, transported by the secondary flow or diffusion to the bearing room, are locally condensing at the water-cooled walls. The fine particles in the liquid product could be the result of this secondary flow, as the particles are milled to smaller sizes by the axel, allowing the fluid stream during the expansion process to transport them through the condenser to the product vessel. Here the bigger ones are separated and found in the liquid product, while the finest fractions leave the product vessel through the control valve to the vent. The presence of solid particles in the exhaust stream is visible in the transparent PTFE-hose, which connects the control valve to the vent.



**Figure 43:** Catalyst coated magnetic axel after the reaction. The visible part is installed in the bearing room section where theoretically no catalyst should be present. The second picture shows the exhaust PTFE-hose. The slight red color is an indicator for the presence of finest catalyst particles in the exhaust gas stream.

The taken liquid samples are analyzed in a *Shimadzu GC-2010 Plus* with an installed *Zebtron ZV-WAXplus™* column. Measurements result in low percentages of methanol, certifying the batch scale plant as well as the self-produced  $Cu/ZnO/Al_2O_3$  catalyst their functionality. As mentioned before, no quantitative result can be noted, since the liquid products are diluted with water from the activation as well as deionized water, preplaced in the product vessel.

#### 4.3.6 Optimization and future improvements

For further research regarding yield, conversion and other characteristics, one must assure the consistency and correctness of the gathered results. Therefore, different experiments are carried out, assuring the detectability of the liquid products and allowing further understanding of the system. Optional additions and improvements of the setup are described as well.

##### 4.3.6.1 Product loss during expansion

Since all liquid reaction products are collected in the product vessel and no continuous sampling of the liquid phase is available, it must be assured that no liquid is lost during the expansion process of the system. To test that, a defined amount of liquid is put in the beaker and placed in the product vessel. The tare of the beaker and the exact amount of water must be weighed beforehand. Then the system is slowly pressurized to a certain pressure with nitrogen (optional increase in pressure by heating), and even slower expanded to ambient pressure. The difference in water mass in the beaker, before and after the experiment, equals the losses caused by the gas flow over the liquid phase.

$$m_{H_2O,After} = m_{Beaker+H_2O,After} - m_{Beaker,Tare} [g] \quad (44)$$

$$\Delta m_{H_2O,Lost} = m_{H_2O,Initial} - m_{H_2O,After} [g] \quad (45)$$

$$m_{H_2O,Regained} = \frac{m_{H_2O,After}}{m_{H_2O,Initial}} * 100 [w\%] \quad (46)$$

As one can see in *Table 6*, almost the entire amount of water can be found after the experiments. The table shows three experiments regarding the liquid discharge from the product vessel without heating, and two experiments where the reactor and therefore the fluid



in it are heated to 300 °C. Comparing the experiments at ambient temperature with those at high temperatures (4 & 5), results in the same range can be observed. Regarding the first experiment, it must be mentioned that in this experiment, a nitrogen stream was applied before the pressurizing of the system. This stream caused splashing of the liquid, so that liquid droplets could be found on the inner product vessel walls. These droplets could not be regained, which explains the comprehensively low percentage of regained water in this experiment. High gas streams are caused by a quick opening of the needle valve after the product vessel, which therefore must be avoided. The expansion of the batch system requires a skilled and patient user to open the needle valve as consistent and slow as possible. Considering the deviations during the procedure of experiment number one, the statement that 99 wt% of the preplaced liquid are findable can be made. Therefore, no significant loss during expansion, of liquid which is located in the product vessel, is occurring.

**Table 6:** Product loss during expansion data

Experiment Number:	1	2	3	4	5
$p_{R,End}$ [bar]	55.15	49.2	54.74	43.57	52.41
$p_{R,Initial}$ [bar]	-	-	-	34.59	41.51
$T_{R,End}$ [°C]	-	-	-	300.00	300.50
$m_{Beaker,Tare}$ [g]	35.2033	35.2040	35.2081	35.2029	35.2033
$m_{H_2O,Initial}$ [g]	5.0700	5.0170	5.0610	5.3292	5.0013
$m_{Beaker+H_2O,After}$ [g]	39.8441	40.1816	40,2378	40.4824	40.1539
$m_{H_2O,After}$ [g]	4.6408	4,9776	5,0297	5.2795	4.9506
$\Delta m_{H_2O,Lost}$ [g]	0.4292	0.0394	0.0313	0.0497	0.0507
$m_{H_2O,Regained}$ [w%]	91.53	99.21	99.38	99.06	98.99

#### 4.3.6.2 Product loss during condensation

For further understanding of the process, the condenser is investigated. To check if the cooling power is sufficient, respectively how much of potentially vaporous products can be regathered, a defined amount of liquid is preplaced in the reactor. The system is pressurized to  $p_R \cong 41 \text{ bar}$  with  $N_2$  and checked for leaks. As no leaks are found, the heating process is started. After  $T_R$  remains at  $300 \text{ }^\circ\text{C}$  for half an hour, the system is depressurized. After the experiment, the difference between the preplaced liquid mass and the regained condensed liquid mass is determined. After depressurization, the product vessel is dismantled, the beaker in the product vessel weighed and the rest of the system flushed to collect liquid which is trapped in the piping and the cooler. The rest of the system is left to cool and opened on the following morning. The differences in liquid mass, weighed before and after the experiment are calculated and used for evaluation.

**Table 7:** Product loss during condensation data

Experiment Number:	6	7
$p_{R,End} [\text{bar}]$	57.15	57.23
$p_{R,Initial} [\text{bar}]$	41.44	41.41
$T_{R,End} [^\circ\text{C}]$	300.14	300.01
$m_{Beaker,Tara} [\text{g}]$	35.2032	35.2006
$m_{H_2O,Initial} [\text{g}]$	5.1051	5.1402
$m_{Beaker+H_2O,After} [\text{g}]$	38.7982	39.0631
$m_{H_2O,Beaker,After} [\text{g}]$	3.5950	3.8625
$m_{H_2O,Other,After} [\text{g}]$	0.5409	0.7477
$m_{H_2O,Total,After} [\text{g}]$	4.1359	4.6102
$\Delta m_{H_2O,Lost} [\text{g}]$	0.9692	0.5300
$m_{H_2O,Regained} [\text{w}\%]$	81.01	89.69

Table 7 shows the results of two experiments. Comparing the regained amount of water to the product loss experiments, one can see a percentual decrease. These results could be caused by different issues. A main difference between the two experimental data sets is the place of liquid placement. While in the product loss experiments, liquid could only be lost due to

bypassing fluid streams, in the latter experiments the liquid had to evaporate, be condensed and “transported” to the product vessel. Due to the cooling of stirrer’s bearings, vapor condenses on the surface of the bearing room’s inner walls. While some of the liquid can be collected and added to the total regained amount, a significant amount remains on the walls due to its surface tension. It is therefore lost and can not be considered in component balances. Another issue may be caused by the rising pipe. During the dismantling of the connection piping and the following flushing, gurgling in the rising pipe, caused by the gas stream passing through liquid, is hearable. This leads to the assumption that the temperature in the rising pipe is not high enough to allow vaporous products to get to the condenser. To encounter the expected issues, further experiments are executed with slightly modified equipment. To assure that no liquid may condense in the rising pipe, an electrical heating strip which heats the pipe to more than 200 °C is applied.

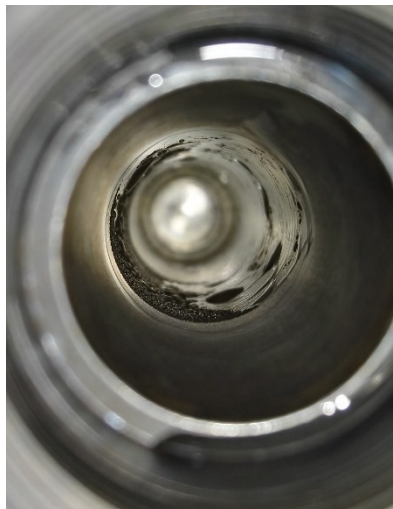


**Figure 44:** View inside the empty bearing room after a re-condensation experiment. The visible liquid droplets at the inner walls of the bearing room cannot be collected. Such a behavior must be considered in future balances.

Regarding the problem of liquid condensing on the inner surfaces of the water-cooled bearing room (as visualized in *Figure 44*), rather tight bearings in combination with a non-hollow axel and propeller stirrer can be installed. In comparison to the original hollow axel and the turbine stirrer, other flow regimes (as described in chapter 4.3.1) apply with this setup. To further improve the amounts of regained water, a bypass heating for the rising pipe is installed and two more experiments are performed. Between these two experiments the rising pipe itself is shortened and thermo couples are installed before the condenser, in the top of the rising pipe,

and after the condenser. Furthermore, the hollow axel and the old stirrer are replaced with a non-hollow axel and a propeller stirrer.

**Table 8:** Product loss during condensation with installed heating of the rising pipe

Experiment Number:	8	9
$p_{R,End}$ [bar]	65.71	56.68
$p_{R,Initial}$ [bar]	41.55	41.66
$T_{R,End}$ [°C]	298.15	294.92
$m_{Beaker,Tara}$ [g]	35.2005	27.7313
$m_{H_2O,Initial}$ [g]	5.2404	5.4279
$m_{Beaker+H_2O,After}$ [g]	38.9080	32.3750
$m_{H_2O,Beaker,After}$ [g]	3.7075	4.6437
$m_{H_2O,Other,After}$ [g]	0.5320	0.2123
$m_{H_2O,Total,After}$ [g]	4.2395	4.856
$\Delta m_{H_2O,Lost}$ [g]	1.0009	0.5719
$m_{H_2O,Regained}$ [w%]	80.09	89.46

Comparing the results in *Table 8*, huge differences in the amounts of water, which is found in other locations than the product vessel, do emerge. As possible reasons for these phenomena different causes seem reasonable. At first, the manipulated rising pipe must be mentioned, which in experiment 9 is shortened, compared to experiment number 8. In addition, there is no proof regarding the temperatures, respectively the effectiveness of the pipe heating, since in experiment number 8 additional thermocouples are not yet installed in the rising pipe. The effectiveness of the current pipe heating is limited because of its temperature range. Furthermore, it might be possible that the depressurization in experiment number 8 may have been performed slower, resulting in a lower volumetric air flow through the condenser. This may have resulted in more liquid, staying in the condenser instead of flowing into the product vessel. In experiment number 9, two additional temperature sensors are installed. One in the top of the rising pipe and one after the condenser. Collected data of these sensors show only

little deviation during the entire experiment and imply therefore that enough cooling power is supplied by the cryostat. In comparison to the results in *Table 8*, the experiments without the additional pipe heating, listed in *Table 7*, do not show a huge difference in the regained amount of liquid. This implies that the current pipe heating, as well as the new axel and the stirrer, do not increase the regained liquid mass noticeably. As both measures, the pipe heating as well as the new stirrer and axel, fail to increase the regained liquid amount, it seems likely that with this setup most of the lost liquid remains in the bearing room, condensed to the walls.

#### 4.3.6.3 *Future improvements*

Although the concept of the new lab scale DSTR plant is proven and validated, different issues should be addressed in order to improve the setup's capability. These optimization opportunities can be divided in three categories:

- Catalyst characterization
- Improving the setup's handling properties
- Adaption and addition of equipment

For the catalyst characterization, the same considerations as described in chapter 4.2.5 must be taken into account. This includes the needed knowledge about the catalyst composition, crucial for an estimation of the water amount, produced during the activation process. This is of utter importance since the lab scale DSTR system's opening would require much time, caused by the need for new pressure tests. Opening of the system between activation and synthetization experiments should therefore be avoided. In addition to the knowledge about the amount of formed water during the catalyst activation, sophisticated knowledge is required to account for the liquid, which is lost because of its condensation in the bearing room. Therefore, test series, with the final setup, are advised.

To assure better handling properties and therefore better reproducibility of all experiments, pressurization and depressurization must not be performed manually. The manual actuation of valves and the, therefore, resulting gas flow depend strongly on the operator. Small movements can result in huge flow spikes, which are very likely to occur, since control valves vary in their movement resistance, depending on how much force was applied to close them. More consistent flow rates during pressurization can be obtained by using the mass flow controllers, which therefore must be recalibrated for higher volumetric flow rates. Regarding a

reproducible procedure for de-pressurization, an electric actuated control valve is necessary. In order to deal with the dispersion of finest catalyst powder, an immobilization of the catalyst and/or the usage of bigger particles in combination with a non hollow axel should be considered. The immobilization could be achieved by the introduction of a catalyst basket.

Finally, different constructive additions should be considered. One addition may be the exchange of the reactor lid to another model, which is equipped with larger connection tubing. Larger diameters should be beneficial for the, in this work tested, approach, allowing increased/less hindered fluid flow to the condenser. At last, new tubing from the product vessel to the reactor in combination with a displacement pump is suggested to establish a recycling stream. Such a recycling stream allows to investigate the impact of the new setup furthermore, as experiments can be performed which aim on the total conversion of fed reactants.

## 5 Conclusion

The main purpose of this work is to implement two different lab-scale reactor systems and test a new  $Cu/MgO$  catalyst as a basis for future research. Therefore, three different tasks are mastered:

- The preparation and validation of a new  $Cu/MgO$  catalyst for methanol synthesis
- The assembly of a therefore suitable lab scale PFR plant
- The assembly and validation of a new DSTR based concept

The idea for the  $Cu/MgO$  catalyst origins in promising results of a bifunctional  $Ni/MgO$  catalyst, used in the methanization of  $CO_2$  [7, 8]. *Loder et al.* were able to reach  $CO_2$  conversions of up to 87% and selectivity for methane  $\geq 99\%$ . This suggests that a combination of a suitable active species such as  $Cu$ , which is very selective for the formation of methanol, with  $MgO$  is suitable to address the challenges in the hydrogenation of  $CO_2$  to methanol. In addition to the results of *Loder et al.* studies show that classical  $Cu/ZnO/Al_2O_3$  catalysts benefit if  $ZnO$  is substituted with  $MgO$  [35]. The catalyst preparation is performed similarly as described by *Loder et al.* The impregnation of  $MgO$  with dissolved  $Cu(NO_3)_2$ , aims for a  $Cu/Mg$  ratio of 3/1. Preparation includes washing- as well as calcination- and activation-steps. For the activation and validation of the formed catalyst, a lab-scale PFR system has to be built and tested.

Before the actual activation and validation of the catalyst in the newly built setup, pressure tests are performed, to assure appropriate safety during the actual experiments. Therefore, the system is pressurized with  $N_2$  at room temperature,  $H_2$  at room temperature,  $H_2$  at reaction/activation temperature (300 °C), and the pressure data logged over time. Leakages are located by soapy water and a  $H_2$ -sensor. The evaluation of the gained data results in a leakage rate of  $\dot{V}_{PFR,Leakage} = 0.10 \text{ ml/min}$ , attesting the system an adequate tightness. Nevertheless, it must be mentioned that the reactor connection fittings have to be tested before each future experiment since they must be disconnected in order to fill or empty the catalyst.

For the activation and the validation experiments, the catalyst has to be installed according to a special procedure (see chapter 4.2.4.1) in the reactor. This is achieved with the use of glass spheres and glass wool ( $m_{gw,top} = 0.14 \text{ g}$  and  $m_{gw,bottom} = 0.13 \text{ g}$ ) as a support to hold the fine catalyst powder in place. A catalyst mass of  $m_{CuMgO} = 2.03 \text{ g}$  with a bulk density of  $\rho_{cat} =$

0.246 g/ml and a particle size smaller than  $d_{p,m} < 600 \mu m$  results in a catalyst bed of approximately 10 cm in height. The so established catalyst bed is activated by a stream of  $\dot{V}_{H_2} = 30 \text{ Nml/min}$  and  $\dot{V}_{N_2} = 10 \text{ Nml/min}$  at  $T_R \cong 300 \text{ }^\circ\text{C}$  and  $p_R \cong 50 \text{ bar}$ . The exothermic activation reaction can be observed, causing an increase in reactor temperature to a maximum of  $360 \text{ }^\circ\text{C}$ . For the validation experiment a feed stream containing  $\dot{V}_{H_2} = 30 \text{ Nml/min}$ ,  $\dot{V}_{CO_2} = 10 \text{ Nml/min}$  and  $\dot{V}_{N_2} = 5 \text{ Nml/min}$  are established at  $T_R \cong 300 \text{ }^\circ\text{C}$  and  $p_R \cong 51 \text{ bar}$ . After a total experimental time of approximately 11 h, a fast increase in pressure indicates that the catalyst bed begins to clog and the experiment has to be aborted. Attempts to restart the experiment are not successful. After the end of the experiment, some liquid is found in the product beaker. Its analysis brings the final evidence, needed for the validation of the self-prepared Cu/MgO catalyst, as well as the built PFR lab-scale plant. As the liquid is found to contain methanol, the validation is successfully complete.

The idea for the implementation of the second, DSTR based lab-scale plant is to investigate the impact of the withdrawal of products during the reaction. Therefore, the DSTR is combined with a condenser and a product vessel. The concept is based on the idea that formed vaporous products will condensate in the condenser, inducing an additional fluid flow from the reactor to the condenser. The withdrawal of vaporous products should hinder the formation of an equilibrium in the reactor. Condensed liquid flows to the product vessel where it is collected and separated from the gas stream.

To minimize the risk during the actual validation experiments, pressure tests, analogous to those for the PFR plant, are performed. This leads to an average leakage rate of  $\dot{V}_{DSTR,Leakage} = 0.13 \text{ ml/min}$ . Additionally, a risk assessment according to EN-60079-10 (2009), is performed, leading to a Zone 1 with an extent of  $r_{sphere} = 1.81 \text{ cm}$ . A time of  $t \cong 9 \text{ min}$  is needed to lower an initial concentration, which equals the UEL, to the LEL.

For the activation and validation experiments, a pulverized Cu/ZnO/Al<sub>2</sub>O<sub>3</sub> catalyst ( $m_{cat} = 17.17 \text{ g}$ ,  $d_{p,m} < 600 \mu m$ ) is used. The activation takes place in a H<sub>2</sub> atmosphere under increased temperature and pressure (up to  $T_R \cong 300 \text{ }^\circ\text{C}$  and  $p_R \cong 50 \text{ bar}$ ). Hereby, a temperature spike can be noted, indicating the exothermic reduction reaction. Because of gas leakages and consequently the abortion of the first activation attempt, a second activation is performed to assure the activation of the whole catalyst. The atmosphere in the reactor during the validation of the activated catalyst is performed in a  $n_{H_2}/n_{CO_2}$  ratio of 3/1 at  $T_R = 300 \text{ }^\circ\text{C}$



and  $p \cong 53 \text{ bar}$ . The reaction is performed over two days and the reactor is shut down and cooled overnight. Combining the experimental times, a total reaction time of  $t_{\text{Reaction}} \cong 13.25 \text{ h}$  can be reached. By opening the product vessel, liquid products can be found which are collected and analyzed in a GC, leading to the result that methanol is present. The exact amount cannot be calculated because of the insufficient knowledge about the water content, either leftover from the preplaced one or formed during the catalyst activation. Additionally, some liquid is present also in the externally cooled bearing room. Furthermore, finest catalyst powder coats the axel in the bearing room and can further be found in the condenser, as well as in the product vessel. Additional experiments have shown that liquid, present in the product vessel, is not carried out during the depressurization of the system (liquid loss  $< 1 \text{ w\%}$ ). First experiments regarding the amount of liquid loss in the bearing room, allow a first approximation, that 10 – 20 w% can not be regained. Modifications of the rising pipe in combination with a pipe heating, as well as the assembly of a new solid axel, do not lead to the desired improvements. Although two challenges regarding the liquid in the bearing room and the catalyst contamination around the system have arisen, the setup and its functionality are validated as the presence of methanol is proven.

By implementing the improvements, described in chapter 4.2.5 investigation of self-prepared catalysts will be possible in the PFR lab-scale plant. Different catalysts (varying in their composition, preparation, particle size distribution, porosity, etc.) can be compared regarding their yield and selectivity for methanol. Furthermore, their performance at different pressures and temperatures, as well as the influence of the residence time or the space-time can be investigated. By performing experiments for a longer time period, statements regarding catalyst endurance and their timely dependent deactivation will be possible. The so gained test results can be used for a statement regarding the potential of copper-magnesia catalysts for large-scale application. The, according to chapter 4.3.6.3, optimized DSTR setup should be further investigated. Therefore, more detailed knowledge about the percentual loss of liquid in the bearing room seems crucial. If this is achieved, the influence of the occurring condensation on the total conversion of a batch can be examined. Additionally, a comprehensive study of the influence of the tubing diameter could lead to interesting results. Finally, the addition of a recycling stream from the product vessel to the reactor could be implemented. Hereby the maximum achievable conversion of all fed reactants, as well as the impact of the condenser, could be investigated.

## 6 References

1. COMMISSION OF THE EUROPEAN COMMUNITIES (2000) Green Paper on greenhouse gas emissions trading within the European Union. (presented by the Commission), Brussels
2. Song C, Liu Q, Deng S et al. (2019) Cryogenic-based CO<sub>2</sub> capture technologies: State-of-the-art developments and current challenges. *Renewable and Sustainable Energy Reviews* 101:265–278. doi: 10.1016/j.rser.2018.11.018
3. Olah GA, Goepfert A, Prakash GKS (2009) Beyond oil and gas. The methanol economy, 2nd updated and enlarged ed. Wiley-VCH, Weinheim
4. Speight JG (2015) 6 - Gasification processes for syngas and hydrogen production. In: Luque R, Speight JG (eds) *Gasification for synthetic fuel production. Fundamentals, processes and applications*, 1. Aufl. Elsevier Reference Monographs, Amsterdam, pp 119–146
5. Aasberg-Petersen K, Dybkjær I, Ovesen CV et al. (2011) Natural gas to synthesis gas – Catalysts and catalytic processes. *Journal of Natural Gas Science and Engineering* 3:423–459. doi: 10.1016/j.jngse.2011.03.004
6. Bertau M, Offermanns H, Plass L et al. (2014) *Methanol: The Basic Chemical and Energy Feedstock of the Future*. Springer Berlin Heidelberg, Berlin, Heidelberg
7. Baldauf-Sommerbauer G, Lux S, Aniser W et al. (2018) Steady-state and controlled heating rate methanation of CO<sub>2</sub> on Ni/MgO in a bench-scale fixed bed tubular reactor. *Journal of CO<sub>2</sub> Utilization* 23:1–9. doi: 10.1016/j.jcou.2017.10.022
8. Loder A, Siebenhofer M, Lux S (2020) The reaction kinetics of CO<sub>2</sub> methanation on a bifunctional Ni/MgO catalyst. *Journal of Industrial and Engineering Chemistry* 85:196–207. doi: 10.1016/j.jiec.2020.02.001
9. Levenspiel O (1999) *Chemical reaction engineering*, 3. ed. Wiley, Hoboken, NJ
10. Hagen J (1996) *Technische Katalyse. Eine Einführung*. VCH, Weinheim
11. Kim Aasberg-Petersen, Kim, et al (2008) Large Scale Methanol Production from Natural Gas. *Research|Technology|Catalysts*.  
[http://scholar.google.at/scholar\\_url?url=https://www.researchgate.net/profile/Rick\\_Mannner/post/CO2\\_Hydrogenation\\_to\\_produce\\_methanol\\_model\\_simulation/attachment/59d6](http://scholar.google.at/scholar_url?url=https://www.researchgate.net/profile/Rick_Mannner/post/CO2_Hydrogenation_to_produce_methanol_model_simulation/attachment/59d6)

- 50a279197b80779a963d/AS%253A503928378884096%25401497157296471/download/Topsoe\_large\_scale\_methanol\_prod\_paper.pdf&hl=de&sa=X&scisig=AAGBfm3aZUKUPAqgA07zdDUF-FZtCHMwMg&nossl=1&oi=scholarr. Accessed 28 Apr 2020
12. Ross JRH (2012) *Heterogeneous catalysis. Fundamentals and applications*. Elsevier, Amsterdam
  13. Pontzen F, Liebner W, Gronemann V et al. (2011) CO<sub>2</sub>-based methanol and DME – Efficient technologies for industrial scale production. *Catalysis Today* 171:242–250. doi: 10.1016/j.cattod.2011.04.049
  14. Saeidi S, Amin NAS, Rahimpour MR (2014) Hydrogenation of CO<sub>2</sub> to value-added products—A review and potential future developments. *Journal of CO<sub>2</sub> Utilization* 5:66–81. doi: 10.1016/j.jcou.2013.12.005
  15. Ross JRH (2018) *Contemporary catalysis. Fundamentals and current applications*. Elsevier, Amsterdam
  16. Hagen J (2015) *Industrial catalysis. A practical approach, Third completely revised and enlarged edition*. Wiley-VCH, Weinheim, Germany
  17. Methanol Institute Price, supply and demand of methanol. <https://www.methanol.org/methanol-price-supply-demand/>. Accessed 28 Apr 2020
  18. William H. Day, Longview Energy Associates, LLC (2016) Methanol fuel in commercial operation on land and sea. *Gas Turbine World*
  19. Air Liquide Engineering & Construction (2017) METHANOL AND PROVEN TECHNOLOGIES FOR OPTIMAL PRODUCTION. Accessed 28 Apr 2020
  20. Sheldon D (2017) Methanol Production - A Technical History. *Johnson Matthey Technology Review* 61:172–182. doi: 10.1595/205651317X695622
  21. CASALE METHANOL PROCESS. M3000-M7000-M2000C. OPTIMIZED PROCESSES FOR ANY PLANT SIZE AND FEEDSTOCK. Accessed 28 Apr 2020
  22. Pérez-Fortes M, Schöneberger JC, Boulamanti A et al. (2016) Methanol synthesis using captured CO<sub>2</sub> as raw material: Techno-economic and environmental assessment. *Applied Energy* 161:718–732. doi: 10.1016/j.apenergy.2015.07.067

23. Bock S, Zacharias R, Hacker V (2019) Experimental study on high-purity hydrogen generation from synthetic biogas in a 10 kW fixed-bed chemical looping system. *RSC Adv* 9:23686–23695. doi: 10.1039/C9RA03123E
24. Pontzen F, Liebner W, Gronemann V et al. (2011) CO<sub>2</sub>-based methanol and DME – Efficient technologies for industrial scale production. *Catalysis Today* 171:242–250. doi: 10.1016/j.cattod.2011.04.049
25. Marlin DS, Sarron E, Sigurbjörnsson Ó (2018) Process Advantages of Direct CO<sub>2</sub> to Methanol Synthesis. *Front Chem* 6:446. doi: 10.3389/fchem.2018.00446
26. Din IU, Shaharun MS, Alotaibi MA et al. (2019) Recent developments on heterogeneous catalytic CO<sub>2</sub> reduction to methanol. *Journal of CO<sub>2</sub> Utilization* 34:20–33. doi: 10.1016/j.jcou.2019.05.036
27. Zhao Y-F, Yang Y, Mims C et al. (2011) Insight into methanol synthesis from CO<sub>2</sub> hydrogenation on Cu(111): Complex reaction network and the effects of H<sub>2</sub>O. *Journal of Catalysis* 281:199–211. doi: 10.1016/j.jcat.2011.04.012
28. Dang S, Yang H, Gao P et al. (2019) A review of research progress on heterogeneous catalysts for methanol synthesis from carbon dioxide hydrogenation. *Catalysis Today* 330:61–75. doi: 10.1016/j.cattod.2018.04.021
29. Lei H, Nie R, Wu G et al. (2015) Hydrogenation of CO<sub>2</sub> to CH<sub>3</sub>OH over Cu/ZnO catalysts with different ZnO morphology. *Fuel* 154:161–166. doi: 10.1016/j.fuel.2015.03.052
30. PII: S0926-3373(01)00203-X
31. Saeidi S, Amin NAS, Rahimpour MR (2014) Hydrogenation of CO<sub>2</sub> to value-added products—A review and potential future developments. *Journal of CO<sub>2</sub> Utilization* 5:66–81. doi: 10.1016/j.jcou.2013.12.005
32. Gao P, Li F, Zhan H et al. (2013) Influence of Zr on the performance of Cu/Zn/Al/Zr catalysts via hydrotalcite-like precursors for CO<sub>2</sub> hydrogenation to methanol. *Journal of Catalysis* 298:51–60. doi: 10.1016/j.jcat.2012.10.030
33. Guil-López R, Mota N, Llorente J et al. (2019) Methanol Synthesis from CO<sub>2</sub>: A Review of the Latest Developments in Heterogeneous Catalysis. *Materials (Basel)* 12. doi: 10.3390/ma12233902

34. Angelo L, Kobl K, Tejada LMM et al. (2015) Study of CuZnMO<sub>x</sub> oxides (M=Al, Zr, Ce, CeZr) for the catalytic hydrogenation of CO<sub>2</sub> into methanol. *Comptes Rendus Chimie* 18:250–260. doi: 10.1016/j.crci.2015.01.001
35. Dasireddy VDBC, Štefančič NS, Huš M et al. (2018) Effect of alkaline earth metal oxide (MO) Cu/MO/Al<sub>2</sub>O<sub>3</sub> catalysts on methanol synthesis activity and selectivity via CO<sub>2</sub> reduction. *Fuel* 233:103–112. doi: 10.1016/j.fuel.2018.06.046
36. Joo O-S, Jung K-D, Moon I et al. (1999) Carbon Dioxide Hydrogenation To Form Methanol via a Reverse-Water-Gas-Shift Reaction (the CAMERE Process). *Ind Eng Chem Res* 38:1808–1812. doi: 10.1021/ie9806848
37. Bioenergy International (2019) MHPS Europe and RWE Power commission CO<sub>2</sub> to methanol pilot plant. Accessed 23 Apr 2020
38. Bioenergy International (2019) CRI seals deal for first CO<sub>2</sub>-to-methanol plant in China. <https://bioenergyinternational.com/technology-suppliers/cri-seals-deal-for-first-co2-to-methanol-plant-in-china>. Accessed 23 Apr 2020
39. (2018) OMV's concrete actions to reduce its CO<sub>2</sub> footprint. Brussels, 25 April 2018
40. Seeger M, Otto W, Flick W et al. (2000) Magnesium Compounds. In: Ullmann's Encyclopedia of Industrial Chemistry, vol 10. Wiley-VCH Verlag GmbH & Co. KGaA, Weinheim, Germany, p 129
41. Zhang J, Richardson HW (2000) Copper Compounds. In: Ullmann's Encyclopedia of Industrial Chemistry, vol 64. Wiley-VCH Verlag GmbH & Co. KGaA, Weinheim, Germany, pp 1–31
42. Heterogeneously Catalyzed Hydrogenation of Supercritical CO<sub>2</sub> to Methanol
43. Schröder V (2002) Explosionsgrenzen von Wasserstoff und Wasserstoff/Methan-Gemischen. *Forschungsbericht / Bundesanstalt für Materialforschung und -prüfung (BAM)*, Berlin, vol 253. Wirtschaftsverl. NW Verl. für Neue Wiss, Bremerhaven
44. Losert O (2017) Explosionsschutz aktuell. Sicherheitskräfte-Tagung des Präventionszentrums Nürnberg am 05./06. April 2017 in Deggendorf. [https://www.bgrci.de/fileadmin/BGRCI/Veranstaltungen/Sifa-Tagung\\_Deggendorf\\_April\\_2017/Dr.\\_Losert\\_Oswald\\_-\\_BG\\_RCI\\_Explosionsschutz\\_aktuell.pdf](https://www.bgrci.de/fileadmin/BGRCI/Veranstaltungen/Sifa-Tagung_Deggendorf_April_2017/Dr._Losert_Oswald_-_BG_RCI_Explosionsschutz_aktuell.pdf). Accessed 20 Apr 2020

## 7 List of figures

<b>Figure 1:</b> Energy levels of a catalyzed and an uncatalyzed exothermic reaction (schematically) .....	8
<b>Figure 2:</b> Energy levels of the uncatalyzed reaction as well as a catalyzed path, where the reactants react on the catalyst surface.....	9
<b>Figure 3:</b> Schematic representation of the reaction steps during a heterogeneously catalyzed reaction .....	10
<b>Figure 4:</b> An overview of the world's main consumers of methanol in the year 2018 [27].....	13
<b>Figure 5:</b> Schematic representation of conversion profiles to reach a certain conversion for a series of fixed bed reactors with intermediate cooling (left) and a single tubular boiling water reactor (right) in which the S-shaped curve represents a symbolic equilibrium conversion ...	17
<b>Figure 6:</b> Overview of the global CO <sub>2</sub> emissions from fuel combustion in the year 2017, sorted by sector [21] .....	19
<b>Figure 7:</b> Conversion of CO <sub>2</sub> and selectivity for CH <sub>3</sub> OH as functions of temperature and pressure, calculated with Aspen; Reprinted with permission from Stangeland et. al. [30] .....	20
<b>Figure 8:</b> Two possible pathways for the hydrogenation of CO <sub>2</sub> to methanol, adapted from [16] .....	21
<b>Figure 9:</b> Number of review articles listed on ScienceDirect containing all of the following keywords over the years 2010 to 2019: CO <sub>2</sub> , methanol, hydrogenation, catalyst .....	22
<b>Figure 10:</b> Temperature profile during the calcination of MgCO <sub>3</sub> to MgO .....	27
<b>Figure 11:</b> Temperature profile during the drying of the filtered and washed catalyst.....	27
<b>Figure 12:</b> The figure shows the white MgO powder (left) and the blue CuNO <sub>3</sub> solution before the MgO is added.....	28
<b>Figure 13:</b> The picture on the left shows the turquoise catalyst precursor filter cake, while the right picture shows it after the drying process. ....	28
<b>Figure 14:</b> Temperature profile during the final calcination step .....	29
<b>Figure 15:</b> The figure shows the catalyst after the calcination step. The previously turquoise particles have become black. ....	29

- Figure 16:** An example for an MFC assembly including the bypass piping, as well as all needed valves.....34
- Figure 17:** PV installed in the PFR setup, a detail photo of the lid connections (when installed in the DSTR setup) and the bottom connection.....35
- Figure 18:** Solenoid valve UV-001, installed in the hydrogen stream and the installed rupture disc SE-001.....36
- Figure 19:** P&ID of the lab scale PFR setup including all sensors, equipment as well as a proposal for an extension for a batch wise gas sampling station.....40
- Figure 20:** Screenshot of Parr Instrument®'s software Spec View, used for monitoring and control of the lab scale PFR system.....42
- Figure 21:** Pressure test with N<sub>2</sub> at ambient temperature .....43
- Figure 22:** Schematic drawing of the PFR unit, including the temperature sensor and the connected tubing. Additionally, a detail of a sectional drawing is shown to demonstrate the structure of the catalyst bed and its support. ....45
- Figure 23:** Temperatures and pressure data during the activation experiment. The activation itself can be seen as an increase of the temperature T<sub>2</sub> (which represents TR), resulting in a steep spike. The experiment is carried on assuring complete activation under the actual validation conditions of TR  $\cong$  300 °C and p<sub>R</sub>  $\cong$  50 bar. ....46
- Figure 24:** Volumetric flow rates and pressure data during the activation experiment. Note that fluid streams, introduced by a manual opening of the bypasses, or their magnitudes, are not shown in this figure. The manually introduced gas streams are a hydrogen stream at the beginning, resulting in a pressure of 9 bar and a hydrogen stream used for pressurization of the system.....48
- Figure 25:** Temperature and pressure data of the validation experiment. Preheating of the system is followed by pressurization with hydrogen. As CO<sub>2</sub> is added to the feed stream, the final pressure and temperatures establish. After several hours the catalyst bed clogs and the experiment has to be terminated.....49
- Figure 26:** Pressures, measured before the reactor (left) and after the reactor (right). The difference results mainly out of the pressure drop across the packed catalyst bed. ....50

<b>Figure 27:</b> Rinsing is followed by manual pressurization. CO <sub>2</sub> and N <sub>2</sub> are added, synthetization is started, and the system is left approaching steady conditions. At $t \cong 11$ h clogging of the catalyst bed occurs. A second attempt results also in clogging and the experiment is terminated.....	51
<b>Figure 28:</b> Metal beaker with formed liquids in the product vessel, opened after the end of the validation experiment.....	52
<b>Figure 29:</b> P&ID of the lab scale DSTR setup.....	57
<b>Figure 30:</b> Pressure peak after pressurization with different slopes of the reactor- ( $p_R$ ) respectively the product vessel-pressure ( $p_{PV}$ ).....	60
<b>Figure 31:</b> Bubbles of soapy water, caused by leaking gas.....	61
<b>Figure 32:</b> Pressure over time curves for a whole pressurization test, using nitrogen.....	62
<b>Figure 33:</b> Pressure decrease during pressure test with nitrogen including a fast decrease at the beginning and constant decrease after two hours.....	63
<b>Figure 34:</b> Volumetric flow rates calculated from measured pressure data.....	63
<b>Figure 35:</b> Pressure test using hydrogen without heating.....	64
<b>Figure 36:</b> Pressure test under increased temperatures using hydrogen. The tightness of the system is tested periodically using a hydrogen sensor.....	65
<b>Figure 37:</b> First activation experiment using Cu/ZnO/Al <sub>2</sub> O <sub>3</sub> catalyst. At $t \cong 40$ min a temperature increase of TR, indicating the exothermic activation reaction, can be seen. The Activation experiment is terminated due to a hydrogen leakage after a second pressurization at $t \cong 133$ min.....	69
<b>Figure 38:</b> Second activation of the Cu/ZnO/Al <sub>2</sub> O <sub>3</sub> catalyst to assure a complete activation.....	70
<b>Figure 39:</b> Validation experiment data of day one including the molar ratio adjustment, prior to the actual experiment.....	72
<b>Figure 40:</b> Adjustment of the desired molar ratio of $n_{H_2}/n_{CO_2} = 3/1$ by depressurization, respectively repressurization with CO <sub>2</sub> .....	72
<b>Figure 41:</b> Validation experiment over two days using the Cu/ZnO/Al <sub>2</sub> O <sub>3</sub> catalyst.....	73
<b>Figure 42:</b> Humid catalyst particles, coating the stirrer with a thin layer.....	74



---

**Figure 43:** Catalyst coated magnetic axel after the reaction. The visible part is installed in the bearing room section where theoretically no catalyst should be present. The second picture shows the exhaust PTFE-hose. The slight red color is an indicator for the presence of finest catalyst particles in the exhaust gas stream. ....75

**Figure 44:** View inside the empty bearing room after a re-condensation experiment. The visible liquid droplets at the inner walls of the bearing room cannot be collected. Such a behavior must be considered in future balances. ....79

## 8 List of tables

<b>Table 1:</b> Design equations of ideal isothermal reactors .....	7
<b>Table 2:</b> Overview of the used MFCs and their properties .....	32
<b>Table 3:</b> List of installed instruments which are connected to the process controller .....	41
<b>Table 4:</b> List of all instruments which are either connected to the Parr Instrument's® process controller, the BüchiGlassUster® process controller or to the National Instruments® hardware. The MFC arrangement is the same as for the PFR plant and they are therefore not listed again. ....	58
<b>Table 5:</b> Measured pressure differences, calculated leaking rates and the expansion of potentially explosive atmospheres for different leakage scenarios .....	67
<b>Table 6:</b> Product loss during expansion data .....	77
<b>Table 7:</b> Product loss during condensation data .....	78
<b>Table 8:</b> Product loss during condensation with installed heating of the rising pipe .....	80

## 9 List of abbreviations and symbols

$A$	Pre-exponential factor
ATR	Autothermal reforming
BWR	Boiling water reactor
$c_i$	Concentration of a component
$c_A$	- component A
$c_B$	- component B
$c_C$	- component C
$C$	Air changes in a system per hour
$C_{DSTR}$	Air changes in the DSTR lab box per hour
$C_{PFR}$	Air changes in the PFR lab box per hour
DSTR	Discontinuous stirred tank reactor
$\varepsilon$	Porosity of a catalyst
$E$	Educt
$E_A$	Activation energy
$f$	Correction factor
$F_A$	Molar flow rate of a component $A$
$F_{A,0}$	-entering the system
$F_{A,out}$	-exiting the system
$\dot{G}$	Maximum leaking rate
$G$	Gibbs free energy
$\Delta G_R^0$	-of reaction at standard conditions
$\Delta G_{F,P}^0$	-of formation, at standard conditions, of products
$\Delta G_{F,E}^0$	-of formation, at standard conditions, of educts
$GHSV$	Gas hourly space velocity
GC	Gas chromatography
GCR	Gas-cooled reactor
$H$	Enthalpy
$\Delta H_R^0$	-of reaction at standard conditions
$\Delta H_{F,P}^0$	-of formation, at standard conditions, of products
$\Delta H_{F,E}^0$	-of formation, at standard conditions, of educts
$k$	Reaction rate constant
$k_s$	Safety factor

---

$K$	Equilibrium Constant
$K_{298}$	-at 298 K
$K_i$	-at a certain temperature $i$
$K_p$	-as a function of partial pressures
$LEL$	Lower explosion limit
$m_{Beaker,Tara}$	Tare mass of a beaker
$m_{Beaker+H_2O,After}$	Mass of a beaker containing condensed $H_2O$ at end of an experiment
$m_{H_2O,Beaker,After}$	Mass of $H_2O$ , present in a beaker after the experiment
$m_{H_2O,Initial}$	Mass of $H_2O$ at the beginning of an experiment
$\Delta m_{H_2O,Lost}$	Amount of $H_2O$ , lost during the experiment
$m_{H_2O,Other,After}$	Mass of $H_2O$ , regained from other locations than the beaker
$m_{H_2O,Regained}$	Amount of $H_2O$ which could be regained after the experiment in $w\%$
$M$	Module M
$M_{H_2}$	Molar mass of $H_2$
MTBE	Methyl-tertiary-butyl-ether
MFC	Mass flow controller
MFM	Mass flow meter
MTO	Methanol-to-Olefins
$n_A, N_A$	Moles of a certain species $A$
$n_{A,0}, N_{A,0}$	-at the beginning of a reaction
$n_{A,out}$	-at the end of a reaction
$n_i$	Moles of a species $i$
$n_{P,out}$	Moles of formed products, at the end of a reaction
$\dot{n}_P$	Molar flow rate of products $P$
$P$	Product
$p$	Pressure
$p_i$	Partial pressure of a species $i$
$p_R$	Reactor pressure
$p_{R,End}$	-at the end of the experiment
$p_{R,Initial}$	-at the beginning of the experiment
$p_{tot}$	Total pressure
$p_{PV}$	Product vessel pressure
PFR	Plug flow reactor
P&ID	Piping and instrumentation diagram
POX	Partial oxidation

---

PV	Product vessel
$\rho_{Bulk}$	Bulk density of the catalyst
$\rho_{H_2}$	Density of hydrogen
$r_{hemisphere}$	Resulting radius if an explosive atmosphere is assumed to be hemispherical
$r_{sphere}$	Resulting radius if an explosive atmosphere is assumed to be spherical
$r_A$	Reaction rate, formulated for a species $A$
$R$	Ideal gas constant
RWGS	Reversed water-gas shift reaction
$s$	Selectivity
$S$	Entropy
$\Delta S_R^0$	-of reaction at standard conditions
$\Delta S_{F,P}^0$	-of formation, at standard conditions, of products
$\Delta S_{F,E}^0$	-of formation, at standard conditions, of educts
STR	Steam reforming
$STY$	Space-time yield
$\tau$	Residence time
$t$	Time
$t_i$	Certain time $i$
$t_{i-1}$	Certain time $i - 1$ (prior to $t_i$ )
$T$	Temperature
$T_{298}$	-at 298 K
$T_1$	- at the lowest position (relative to $T_2$ and $T_3$ ) in the PFR
$T_2$	- in the middle position
$T_3$	-at the upper most position
$T_i$	A certain temperature $i$
$T_j$	Jacket temperature, measured in a heater unit
$T_R$	Reactor temperature
$T_{R,End}$	-at the end of an experiment
$T_{Set}$	Set temperature
TOF	Turn over frequency
UEL	Upper explosion limit
$\nu_A$	Stoichiometric coefficient of a species $A$
$\nu_P$	Stoichiometric coefficient of products $P$
$v$	Flow velocity

---

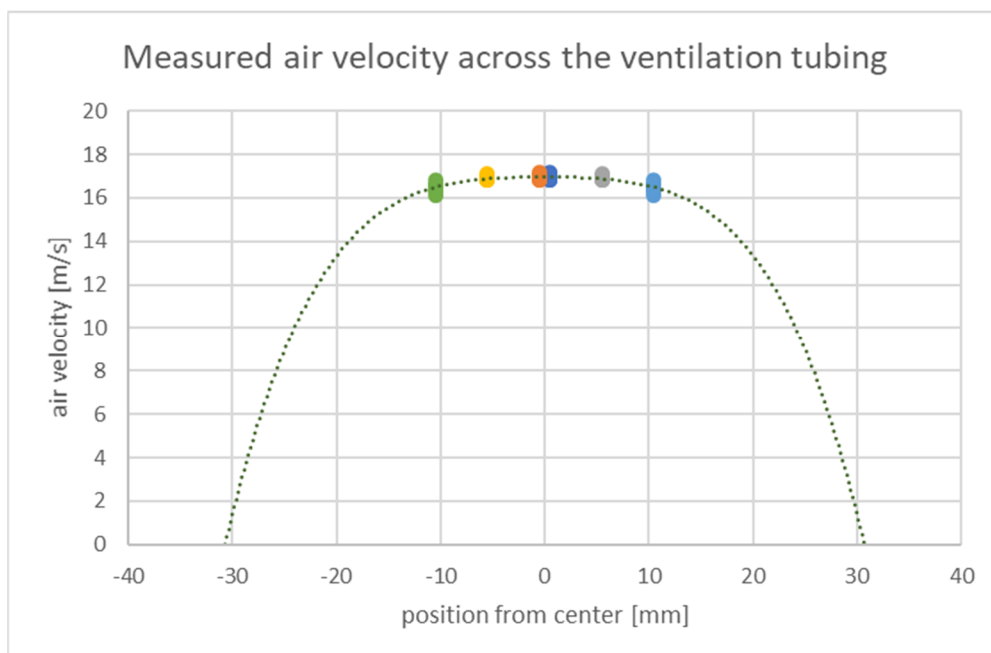
$v_{space}$	Space-time velocity
$V$	Volume
$V_{cat}$	Catalyst volume
$V_{Cylinder}$	Volume of a measuring cylinder
$V_m$	Molar volume
$V_{system}$	Volume of the pressurized system, needed for leakage calculation
$V_z$	Volume of potentially explosive atmosphere
$V_{z,Theo}$	-theoretically
$V_{z,Eff}$	-effective
$\dot{V}_{feed}$	Volumetric feed flow
$\dot{V}_{DSTR,Vent}$	Volumetric flow of the DSTR lab box ventilation
$\dot{V}_{fresh,min}$	Minimum volumetric flow to dilute a potentially explosive atmosphere
$\dot{V}_{PFR,Leakage}$	Leakage flow rate during the pressure test of the PFR-setup
$\dot{V}_{PFR,Vent}$	Volumetric flow of the PFR lab box ventilation
$x$	Molar amount of a component
$x_A$	-component A
$x_B$	-component B
$x_C$	-component C
$X_A$	Conversion of a species $A$

# 10 Appendix

## Calculations for the batch scale PFR setup

Ventilation measurement and calculation PFR box		
vmean/vmax	0,8	Assumption from fluid dynamics
vmean	13,76 [m/s]	Calculated (see measurements)
di_pipe	0,061 [m]	
A_pipe	0,003 [m <sup>2</sup> ]	
Vdot	0,041 [m <sup>3</sup> /s]	
Vdot	2,445 [m <sup>3</sup> /min]	
Vdot	146,672 [m <sup>3</sup> /h]	
V_PFRBoxx_Total	5,198 [m <sup>3</sup> ]	Calculated from $l \cdot h \cdot w = V$
C_Air	28,220 [times/h]	

Mes. Nr.	Position from wall [mm]; Air velocity in [m/s]		
	38	33	28
1	17,1	16,8	16,6
2	16,9	17	16,5
3	16,8	16,9	16,8
4	16,9	16,8	16,6
5	17,2	17,1	16,5
6	17	16,9	16,4
7	17	16,9	16,1
8	16,8	16,8	16,5
9	17	16,9	16,3
10	17	17	16,5
Mean velocity	16,97	16,91	16,48



Calculation of the pressurized volume of the PFR system			
I_MFC-ThreeWayValve	351 [cm]	s_pipe	0,12 [cm]
I_TWV-REACT	150 [cm]	d_1/4"	0,64 [cm]
R-Chill	40 [cm]	d_eff_1/4"	0,39 [cm]
Chill-pV	15 [cm]	A_1/4"	0,12 [cm <sup>2</sup> ]
PV-PCV	95 [cm]		
PCVBypass	25 [cm]	d_3/8"	0,95 [cm]
I1/4"	676 [cm]	d_3/8" _eff	0,70 [cm]
		A_3/8"	0,389 [cm <sup>2</sup> ]
I_cond_3/8"	50 [cm]		
I_reakt	59,5 [cm]	V_1/4"	79,14 [cm <sup>3</sup> ]
d_Reakt	1,27 [cm]	V_3/8"	19,44 [cm <sup>3</sup> ]
d_reakteff	0,94 [cm]	V_Reakt	41,27 [cm <sup>3</sup> ]
A_React	0,69 [cm <sup>2</sup> ]	V_PV	600 [cm <sup>3</sup> ]
V_reakt	41,27 [cm <sup>3</sup> ]	Vtot_System	739,85 [cm <sup>3</sup> ]
			7,40E-04 [m <sup>3</sup> ]

## Calculations for the batch scale DSTR setup

Ventilation measurement and calculation DSTR box			
vmean/vmax	0,80		Assumption from fluid dynamics
vmean	7,28 [m/s]		Calculated (see measurements)
di_pipe	0,104 [m]		
A_pipe	0,008 [m <sup>2</sup> ]		
Vdot	0,062 [m <sup>3</sup> /s]		
Vdot	3,711 [m <sup>3</sup> /min]		
Vdot	222,633 [m <sup>3</sup> /h]		
V_BatchBox_Total	1,449 [m <sup>3</sup> ]		Calculated from $l \cdot h \cdot w = V$
C_Air	153,646 [times/h]		

Mes. Nr.	Position from wall [mm]; Air velocity in [m/s]				
	58	48	38	33	23
1	8,8	8,4	8,5	8,1	7,9
2	8,9	8,5	8,4	8,1	8
3	9	8,6	8,5	8,1	8
4	9,1	9	8,5	8,2	8,1
5	9	8,7	8,4	8,2	8
6	9	8,6	8,5	8,3	8
7	8,8	8,6	8,4	8,1	7,9
8	9	8,7	8,5	8,1	8
9	9	8,6	8,6	8,2	7,9
10	9	8,6	8,5	8,1	7,9
Mean velocity	8,96	8,63	8,48	8,15	7,97



Calculation of the pressurized volume of the DSTR system			
$l_{\text{beforeReact}}$	87 [cm]	$l_{\text{cond}_{3/8''}}$	50 [cm]
$l_{\text{rising}}$	25 [cm]		
$l_{\text{afterCond}}$	10 [cm]		
$l_{1/4''}$	122 [cm]		
$s_{\text{pipe}}$	0,124 [cm]	$d_{3/8''}$	0,9525 [cm]
$d_{1/4''}$	0,635 [cm]	$d_{3/8''_{\text{eff}}}$	0,70358 [cm]
$d_{\text{eff}_{1/4''}}$	0,386 [cm]	$A_{3/8''}$	0,38879158 cm <sup>2</sup>
$A_{1/4''}$	0,117 [cm <sup>2</sup> ]		
$V_{1/4''}$	14,28 [cm <sup>3</sup> ]		
$V_{3/8''}$	19,44 [cm <sup>3</sup> ]		
$V_{\text{Reakt}}$	485 [cm <sup>3</sup> ]		
$V_{\text{PV}}$	600 [cm <sup>3</sup> ]		
$V_{\text{tot\_Syste}}$	1118,722 [cm <sup>3</sup> ]		
	1,12E-03 [m <sup>3</sup> ]		